Terms and Conditions of Use of Digitised Theses from Trinity College Library Dublin

Copyright statement

All material supplied by Trinity College Library is protected by copyright (under the Copyright and Related Rights Act, 2000 as amended) and other relevant Intellectual Property Rights. By accessing and using a Digitised Thesis from Trinity College Library you acknowledge that all Intellectual Property Rights in any Works supplied are the sole and exclusive property of the copyright and/or other IPR holder. Specific copyright holders may not be explicitly identified. Use of materials from other sources within a thesis should not be construed as a claim over them.

A non-exclusive, non-transferable licence is hereby granted to those using or reproducing, in whole or in part, the material for valid purposes, providing the copyright owners are acknowledged using the normal conventions. Where specific permission to use material is required, this is identified and such permission must be sought from the copyright holder or agency cited.

Liability statement

By using a Digitised Thesis, I accept that Trinity College Dublin bears no legal responsibility for the accuracy, legality or comprehensiveness of materials contained within the thesis, and that Trinity College Dublin accepts no liability for indirect, consequential, or incidental, damages or losses arising from use of the thesis for whatever reason. Information located in a thesis may be subject to specific use constraints, details of which may not be explicitly described. It is the responsibility of potential and actual users to be aware of such constraints and to abide by them. By making use of material from a digitised thesis, you accept these copyright and disclaimer provisions. Where it is brought to the attention of Trinity College Library that there may be a breach of copyright or other restraint, it is the policy to withdraw or take down access to a thesis while the issue is being resolved.

Access Agreement

By using a Digitised Thesis from Trinity College Library you are bound by the following Terms & Conditions. Please read them carefully.

I have read and I understand the following statement: All material supplied via a Digitised Thesis from Trinity College Library is protected by copyright and other intellectual property rights, and duplication or sale of all or part of any of a thesis is not permitted, except that material may be duplicated by you for your research use or for educational purposes in electronic or print form providing the copyright owners are acknowledged using the normal conventions. You must obtain permission for any other use. Electronic or print copies may not be offered, whether for sale or otherwise to anyone. This copy has been supplied on the understanding that it is copyright material and that no quotation from the thesis may be published without proper acknowledgement.

Microphone array techniques for aeroacoustics

Peter Jordan

Department of Mechanical Engineering,
Trinity College,
Dublin

October 2000

A degree submitted to the University of Dublin for the degree of Ph.D

Abstract

The capacity for source localisation and measurement in aeroacoustics can be enhanced through the use of a microphone array. Although arrays have been used in a variety of applications, there are a number of problems manifest in their use for analysis of specific systems. The first of these is the dependence of the response characteristic of an array on the source frequency of the system being analysed. This can lead both to spurious source identification and erroneous source measurement. In this work a technique developed for radio antenna applications is adapted to give additional response control for linear arrays with commensurate element spacing. This is then applied to an aeroacoustic system consisting of twin high-speed propellers where the noise generated by one propeller is to measured, while contributions from the other are filtered out. The second problem arises due to aeroacoustic source directivity. This problem is illustrated by means of a simple model, which shows that erroneous results are obtained when a dipole source is measured using an ordinary beamformer. A procedure which allows the location and orientation of such a source to be identified is proposed, and a correction applied to the beamformer such that it correctly measures the source. This procedure is then applied to an experimental aeroacoustic system containing a single dipole in the form of a cylinder in cross-flow. A general methodology for aeroacoustic analysis based on these developments is proposed and its implementation discussed.

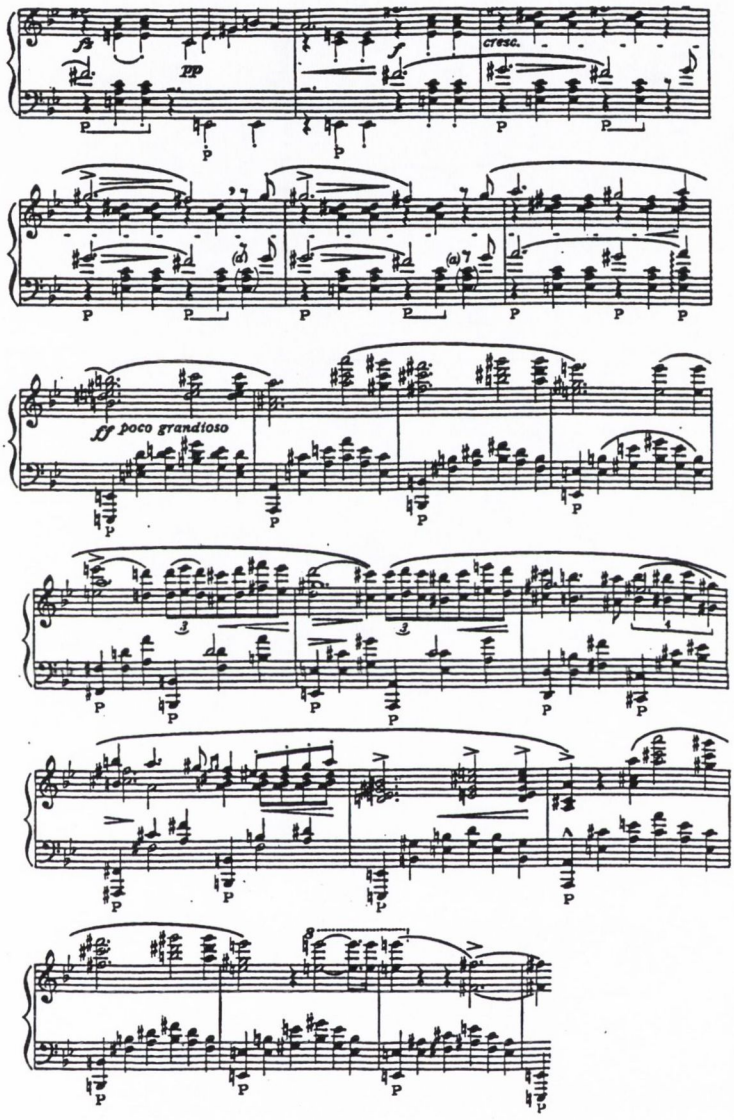

Fryderyk Chopin, Opus 23 bars 82-100

Declaration

I declare that I am the sole author of this thesis and that all the work presented in it, unless otherwise referenced, is my own. I also declare that this work has not been submitted, in whole or in part, to any other university or college for any degree or other qualification.

I authorise the library of the University of Dublin to lend this thesis.

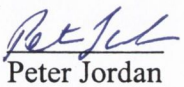

Peter Jordan

October 2000

Acknowledgements

There are a number of people who I would like to thank for their support over the course of the last four years. Firstly John Fitzpatrick, who has been a continual source of guidance and enthusiasm. Thanks also to my colleagues in the fluids and vibrations group for their technical assistance, in particular Craig Meskell, Michael Carley and Conor Sweeney. And finally, thanks to my family and friends for four years of fun and friendship.

Contents

List of Figures

Chapter 1

Introduction

1.1 Engineering and noise

Noise pollution is an unfortunate consequence of many engineering developments and is one of the major drawbacks of technological advance in automotive transport systems. Although industrial noise has always been a problem, recent legislation for environmental noise pollution has become more stringent making the acoustic design of engineering systems a higher priority. Although the full effect of noise on society is not yet fully understood, there is little doubt that the psychological effects are very real. A comparison between a modern capital city and that city two hundred years ago is most remarkable for the difference in ambient noise. City sounds today are dominated by the sound of automotive engine noise, whereas the ambiance of two hundred years ago was dominated by the sounds of human conversation.

The problem of noise control is of particular concern for the aircraft industry, as the more advanced aircraft become in terms of performance the more sound they are liable to generate, a consequence of the relationship between the intensity of sound generated by an aircraft's propulsion system and its velocity. Depending on the type of aeroacoustic source, sound intensity can vary with the fourth, sixth or eighth power of velocity. This fact, together with the ever increasing volume of air traffic through most modern airports,

emphasises the necessity for improved research in the acoustic design of aircraft. In recent years the number of complaints received from residents living near the major European airports has increased substantially, despite large reductions in noise levels, indicating that the public are becoming more sensitive to environmental noise and are less prepared to tolerate this intrusion into their homes.

1.1.1 Aeroacoustic noise

The noise pollution evident around any modern airport is an example of aeroacoustic noise, aeroacoustics being that branch of acoustics concerned with sound generated by aerodynamic phenomena. Just as the mechanical workings of large industrial machinery generate noise, the aerodynamic 'workings' of modern aircraft also generate large amounts of unwanted sound. Aeroacoustic systems tend to be more difficult to analyse than mechanical systems however, due largely to the fact that the mechanisms responsible for the noise are usually invisible and complex. While sound generated by mechanical systems is due in the main to the vibration and contact of machine components, sources of aeroacoustic sound are most often due to aerodynamic mechanisms which remain undetectable to the naked eye, for example turbulence and fluid-structure interactions.

The most obvious sources of aeroacoustic sound are manifest in the aircrafts' propulsion systems, be they jet, propeller or otherwise. However, although a large proportion of the total sound energy can be attributed to the propulsion system, it does not account for all of the noise. As propulsion noise is reduced, other less obvious sources of sound such as undercarriage noise or flap-edge noise become more dominant.

Aeroacoustic sound is the result of disturbances in a sonic medium caused by aerodynamic effects. As the aerodynamic and acoustic fields are intrinsically linked, it is clear that for any complex aerodynamic system, there will be an equally complex acoustic field, and it is this complexity which makes

aeroacoustic systems so difficult to analyse

1.1.2 Reducing noise levels

It is clear, that if the problem of environmental noise pollution is to be addressed and successfully treated, sources generating noise and their associated physical mechanisms must be evaluated and understood, as it is only then that better design techniques for the reduction of noise can be developed. The task facing the acoustic engineer can be stated as follows: how can a noisy engineering system be most thoroughly analysed, in order to identify the major sources of sound? The primary requirement is that the system be broken down into its fundamental components, and that these components and their respective interactions be studied to determine the mechanisms generating the resultant acoustic field. Aeroacoustic systems generally consist of a large collection of arbitrarily correlated individual source components. Thus, important sources may often be embedded in a background of noise, making them extremely difficult to identify. Separation of these components for examination necessitates a capacity for the examination of very specific regions of space-time, i.e. regions of space over a given time period. This thesis is concerned with the investigation and development of an experimental tool, based on the principles of microphone array technology, capable of this kind of measurement.

1.2 The microphone array

As sound is the direct result of physical mechanisms which cause distinctive pressure disturbances in the surrounding medium, the resultant behaviour of that medium gives valuable information concerning the nature of the source mechanism. The microphone array is a device which can focus on specific regions of space in order to determine the nature of the acoustic or aeroacoustic sources in that region.

In particular this thesis is concerned with sound generated by aerody-

namic phenomena. These generate distinctive acoustic fields depending on the source mechanism, and so, through the medium of sound relay information which, when appropriately processed, can reveal the nature of the source. The primary focus of this thesis is on two specific aspects of microphone array applications.

- **Optimisation** The way in which the microphone signals are combined, together with the characteristics of the system being analysed, play a large part in determining the response characteristic which will result. Through an examination of basic beamforming, and the mathematical formulation of this mechanism, the difficulty of antenna optimisation is addressed.

- **Source directivity** Ordinary beamforming procedures do not allow for the directional nature of certain sources. This thesis demonstrates by means of numerical models, which are subsequently validated using a simple aeroacoustic system, the effect of a single dipole source on the response of an array. It is shown how the beamformer fails to locate and measure the source, and a technique is developed which adapts the array processing to suit the distinctive characteristics of that source.

Chapter 2

Review of array techniques

2.1 Historical perspective

Throughout the twentieth century advances in technology proceeded at what appears to have been an exponential rate. Technologies which, at the beginning of the century were in their infancy, developed to become the foundation technologies of today's engineering environment. The concept of array processing is one such technology. Initially developed for military purposes, in the form of radar and sonar, it has today become a vital element in areas such as telecommunications and navigation.

Examples of array techniques can be found as early as the first world war where arrays of acoustic receivers were used to 'listen' for the approach of enemy aircraft, as shown in figure 2.1. This particular device could be manually rotated so as to aim it in different directions, and thus identify the presence of incoming aircraft. This technology was rapidly developed for military advantage in the form of radar and sonar detection systems. Radar, which was being developed by the Germans as early as 1933, uses electromagnetic radiation to search space for the presence of solid bodies. Portions of the electromagnetic field reflected by a solid body can be manipulated according to the principles of array processing so that the location of the body can be determined [1]. This technique was developed during world war two into a highly efficient

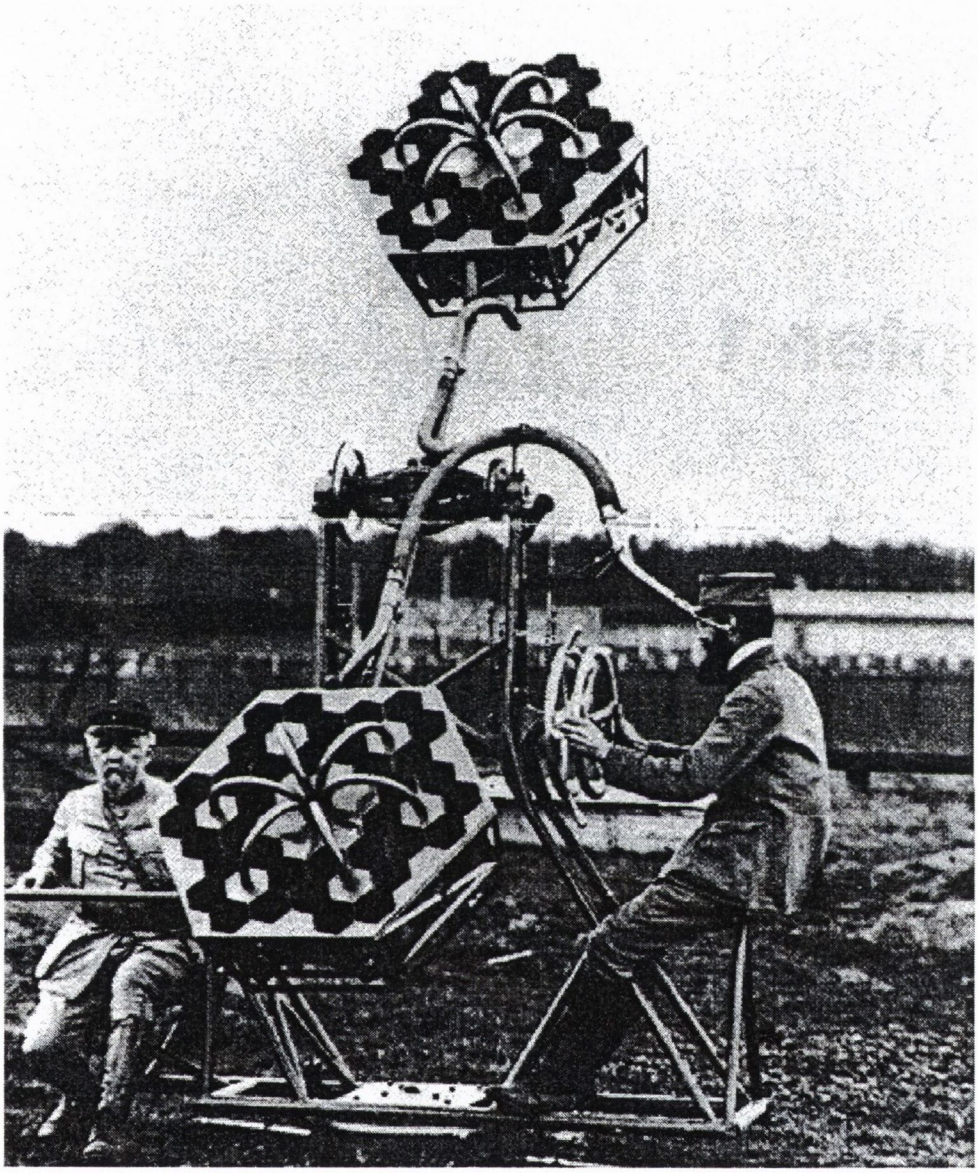

Figure 2.1: Early acoustic array

device for locating and tracking aircraft, and has today become an essential tool in the global transport industry. Sonar systems are used in a similar fashion to search the seas for submarines and fish, as well as being used by a large variety of water craft to identify the depth and topology of the local sea bed [2]. There are two basic modes of operation of a sonar system, active and passive. Active sonar consists in the radiation of an acoustic field which, when reflected by a solid body and processed in a similar fashion to the electromagnetic wave fields of radar systems, can be used to determine the location of that body. Passive sonar consists in 'listening' for the acoustic signature of underwater craft, and so can only detect objects which generate sound. It is in this passive manner that microphone arrays are usually employed. Sonar is an inefficient tool for application in air, due to the relatively slow speed of sound propagation compared with the speed of modern aircraft. This difference in velocity means that by the time the sound from an aircraft has reached the receiver, the position of the aircraft has changed and so the location identified by the sonar system will always be in error. In underwater applications it is more efficient as the sonic velocity is four times that of air, and this, combined with the relatively slow speed of underwater craft make sonar a viable option. Other examples of array processing are the telescopes used in radio astronomy, whose foci roam about in deep space, probing and gathering new information [3]. Instead of microphones these telescopes consist of collections of satellite dishes. The VLA (very large array) in New Mexico shown in figure 2.2 is an example. Each satellite dish receives electromagnetic radiation from outer space which can be processed and then combined with signals from the other satellite dishes so that radio waves which have been bombarding the earth for millions of years can be used to determine the nature of their source. Another growth area of array processing is the telecommunications industry. All radio antennae (receivers or emitters) use array processing in some form or other, mobile phones are a recent example. In the case of telecommunications the emphasis is on array emitters which concentrate the majority of the signal

Figure 2.2: VLA, New Mexico

power in a given direction, thus avoiding radiation into redundant regions of space. Much of the research in this area is concerned with the optimisation of radiation patterns. Dolph [4] developed a technique which maximises radiation resolution, i.e. the majority of the signal power is concentrated in as narrow a beam as possible. Bouwkamp et al. [5] argued that there is no exact solution to the problem of optimum current distribution for linear radio antennae and they developed a method to realize any radiation pattern by suitable choice of current distribution. Riblet, [6] extended the theory of Bouwkamp to two-dimensional current distributions to enable the same radiation pattern specification for planar antennae.

These techniques are examples of antenna emmitters used in the telecommunications industry. The acoustic array is an example of an antenna receiver, which was developed as a result of the success of radar and sonar as an experimental tool for acoustic source localisation in a number of different applications. Billingsley and Kinns [7] for example have applied a microphone array to jet noise and Marcolini and Brooks [8] more recently used an array for the analysis of helicopter rotor noise. In acoustics, the principle is usu-

ally applied to a collection of microphones (or hydrophones, depending on the application), known collectively as an acoustic array. The layout of the microphones depends on the system it has been designed to analyse. The microphone signals can be processed individually and then combined in one of any number of different ways (multiplied, added, convolved etc.), depending on what is required of the measurement. The array treats incoming sound waves in a similar fashion to the treatment of electromagnetic radiation by radar systems, and, in the same way, is capable of discovering the direction from which a given sound field emanates. Just as radar is used to determine the positions of objects in space, an acoustic antenna can determine the source of a given sound field.

Arrays can be used to analyse noisy engineering systems in order to obtain a better understanding of the noise sources through more accurate measurement. With this more fully developed understanding of the sources responsible for the sound, the engineer is in a better position to reduce overall noise levels. Meadows et al. [9] for example performed measurements on a NACA 63_2-215 wing section with a 30 percent chord half-span flap. Using two directional arrays, correlated with an array of unsteady surface pressure transducers, they identified that locally dominant noise sources existed on the flap-side edge.

Before the most recent developments in computing power, acoustic mirrors were the preferred tool of acousticians seeking to analyse complex noise producing systems. The acoustic mirror is an acoustically reflective surface of parabolic shape, with a microphone located at the inner focal point (shown in figure 2.3 as F1). The mirror is arranged such that the area of interest lies at the outer focal point (shown in figure 2.3 as F2). In this way the majority of the system's energy is focused on the inner microphone, while sound generated by regions away from the outer focal point is scattered so as to cause destructive interference in the vicinity of the inner microphone. These devices proved quite successful, although they have a number of drawbacks. The main problem is that their spatial resolution is inversely proportional to the diameter

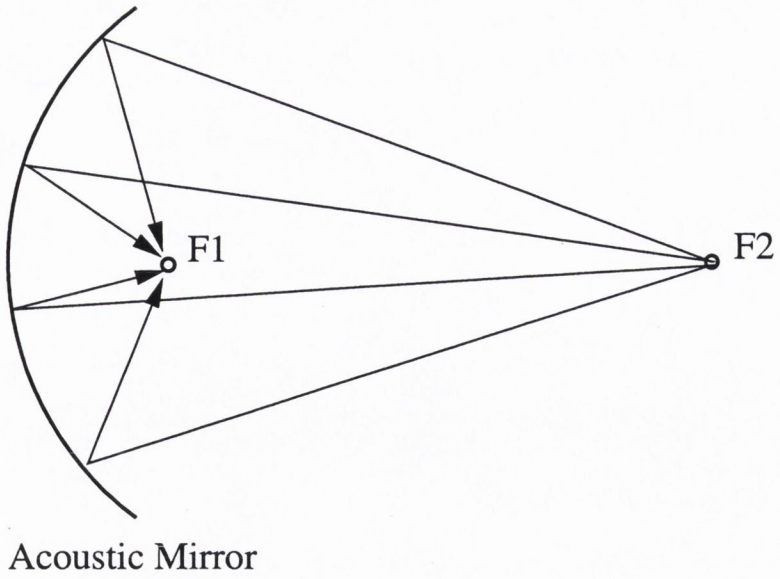

Figure 2.3: Acoustic Mirror

of the mirror. Thus, for good resolution huge mirrors are necessary and this poses obvious problems from a manufacturing perspective. Another limitation is that any modification of the focus position requires that the whole device be mechanically translated and/or rotated.

As long as digital signal acquisition and processing remained inefficient the acoustic mirrors were a viable option. However, with the recent advances in computing power, these devices have, for the most part, become redundant. The speed at which data can be acquired and processed has given rise to a renewed interest in microphone array systems. There has been an abundance of research in the past few years in a wide variety of areas, from the tracking of zooplankton [10] to jet noise source localisation [11].

2.2 Beamforming and some of its problems

The most common technique employed with microphone arrays is known as beamforming, also referred to as delay-and-sum beamforming, as used for example by Billingsley and Kinns [7] in a study of jet noise. The concept consists

of using a number of transducers at discrete spatial locations in order to sample a given wave field. The signals are then processed such that signal power from a specified region is enhanced, whereas signal power from all other regions is attenuated. The underlying principle is quite simple; if a propagating wave field is incident on a collection of transducers, it will arrive at each of the transducers at a different time, depending on the source-transducer distance. Because the relative time differences are simply dependent on the source position, the transducer signals can be modified to eliminate the time difference, or phase-difference in the frequency domain. The time differences are manipulated such that the temporal coordinates of the microphone signals become the same, thus forcing the signals into phase with one another with respect to a specified source. In this way, those portions of the transducer signals which came from a point in space defined by that set of phase shifts, when summed, will interfere constructively. Similarly, portions of signals emanating from any other region will interfere destructively. By appropriate manipulation of the signals' phases the focus of the array can be shifted about in space, boosting the signal to noise ratio of specified regions. This technique can be thought of as an adaptable acoustic mirror. Whereas variation of a mirror's focus position and resolution requires mechanical alteration of the device, all array adaptation can be achieved electronically. Figure 2.4 illustrates this technique.

2.2.1 Directivity

The performance of an array is often characterised by what is known as its directivity pattern, which defines the spatial sensitivity of the array. For any given focus position it gives an indication of how susceptible the array will be to sources of contamination in other regions of space. An example can best illustrate this point. Figure 2.5 shows a linear array of thirty microphones, which has been set up to examine a linear region of space. The directivity of the array defines its sensitivity to potential sources of contamination from a

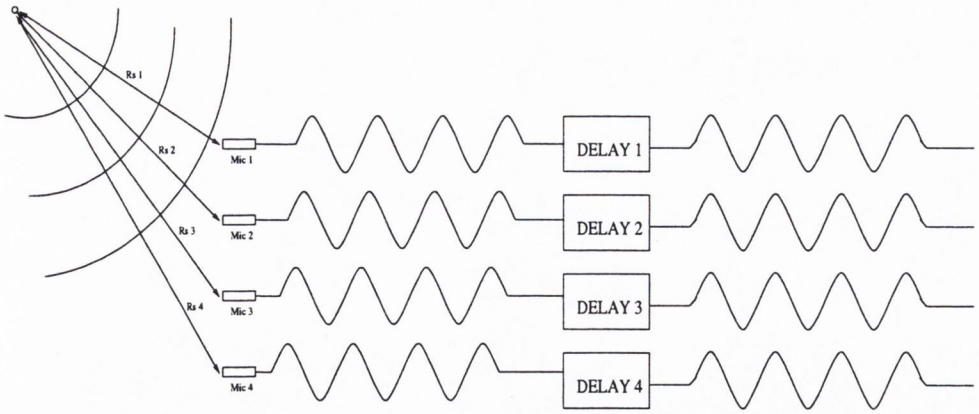

Figure 2.4: Beamforming

selected region, in this case the linear region AB, parallel to the array axis. Figure 2.6 shows the directivity for a $1000Hz$ source located directly opposite the mid-point of the array. This directivity pattern is generated by moving the array focus from point A to point B in increments of a given size. On examination of the directivity it can be seen that the pattern consists of a mainlobe (or major lobe), centered on the source position, and a series of sidelobes (or minor lobes) to either side of the mainlobe. The peak of the mainlobe corresponds to thirty signals which are perfectly in phase, and so interfere constructively to give a maximum. The sidelobes, a result of partial constructive interference, are a major problem associated with array measurement and the focus of much research in this area, for example the techniques of Dolph [4] and Riblet [6], described earlier, achieved equal minor lobe amplitudes and an improved mainlobe width. The effect of the sidelobes is to contaminate the measurement, especially if a second source coincides with their position. An array's directivity pattern is a function of array geometry, source frequency and array-source distance. Thus it can be seen that the response characteristic of an array is dependent, not only on the array configuration, but also on the frequency of the source being analysed. Much of the research effort where arrays are concerned has been with a view to developing optimum directivity patterns for specific applications, as this will determine the quality of

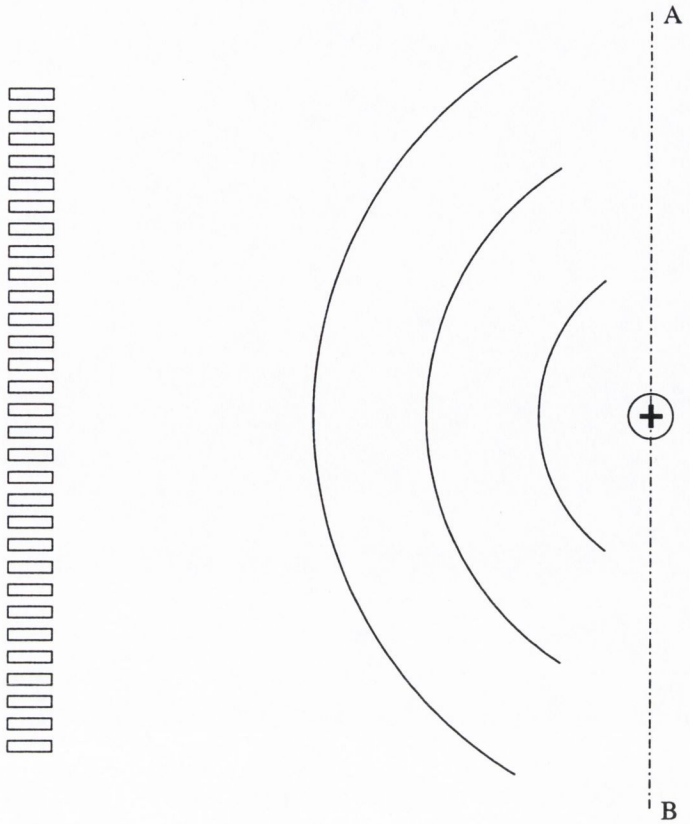

Figure 2.5: Linear array

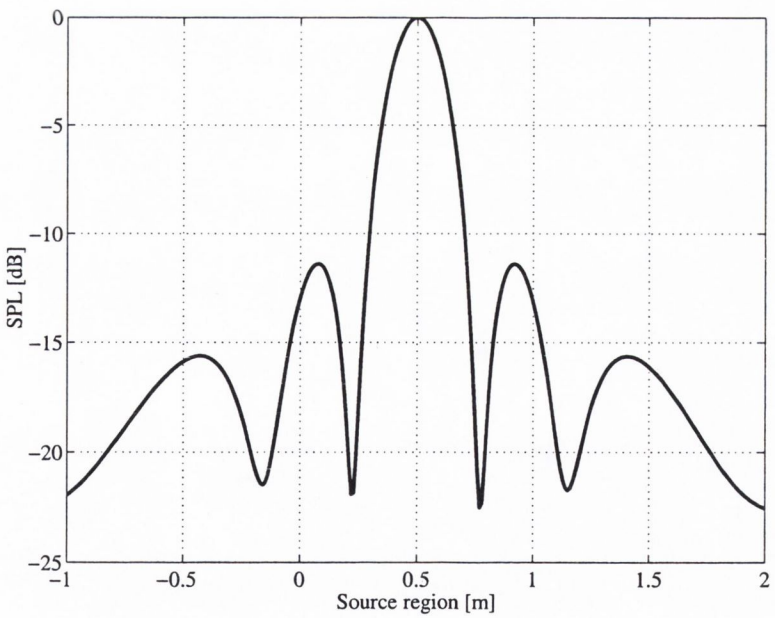

Figure 2.6: Array directivity

the measurements which can be taken, for example Marcolini and Brooks [8] developed a technique which produced constant measurement resolution for different frequencies and applied it to a helicopter rotor in order to obtain quantitative measurements.

2.2.2 Source localisation in acoustics and aeroacoustics

In 1976, Billingsley and Kinns [7] developed a microphone array for the location of noise sources on a full scale jet engine. By means of statistical averages, this system could calculate time varying source distributions with respect to position and frequency. This is an early application of beamforming to an aeroacoustic system, they called the device an 'acoustic telescope'. In an attempt to improve the measurement capacity of array systems many researchers deviate from the traditional delay-and-sum technique. Berman and Clay [12], examined the possibility of using a method other than the usual linear operation of adding element outputs for an acoustic receiving array. Replacing the linear operation with a form of non-linear processing, they showed that with these non-linear operations, a directivity equivalent to that of an array with a large number of elements could be obtained using substantially fewer elements. Brown and Rowlands [13] investigated further the merits of this technique. They demonstrate the improvements in directionality through the use of non-linear operations, and show that, for the noiseless case, a two element array can be made to yield patterns equivalent to those produced by an n-element linear array. These techniques were developed for the noiseless case and could be approximated for the case of very high SNR. Kinns [14] used a technique in which sources were examined through use of the coherence and phase spectra of signals from a closely spaced pair of microphones. These were used to compute the moments (i.e. statistical characteristics) of a line distribution of arbitrarily correlated omnidirectional sound radiators. This work established that, from a single binaural measurement the source location could be determined. Flynn and Kinns [15] performed a comparison between

multiplicative signal processing and additive processing. They found that by using multiplicative methods the resolution of an array's response could be improved. Again this technique was for the case of very high SNR.

The spatial resolution of an array is a function of the frequency of the source being measured, which means that the characteristics of a given measurement depend on the frequency of interest. Marcolini and Brooks [8] addressed this problem using a method which can be illustrated more clearly through an examination of figure 2.6. They considered their *effective* measurement region to be that region bounded by the -3dB points, although in their case the measurement region was two dimensional, and so the -3dB points are represented by a contour line. The size of this region (i.e. the resolution of the array) depends on the source frequency, clearly an undesirable effect. Marcolini and Brooks [8] developed a blending type procedure in order to generate constant beam-width for varying source frequency. In effect this meant that regardless of the source frequency, the position of the -3dB points remained constant, giving a constant effective measurement region. The array system which they developed was for the analysis of helicopter rotor noise. They successfully achieved spatial resolution of the main directional lobe which was independent, not only of frequency, but also of look angle. They obtained good agreement in a comparison of the spectral results from the array with predicitons of broadband self noise, and with total rotor noise measurements obtained from individual microphones of the array. Due to the anechoic environment, side-lobe position and size was not a major concern.

In 1997 Meadows et al. [9] performed tests on a wing-flap configuration using two directional arrays, one large aperture directional array (LADA) and another small aperture directional array (SADA). The LADA was for identifying the dominant sources of sound and had a spiral microphone layout, which gives good gain characteristics. This means that the difference between the mainlobe level and the highest sidelobe is maximised. The SADA was used for quantitative spectral analysis of the dominant sound generating regions and

included the blending procedure of Marcolini and Brooks. This application was for high frequency source analysis ($2 - 30kHz$). At these fequencies there will be a large number of sidelobes very close to the main lobe and so it is vital that the gain of the array is optimised, in order to minimise contamination. For low fequency applications this optimum gain is not as important because the first sidelobe will often lie outside the sound generating region. This will be demonstrated in the case study discussed in chapter 3.

2.2.3 Microwave antennae

As the beamforming principle derives from antenna theory it is useful to examine some of the work conducted in this area. Radio antennae use the same principle in order to achieve directional electromagnetic radiation. Much of the radio literature is concerned with the synthesis of optimum directivity patterns for linear point arrays, or antennae with continuous current distributions. Schelkunoff [16] formulated the problem according to a far-field model, and using this model approximated the directivity of an array as a polynomial. Dolph [4] was concerned with the control of mainlobe width and sidelobe suppression, and he developed a technique which was extended by Riblet [6] to two dimensions. Duhamel [17] modified the techniques of Dolph and Riblet so that a common design procedure could be used. Ziehm [18] worked on the optimisation of circular array directivity while Elliot et al. [19] were concerned with planar systems. Woodward et al. [20] present a mathematical theory for two-dimensional arrays which suggests the possibility of unlimited directivity control, although in practice the application of this theory is limited by unrealistic excitation amplitudes. The work of Dolph and Riblet was adapted for application to an acoustic antenna by Pritchard [21], who realised the potential of these techniques for application to acoustic arrays.

The original work of Dolph [4] showed that through specification of equal minor lobe amplitudes (side lobes, shown in figure 2.6), the major lobe width (mainlobe width) could be minimised, and conversely if the major lobe width

was specified the minor lobe levels could be minimised. Further to these observations, Dolph [4] showed that the relevant element excitations required to produce an equal minor-lobe pattern could be found. The method involved transforming the array's directional characteristic to a polynomial in a suitable variable, and then applying an appropriate transformation with Tchebycheff polynomials - which possess the property that all extrema are of the same amplitude. Pritchard [21] extended these techniques to steered or 'compensated' arrays. The importance of transducer spacing was discussed at some length and it was noted, in particular, that spacings equal to the sound wavelength resulted in unacceptably large secondary lobes. Arrays with spacing equal to or less than a wavelength are referred to as 'super-gain' arrays by Riblet [6]. In present day array design, it is a prerequisite that the transducer spacing be less than half a wavelength. Pritchard [21] also found that as the array length was increased the major lobe width decreased (for constant transducer spacing), a now well established consequence.

The effect of source frequency and array length on the response of an array are illustrated in figures 2.7 and 2.8. For a system set-up as in figure 2.5, with the source region at a distance of $2m$ from the array, and for a thirty element, $2m$ array, the directivities for monochromatic sources of $1000Hz$ and $2000Hz$ are shown in figure 2.7. It can be seen clearly that as the source frequency is increased the array's resolution improves. The effect of array length is illustrated in figure 2.8 which shows directivities for 1 and $2m$ arrays in the presence of a $2000Hz$ source.

2.3 Summary

Acoustic antennae have been developed for application in a wide variety of areas. This thesis focuses on applications involving aeroacoustic systems, where individual source components correspond to different aerodynamic phenomena. Because of the complexity of aeroacoustic systems, it is crucial that the

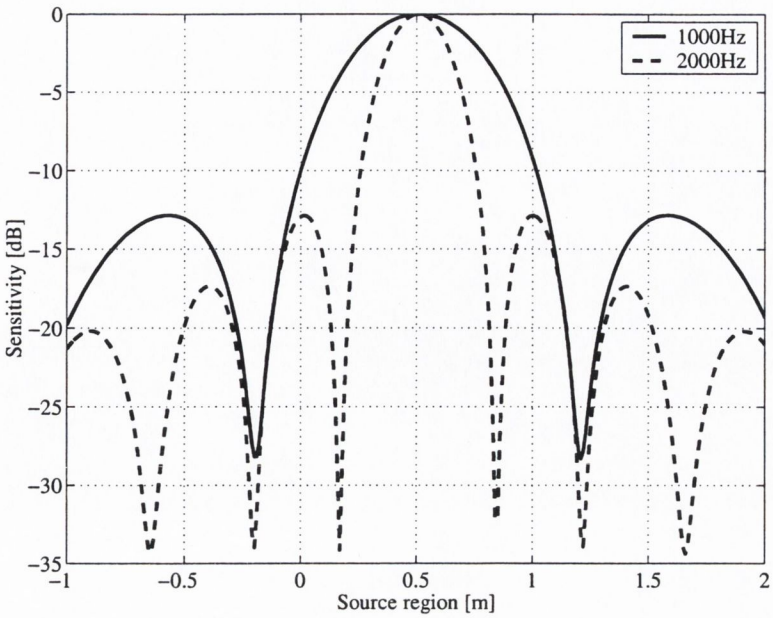

Figure 2.7: Effect of source frequency

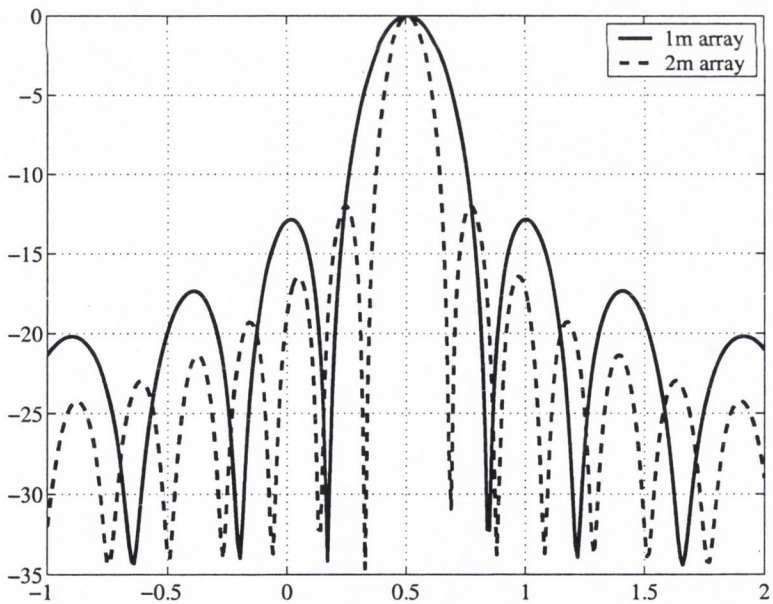

Figure 2.8: Effect of array length

array be designed so as to minimise the potential for spurious interpretation and contamination from unwanted sources. This requires that the array response characteristics be well known for all system set-ups. Emphasis is placed on the necessity for directivity control, or where this is not possible, the need for a thorough knowledge of the response characteristics of the array.

There are two specific aspects of array measurement which will be investigated in this work. The first is the problem of directivity control, an area which has received much attention in the area of microwave antenna, but which has not been fully exploited in acoustic and aeroacoustic applications. The second aspect is the identification of specific types of aeroacoustic source. If an array is to be used to its full potential, it is crucial that both these aspects be given due consideration.

Chapter 3

Directivity modelling and control

3.1 Introduction

The dependence of array response on parameters such as source frequency, array geometry, position and orientation poses real problems in the practical implementation of these devices. The external control of directivity is something which has been dealt with in some detail in telecommunications research, as was seen in the last chapter. Similar control has not been used as extensively however in acoustic array design, and so, in this chapter the problem of acoustic antenna optimisation is addressed. The problem is formulated mathematically according to both near and far field models, thus allowing the specific difficulties of directivity control to be identified.

3.2 Near field formulation of array response

Using the coordinate system shown in figure 3.1, for a microphone at point M, and a source of wavenumber k at point S, the microphone signal due to that

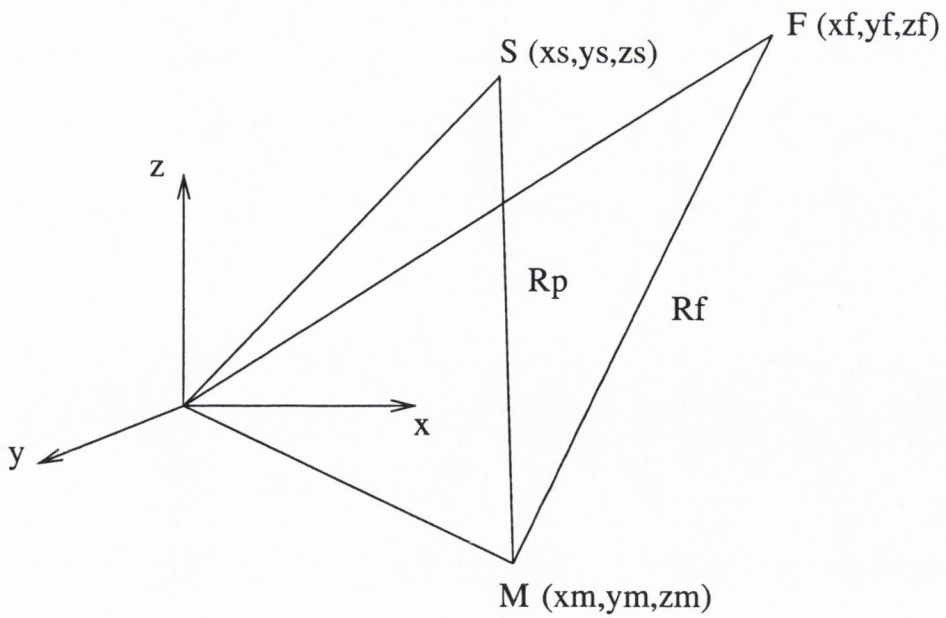

Figure 3.1: System reference frame

source is given by

$$P(k, R_p) = \frac{e^{-jkR_p}}{4\pi R_p} \tag{3.1}$$

Equation 3.1 is the monochromatic solution of the acoustic wave equation. When this signal is weighted for focus on point F it becomes

$$P(k, R_p, R_f) = \frac{e^{jk(R_f - R_p)}}{4\pi R_p} \tag{3.2}$$

Which in terms of the cartesian coordinates of the source, microphone and focus position is

$$P(k, R_p) = \frac{e^{-jk([(x_m-x_f)^2+(y_m-y_f)^2+(z_m-z_f)^2]^{1/2}-[(x_m-x_s)^2+(y_m-y_s)^2+(z_m-z_s)^2]^{1/2})}}{4\pi[(x_m - x_s)^2 + (y_m - y_s)^2 + (z_m - z_s)^2]^{1/2}} \tag{3.3}$$

This equation represents a single phase-weighted microphone signal, thus the array output can be written as

$$S_p = \Sigma_{m=1}^{N} \frac{1}{4\pi} \frac{e^{-jk([(x_m-x_f)^2+(y_m-y_f)^2+(z_m-z_f)^2]^{1/2}-[(x_m-x_s)^2+(y_m-y_s)^2+(z_m-z_s)^2]^{1/2})}}{[(x_m - x_s)^2 + (y_m - y_s)^2 + (z_m - z_s)^2]^{1/2}} \tag{3.4}$$

Equation 3.4 is the array response to a sound source at position S, when the focus position is F, for microphone coordinates (x_m, y_m, z_m) and $m = 1 : N$, where N is the total number of microphones. This represents the sensitivity of the array at spatial coordinate (x_f, y_f, z_f) and constitutes a single equation with $3N$ unknowns, or $4N$ if microphone weights are included. This is clearly insoluble. However, given that a selection of spatial coordinates and their corresponding requisite sensitivities can be specified, this equation can be extended to a system of $4N$ equations with the same $4N$ unknowns (microphone coordinates and weights). The equation system can be easily over determined by increasing the number of spatial coordinates accordingly.

It would seem from this that any arbitrary directivity pattern can be specified and a set of microphone coordinates and/or coefficients calculated, in order to achieve that directivity. Unfortunately, due to the ill-conditioned nature of this equation system, obtaining a useful solution is virtually impossible. This ill-conditioning is due to a long established tenet of acoustics, namely - *for any given wave field, there exists no unique solution representing the source.* If the array elements are thought of as a collection of point sources, and the directivity pattern the resultant sound field (which is mathematically identical to the more usual formulation), then it becomes clear that any exact directivity control will not be achieved by straightforward means. It may be possible, using very powerful computers, to design optimisation algorithms capable of perfect directivity control, however in the absence of supercomputing it is neccessary to consider an alternative approach. One such approach is to formulate the problem for a farfield setup, and examine how the governing equations change. This is addressed in the next section using the radio antenna theory of Schelkunoff [16].

3.3 Far field formulation of array response

When considering an array system located in the far field of an acoustic source, the problem is exactly analagous to a radio transmitting antenna. This is because the target region of a radio transmitter lies in the emmiter's far field, so that the wave field in that region can be considered to consist of plane waves. It is for this reason that the far field assumption is valid for all radio transmitters. Much of the successful directivity control reported in the radio literature is based on the foundation work of Schelkunoff [16], which expresses the problem in concise mathematical terms.

Consider the system shown in figure 3.2, consisting of a linear array of receivers, equally spaced and in the far field of some acoustic source, whose wave field approaches at velocity c (or wavenumber $k = 2\pi f/c$). Because the receivers are in the farfield, the waves can be considered plane when they arrive at the array. The signal received on any of the transducers can be written as

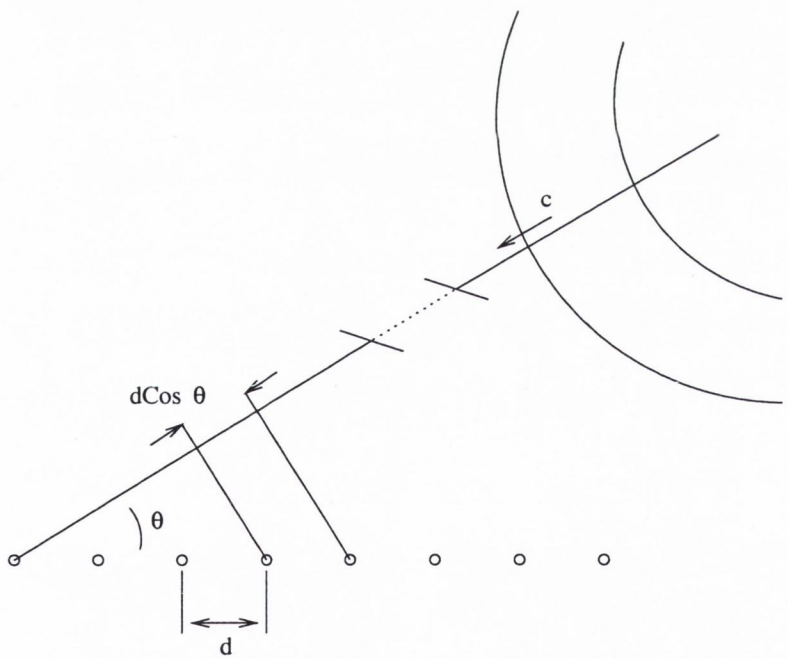

Figure 3.2: Far-field setup

$$P = A_n Cos(nkdCos\theta) \tag{3.5}$$

where θ is defined in figure 3.2. The $nkdCos\theta$ term here accounts for the phase-shift due to the signal arriving at each transducer at a different time. Writing this in the more general form of

$$P = A_n z \tag{3.6}$$

where

$$z = e^{j\phi} \tag{3.7}$$

and

$$\phi = kdCos\theta - \beta \tag{3.8}$$

where β is the phase modification associated with focussing, the array output can now be written as

$$P = |A_0 + A_1 z + A_2 z^2 + A_3 z^3 + ... + A_{n-1} z^{n-1} + A_n z^n| \tag{3.9}$$

It can be seen then that when the array response is formulated according to the far field assumption, it can be written as a polynomial. This leads to Schelkunoff's first theorem, which states that *every linear array with commensurable separations between elements can be represented by a polynomial and every polynomial can be interpreted as a linear array.* It can be seen from equation 3.8 that ϕ is a function of θ, i.e. the angle between the array and any look direction. ϕ is a real valued function, so that the absolute value of z is equal to 1, implying that z always lies on the circumference of a unit circle.

If the spacing between the elements is equal to $\lambda/2$ (where λ is the sound wavelength) then the range of z is equal to 2π, and as θ, the look direction, changes from 0° to 180°, z describes one complete circle. In this case there is a one to one relationship between points on the circumference of the unit circle and directions in space. If the separation between the elements is less than

$\lambda/2$, z describes a semi-circumference. So, depending on the element spacing and the source frequency, regions of space correspond to different regions of the circumference of the unit circle.

Consideration of the fact that the product of two polynomials is a polynomial leads to Schelkunoff's second theorem, which states that *there exists a linear array with a directivity (or space factor) equal to the product of the directivities of any two linear arrays.* An example can illustrate this point. Consider the two element array whose directivity is given by

$$P_1 = |1 + z| \tag{3.10}$$

multiplying this directivity by itself gives

$$P_2 = |1 + z|^2 = |1 + 2z + z^2| \tag{3.11}$$

which is a three element array with transducer magnitudes of 1,2 and 1. From theorem 2 it can be said that in a direction where P_1 has a sensitivity of $\frac{1}{2}$, P_2 will have a sensitivity of $\frac{1}{4}$.This shows that the microphone signals of an array can be weighted such as to modify the directivity pattern, and the relationships between these weight distributions and the resulting directivities can be known through the knowledge of the directivity pattern of the equivalent array to which these weights correspond.

Now consider a pair of transducer signals of amplitude 1, $-t$

$$P = |z - t| \tag{3.12}$$

The complex number $z - t$ represents a line from z to t, so the sensitivity of the two element system in the direcion z is given by the length of the line zt. For the sensitivity to be zero in any direction, the null of the polynomial $|z-t|$ must be in the range of z and must be on the circumference of the unit circle.

Now, any polynomial of degree $(n-1)$ has $(n-1)$ roots and can be factorised into $(n-1)$ binomials, thus the sensitivity given in equation 3.9 can be written as

$$P = |(z - t_1)(z - t_2).....(z - t_{n-1})| \tag{3.13}$$

Each of these binomials represents the directivity of a two element array, which leads to Schelkunoff's third theorem which states that *the directivity of a linear array of n elements is the product of the directivities of* $(n-1)$ *virtual couplets, with their null points at the zeros of* P.

The implication of Schelkunoff's work for acoustic receiving arrays is that the positions of the nulls of an array's directivity pattern can be chosen by generating a polynomial whose roots lie at the appropriate positions on the unit circle. The coefficients of this polynomial are then the weights which need to be applied to the elements of the array system in order to achieve the said null positions.

3.4 Application of Schelkunoff's theory

The applicability of Schelkunoff's theory to an acoustic array for both near and farfield formulations was examined using Matlab based models. Directivity patterns were generated in order to compare true array directivity (nearfield formulation) with the approximated directivity (Schelkunoff's farfield polynomial formulation), and, using these, the effect of sidelobe null specification on the nearfield model was assessed.

3.4.1 Directivity comparison

Near and far-field directivity patterns were generated through numerical imlementation of equations 3.9 and 3.4 . These are shown in figure 3.3 for a source frequency of $1kHz$.

The discrepancy between the models is due to the approximate nature of the farfield formulation. Schelkunoff represents the array sensitivity using a polynomial, whereas this is not actually the case. The true mathematical formulation for beamformer sensitivity is more complex than this (equation 3.4). There is good qualitative agreement between the models however, which means that effects which can be produced in the farfield model should be reproduce-

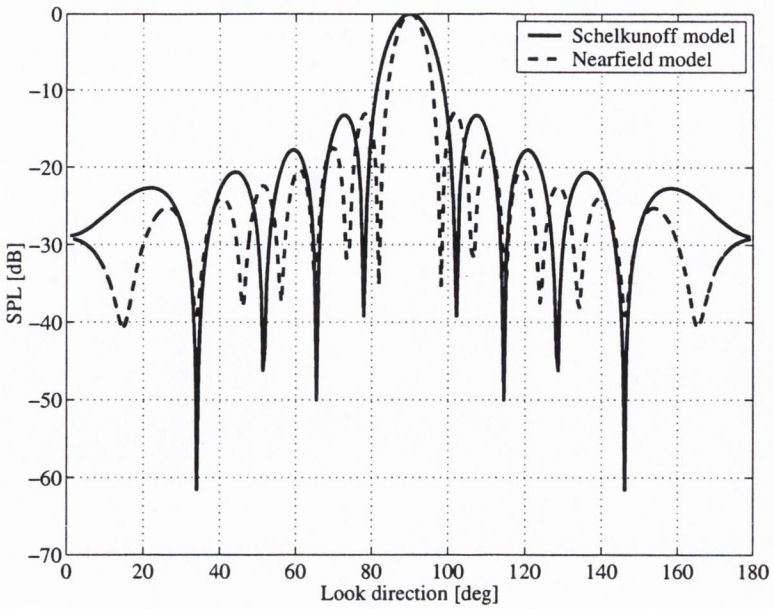

Figure 3.3: Near and farfield directivities

able, at least qualitatively, in the nearfield case. The following example was used to investigate this possibility. Consider a $3m$ linear array with thirty commensurably spaced elements taking measurements from a linear source region, parallel to the array axis, and at a distance of $7m$. The directivity for this sytem, according to Schelkunoff's model is shown in figure 3.4. The sidelobe nulls directly adjacent to the mainlobe are located at 78° and 102°.

Using the method described in the previous section the directivity can be manipulated in order to shift these nulls, and this can be done exactly. In this example, a decision is taken to move the nulls to 80° and 100°. Using these positions a polynomial is generated whose roots lie at these positions and the coefficients of this polynomial are the weights necessary to produce the desired effect. It is shown in figure 3.4 that the nulls are shifted to the locations specified. A side effect of this directivity manipulation is a reduction in mainlobe level and an increase in sidelobe levels. If the nulls are moved in the other direction, the side effects are reversed, i.e. the mainlobe level is increased and the sidelobe levels decreased. In order for this technique to be

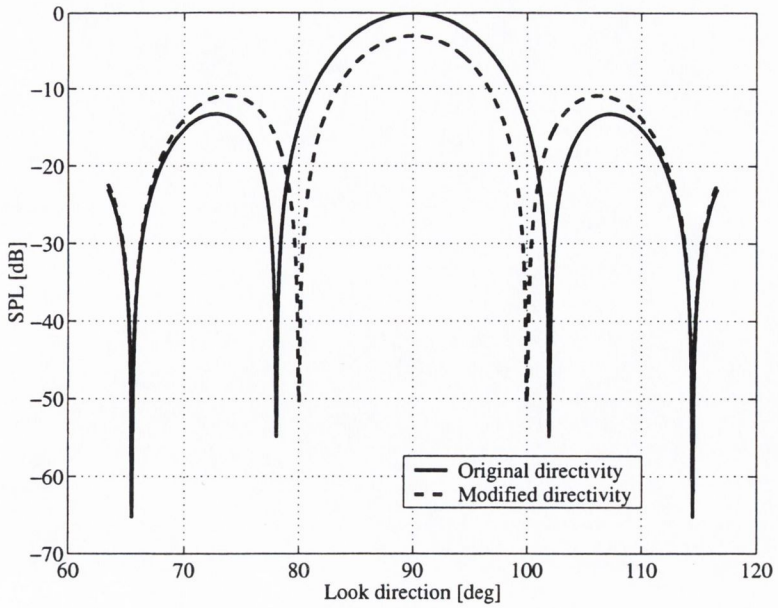

Figure 3.4: Farfield directivity manipulation

of benefit for an actual acoustic array, the effect on the nearfield model must be assessed, so, using the same test parameters the procedure was repeated using the nearfield formulation. Figure 3.5 shows the result.

It is clear that the same effect has been produced on the nearfield model. The sidelobes adjacent to the mainlobe have been shifted by approximately the same amount as was achieved using the farfield formulation, and a similar change is evident in both mainlobe and sidelobe levels. From this it is clear that the technique can be used effectively with a real array. Depending on the modification required, these numerical models can be used to identify an appropriate set of microphone weights.

3.5 A case study

To illustrate the need for optimising both array geometry and processing for specific applications, a real experimental campaign is here used as an example. The experiments are to be performed as part of a European project known as

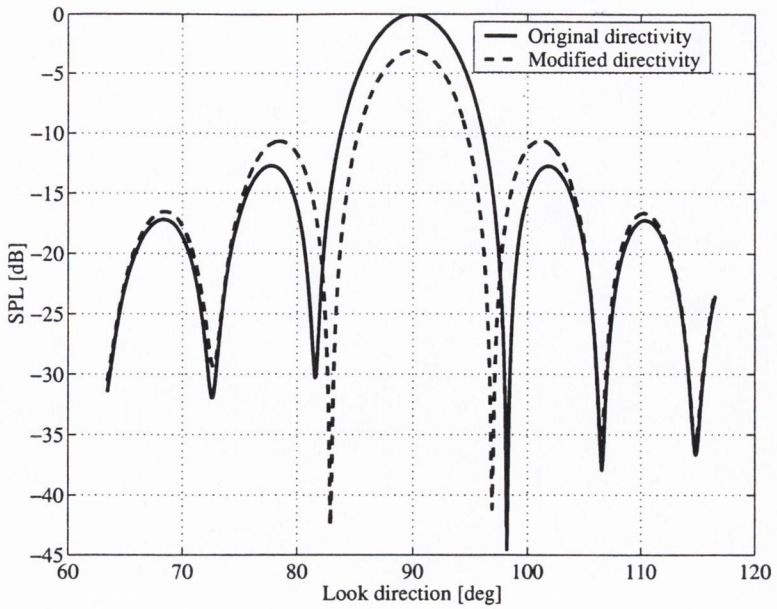

Figure 3.5: Nearfield directivity manipulation

APIAN (**A**dvanced **P**ropulsion **I**ntegration **A**erodynamics and **N**oise). The objective of this project is to study the aeroacoustics of installed high-speed propellers. A microphone array is to be used in these tests to identify the contribution to the overall sound field of a single propeller. This requires that contamination from the second propeller, as well as acoustic reflection from the fuselage, be minimised. Thus, as the major source of contamination in this case is the second propeller, the primary design criterion for the array is that the contribution of this propellers be entirely filtered out. It is not often the case in array applications where there are two such coherent sources of noise of similar orders of magnitude and frequency, and so, it is often sufficient to design an array with good gain characteristics and then not worry about sidelobe contamination. In this case however, as the source of contamination is at exactly the same frequency, and of similar strength, it is necessary to achieve a higher degree of attenuation. This can be achieved by ensuring that the second propeller lies in a region of the sensitivity pattern where attenuation is a maximum, i.e. a sidelobe trough. A number of optimum array geometries

were developed for this application based on test parameters such as model size, source frequency, array-source distance, and the relative strengths and weaknesses of each was assessed in order to choose the most suitable design.

3.5.1 Test set-up

The APIAN model geometry is shown in figures 3.6(a) and (b). The model has a wingspan of $3m$ and the propeller nacelles are separated by a distance of $1m$. This means that at the fundamental frequency, the array sensitivity pattern must be such that the distance between the mainlobe peak and the first sidelobe trough is roughly equal to $1m$. The propellers, which have a diameter of $0.5m$, are not shown in this diagram. The model is to be tested in the closed-loop open-section wind tunnel at DNW (the Dutch-German wind tunnel), and will be positioned as shown in figure 3.7. The DNW open-section facility has anechoic treatment which eliminates acoustic reflection. This means that sidelobes pointing away from the source region are of no concern. In view of this the directivity pattern of the array only needs to be considered in the region of the aircraft model. The model is approximately $5m$ from the wind tunnel nozzle and at a height of $3m$. Acoustic measurements will be taken using an out-of-flow microphone array positioned immediately below the wind tunnel nozzle. At this point the array is a close as possible, in terms of angle, to the propeller axis and will give a measure of the sound radiated in the forward direction. This position gives a source-array distance of approximately $7m$. If this distance is known, and the positions of the main sources of noise are known (i.e. the propellers) an array geometry can be chosen with an aperture such that one of the propellers lies in the trough of a sidelobe for the frequency of interest. For these particular tests the rotational speed of the propellers is $8000rpm$, which for a six bladed propeller corresponds to a fundamental or blade-pass frequency of $800Hz$. A variety of array geometries are now considered and the relative merits of each are assessed.

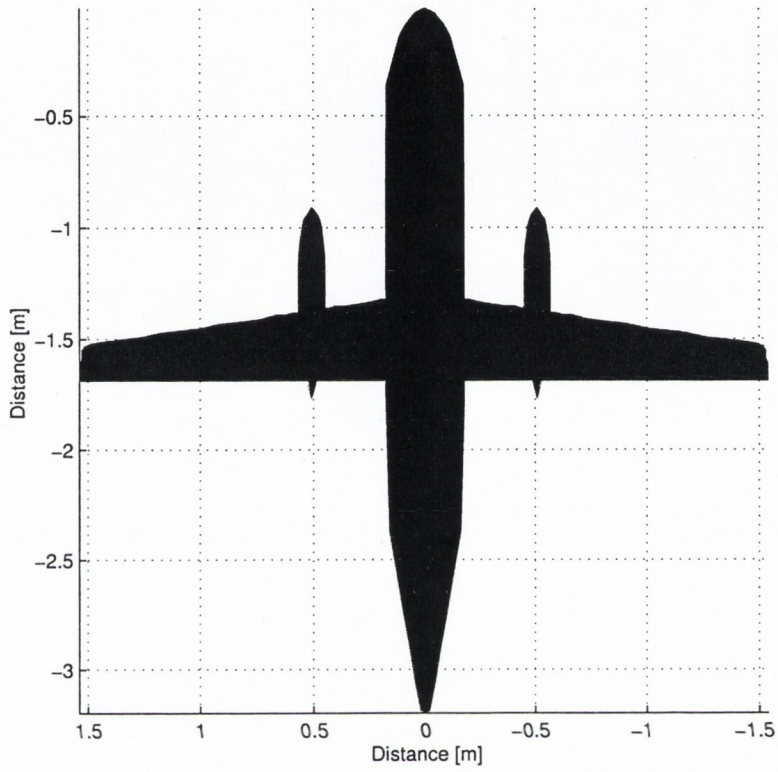

(a)

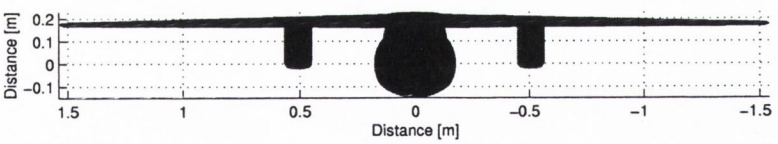

(b)

Figure 3.6: Apian model geometry

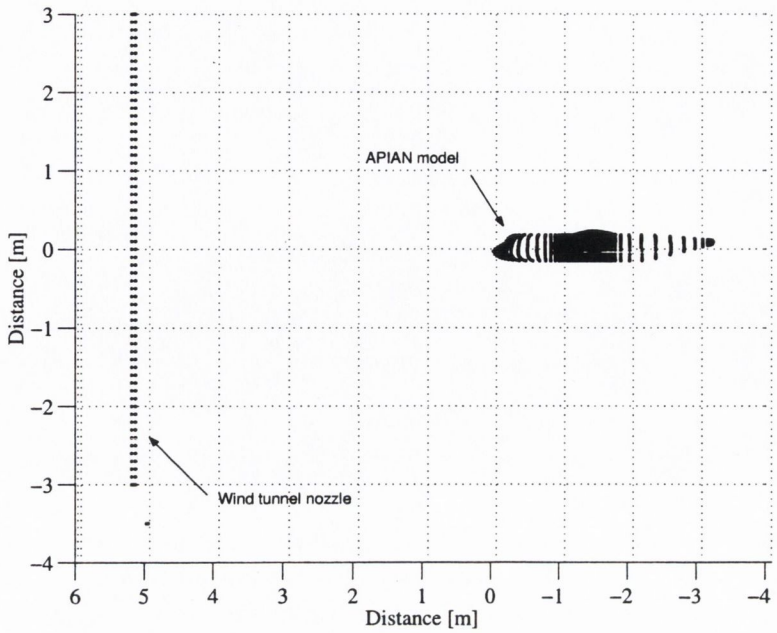

(*a*) Elevation

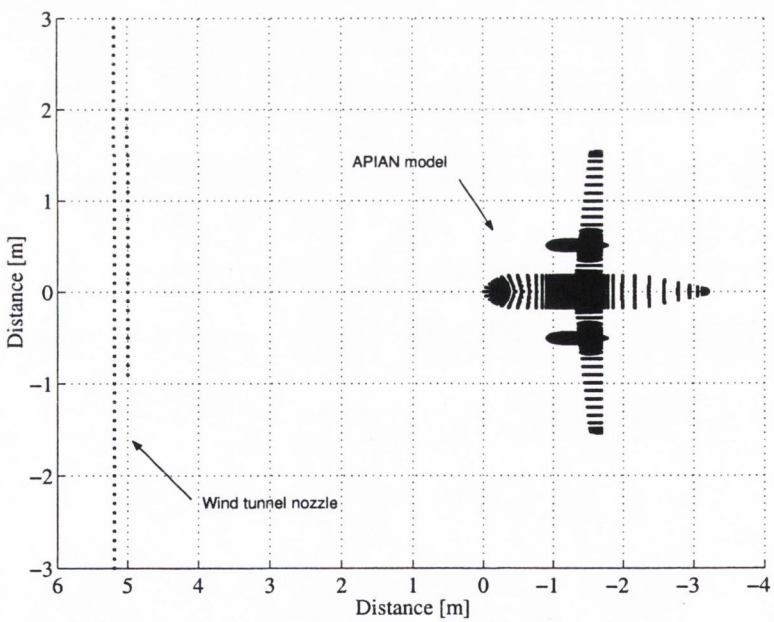

(*b*) Plan

Figure 3.7: Experimental setup

3.5.2 The linear array

A linear microphone array gives good spatial discrimination along an axis parallel to its own axis, in other words, it can not spatially filter along axes perpendicular to its own. Thus for a horizontal linear array the sensitivity pattern is a function of horizontal distance only. As the source distribution in the APIAN case is approximately linear, a linear array is an appropriate design. The setup showing a linear array is shown in figure 3.8(a). For a fundamental frequency of $800Hz$ the optimum array length is $3m$. At this length, the right hand propeller lies in a region of the sensitivity pattern where the attenuation is of the order of $-28dB$. This is shown in figure 3.8(b).

3.5.3 The cross array

The second array design considered for these experiments was a cross array, which gives better discrimination for a planar source region. An optimum cross array for the APIAN setup is one with a length of $4m$ (this is the distance from the tip of one arm to the tip of its opposite member). This setup is shown in figure 3.9(a). It can be seen that the array is physically very large, in fact it is obstructed by the wind tunnel nozzle. The sensitivity pattern for this array is shown in figure 3.9(b). Good attenuation is again achieved on the right hand propeller, and a certain amount of vertical discrimination also results. This is manifest in the improved attenuation seen in certain regions of the fuselage. This design gives a better sensitivity pattern in terms of better attenuation on the model fuselage, but the size of the array poses a problem.

3.5.4 The circular array

Another possible geometry is the circular array, and it is found that for this case the optimum geometry consists of a $2.5m$ diameter circular arrangement, shown in figure 3.10(a). The sensitivity pattern for this array is shown in figure 3.10(b), where again it can be seen to give good attenuation on the right

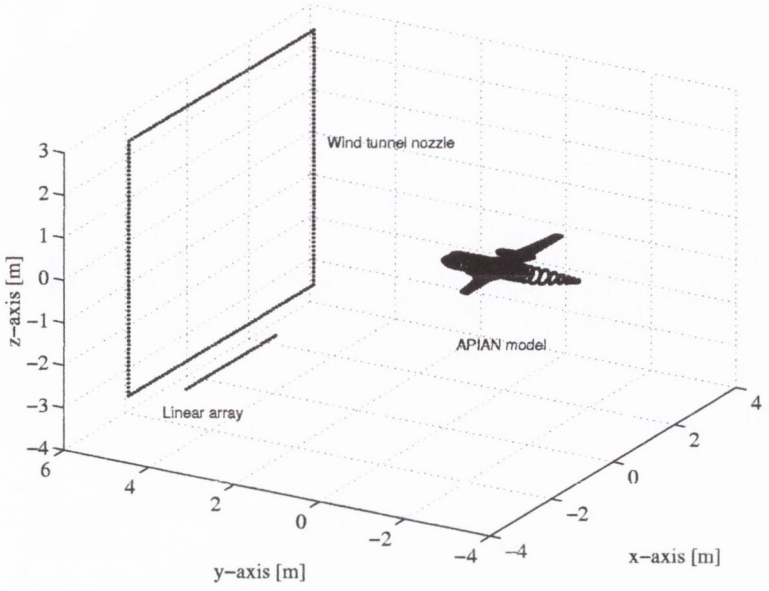

(a)

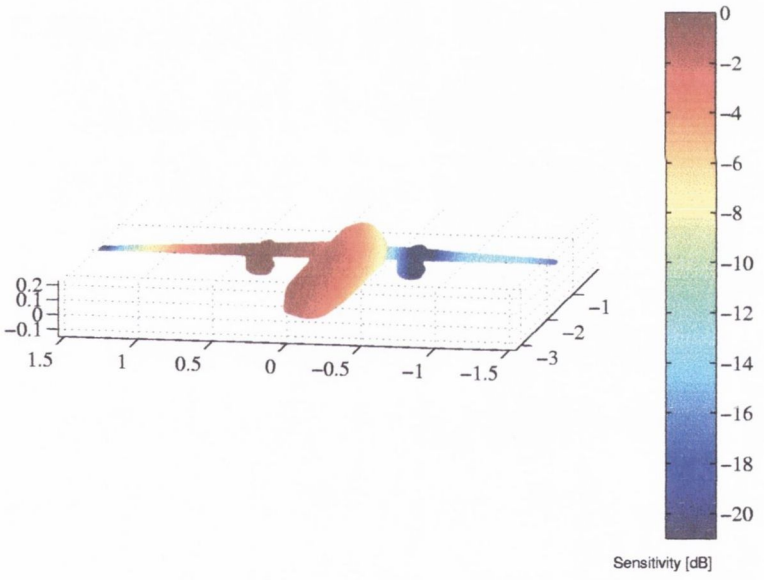

(b)

Figure 3.8: Linear array setup and directivity

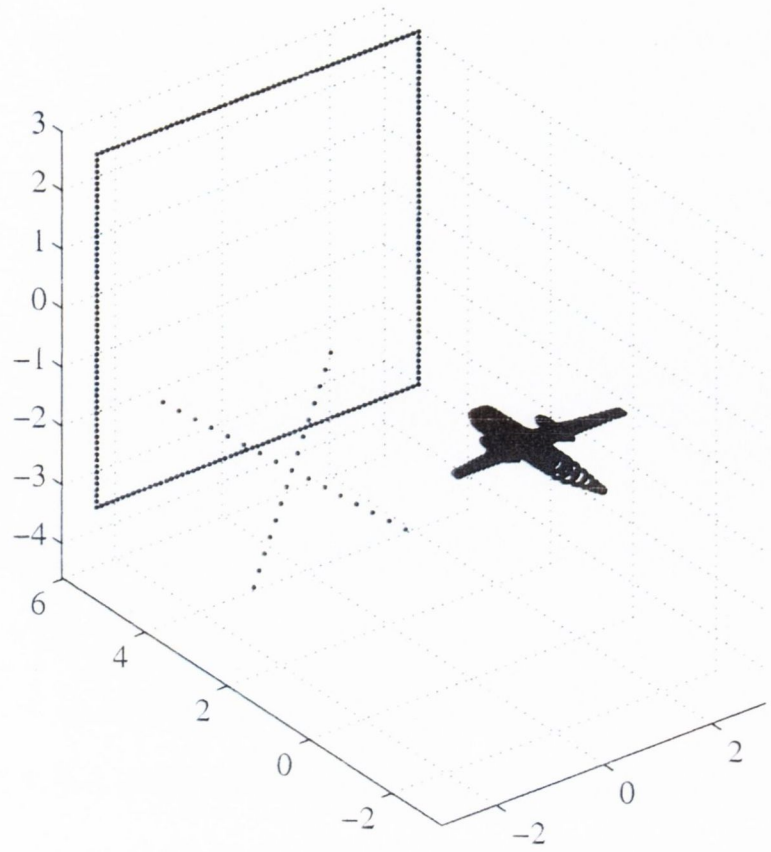

(a)

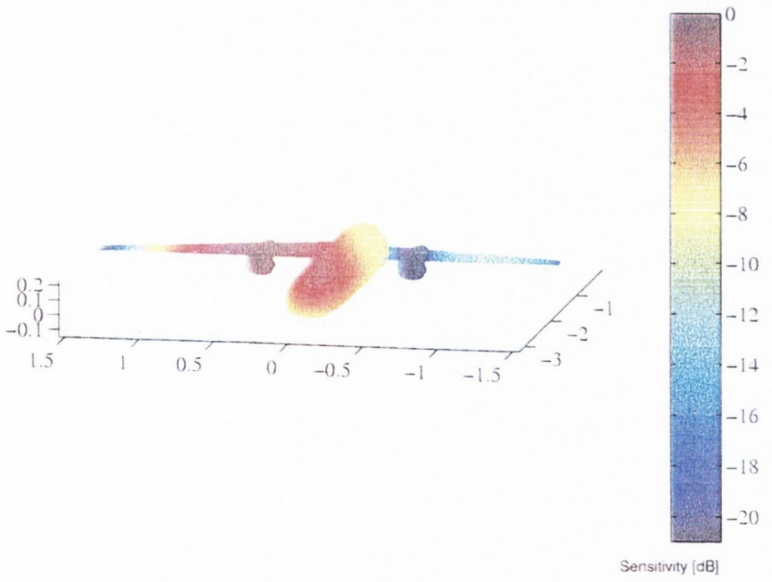

(b)

Figure 3.9: Cross array setup and directivity

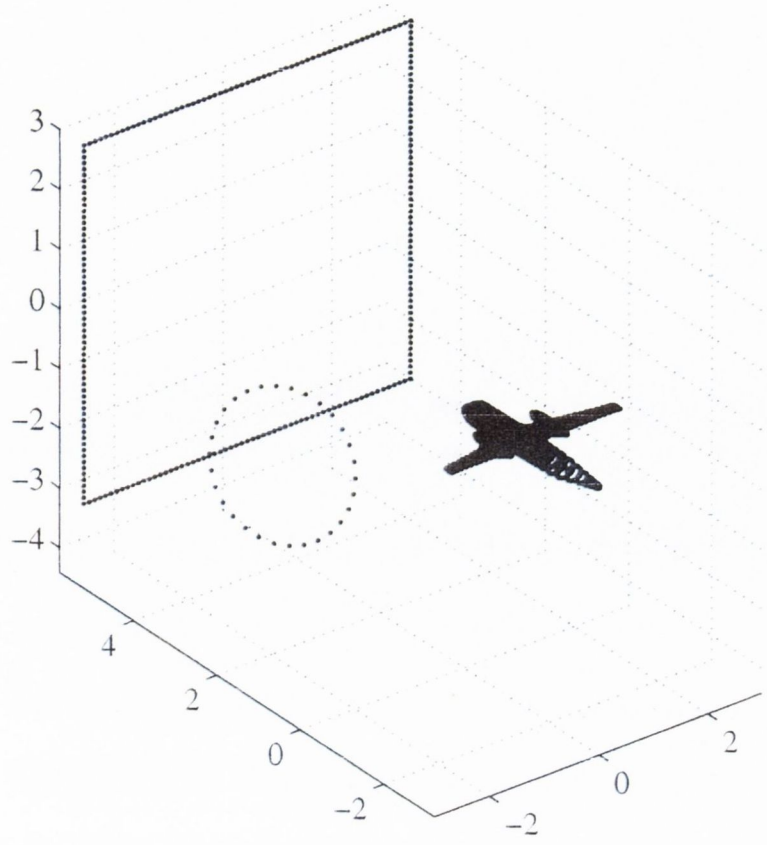

(a)

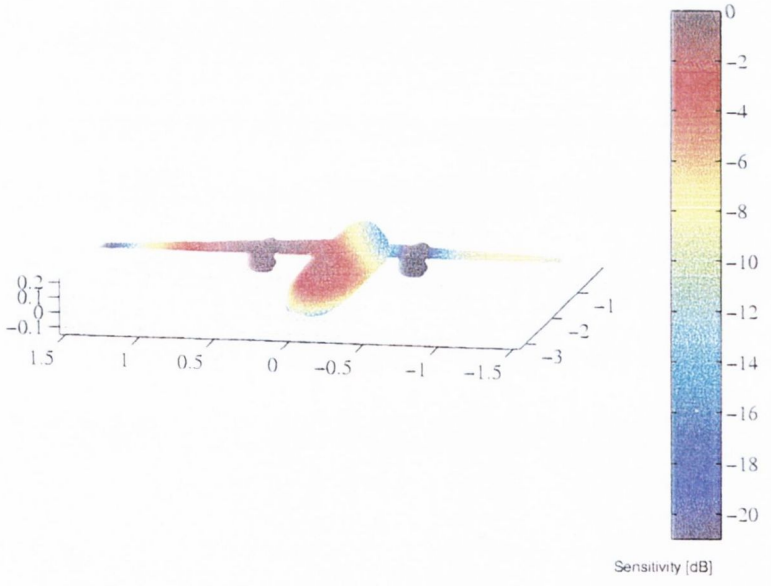

(b)

Figure 3.10: Circular array setup and directivity

hand propeller. As was the case with the cross array, this array geometry provides a degree of vertical discrimination, again showing better attenuation on regions of the fuselage than can be achieved with a linear array. However, as was the case with the cross array, it is physically too large.

3.6 Discussion

The previous section illustrated the performance potential of a number of different array geometries. The purpose of this discussion is to illustrate the process whereby an optimum array can be chosen based on its performance characteristics with respect to a specific system.

It can be seen in each case that an optimum array size can be chosen so as to ensure that the right hand propeller lies in a region of high attenuation. However, a difficulty with these planar designs becomes clear as focussing is attempted at frequencies other than the fundamental. In these cases the side-lobes will move, causing the amount of attenuation at the right hand propeller to change. This means that measurement at frequencies other than the fundamental will be prone to varying degrees of contamination. In the case of the linear array however, through application of the technique described earlier in this chapter the sensitivity pattern can be manipulated so as to ensure that the propeller remains in a region of high attenuation. This is illustrated by changing the measurement frequency to $600Hz$ and observing the change in array sensitivity. The result is shown in figure 3.11. It is clear from this that the beamformer is no longer performing at its optimum. The attenuation on the second propeller has now changed from $-28dB$ to $-9dB$. This will result in considerable contamination of the measurement. Another consequence of this change in array sensitivity is that measurements taken at the two different frequencies will not be comparable, due to the varying degrees of contamination. Using the null specification technique based on Schelkunoff's theory of

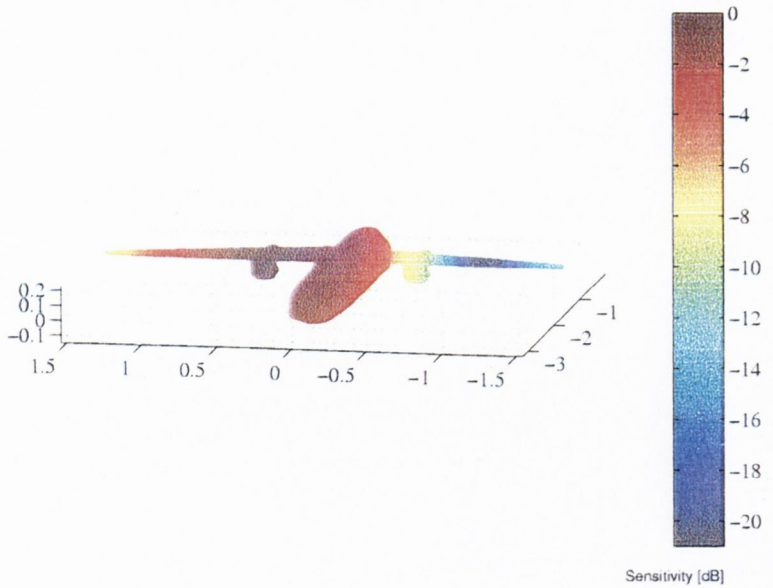

Figure 3.11: Array sensitivity for 600Hz

the second propeller has now changed from $-28dB$ to $-9dB$. This will result in considerable contamination of the measurement. Another consequence of this change in array sensitivity is that measurements taken at the two different frequencies will not be comparable, due to the varying degrees of contamination. Using the null specification technique based on Schelkunoff's theory of arrays, the sensitivity pattern can be manipulated in order to re-optimise the array system. A simplified representation of the directivity pattern is shown in figure 3.12. For the system setup the propeller being measured is located at 90° and the second propeller at 98°, indicated by the dashed line. From figure 3.12 the maximum attenuation is shown at 101°, so a modification of 3° is required in order to re-optimise the array. The directivity as represented by Schelkunoff's approximation is shown in figure 3.13. Because of the discrepancy between the two formulations it is not possible to give the actual location of the second propeller for null specification. However, the amount of modification required is known, and so an appropriate null location can be chosen. The best result is given when a modification of 4° is specified. The resulting changes in both directivies are shown in figures 3.14 and 3.15. The

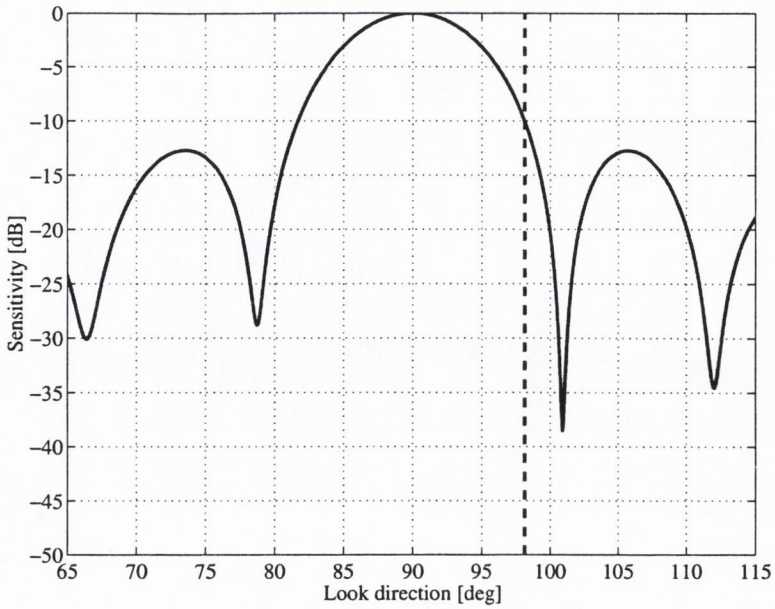

Figure 3.12: Nearfield array sensitivity for 600Hz

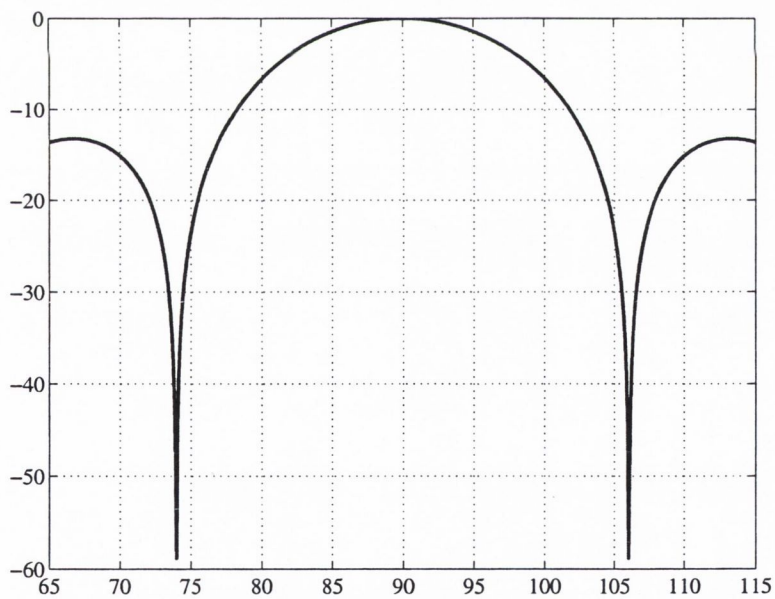

Figure 3.13: Farfield array sensitivity for 600Hz

that the array has been sucessfully optimised for operation at $600Hz$. In this case the increased sidelobe levels are not a problem as there are no sources of sound at these locations. The attenuation at the second propeller is now of the order of $-28dB$, an improvement of $19dB$.

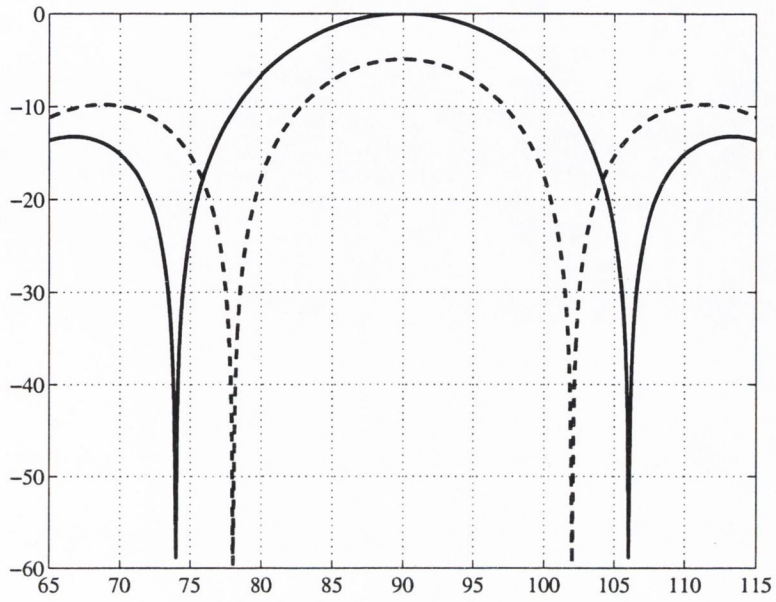

Figure 3.14: Modified farfield array sensitivity for 600Hz

3.7 Conclusion

The foregoing discussion illustrates how a microphone array can be customised in order to suit the characteristics of the system it is being used to analyse. In the case of the APIAN experiments the source region is approximately linear and so the superior performance of the cross and circular arrays, in terms of their two-dimensional discrimination capabilities, could be considered an overdesign. However, in considering directivity manipulation, the linear array is ideally suited to this application because of the control possible using the technique of Schelkunoff. Using this technique it has been shown how the sensitivity of the linear array can be controlled in order to ensure that the second

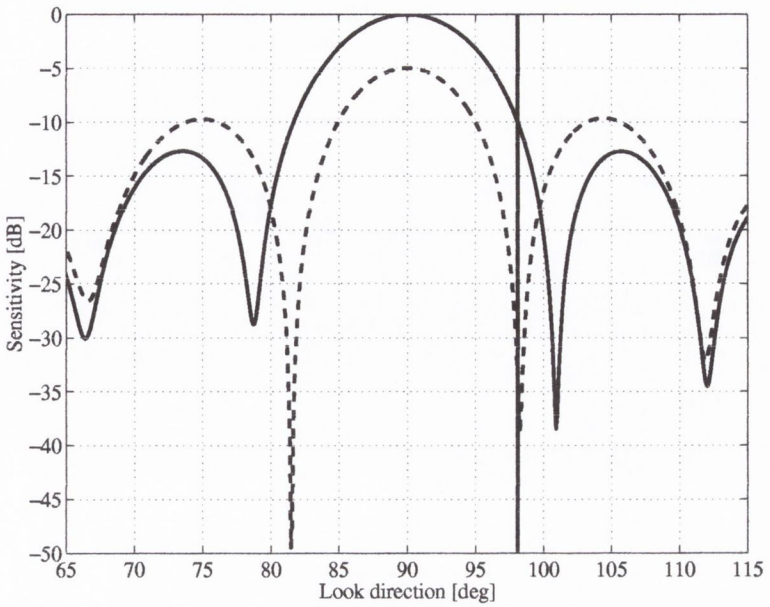

Figure 3.15: Modified nearfield array sensitivity for 600Hz

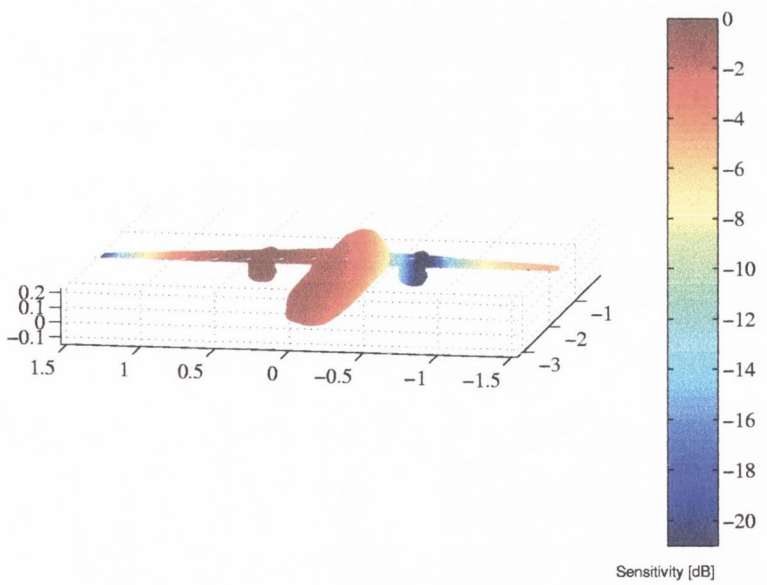

Figure 3.16: Modified farfield array sensitivity for 600Hz

propeller always lies in a region of high attenuation, and so, measurements can be taken from the propeller of interest in the confidence that contamination from the other propeller is minimised.

Before a system is analysed using an array, an initial study must be performed which identifies the significant parameters with respect to array response. These parameters include, the dominant source frequencies, the geometry of the system, the distance at which the array will be positioned relative to the source, and the estimated source distribution. Using these parameters, response characteristics for the array can be calculated, and thus an optimum design developed.

Chapter 4

Application to aeroacoustics

4.1 Introduction

The far-field characteristics of an aeroacoustic system depend on the aerodynamic source mechanisms and the manner by which they interact. It is important to identify these mechanisms, so that their individual contributions to the acoustic far-field can be assessed. There are three fundamental aeroacoustic sources each of which corresponds to a different physical mechanism. These are the *monopole*, the *dipole* and the *quadrupole*. The acoustic field of an aerodynamic system is a result of the interaction of these three sources, and so, any aeroacoustic analysis requires that they be well understood.

4.1.1 The monopole

The simplest aeroacoustic source is the *monopole*, which can be thought of as a small sphere of fluid, radius a_m, whose volume V_o fluctuates, as shown in figure 4.1. Its rate of change of volume, $dV_o/dt = \dot{V}_o$, is called its strength, and if U_m is the radial velocity of the surface of the sphere, then $\dot{V}_o = 4\pi a_m^2 U_m$. The motion of the boundary induces outgoing waves in the surrounding fluid, symmetrical about the sphere, and the pressure in this outgoing wave is

$$p_M(t;\mathbf{x}) = \frac{\rho_o}{4\pi x}\frac{\dot{V}_o^*}{dt} = \frac{\rho_o a_m^2}{x}\frac{dU_m^*}{dt} \tag{4.1}$$

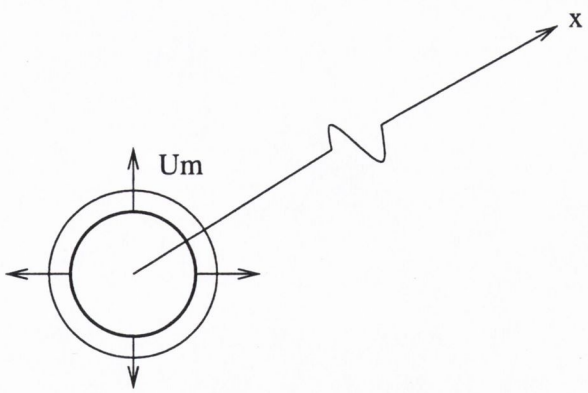

Figure 4.1: The monopole

where ρ_o is the density of the undisturbed medium and c is its sound speed. Due to the finite length of time required for propagation of the sound field, the pressure $p(x,t)$ at the point x is generated by the motion at the origin at a time x/c earlier, i.e. at time $(t - x/c)$ which is indicated by the operator $(t)^*$. The monopole is associated with volumetric displacement of the sonic medium. The blades of a propeller for example cause periodic volumetric displacement of the surrounding fluid as they turn, thus generating monopole sound.

4.1.2 The dipole

The *dipole* source is the second type of fundamental aeroacoustic source and can be constructed from a pair of point monopoles of opposite sign and a very small distance y apart, shown in figure 4.2. In the far field there would be total cancellation if it were not for a difference in the time delay. Because signals arriving at x at the same instant must leave at times $\delta t = (y\cos\theta)/c$ apart, the time-varying source velocities differ by an amount $\delta t.d/dt.(dU_m/dt)$. Consequently, the net sound pressure in the far field at x is

$$p_D(t;\mathbf{x}) = \frac{y\cos\theta}{c}\frac{dp_M}{dt} = \frac{\rho_o a_m^2}{x}\left(\frac{y\cos\theta}{c}\right)\frac{d^2U_m^*}{dt^2} \tag{4.2}$$

It is zero on the plane where points are exactly equidistant from each of the constituent sources, and of opposite sign on the two sides of it. This source

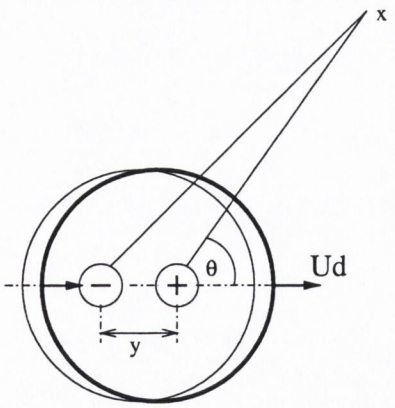

Figure 4.2: The dipole

can be thought of as a sphere which oscillates in the y-direction with velocity U_d. The component of velocity in the x-direction of the local velocity of a point fixed on the sphere is $U_{d,x} = U_d \cos\theta$, and in terms of this

$$p_D(t;\mathbf{x}) = \frac{\rho_o a_d^2}{x}\left(\frac{a_d}{2c}\right)\frac{d^2 U^*_{d,v}}{dt^2} \tag{4.3}$$

The sphere could be made to oscillate because of a force F acting on it in the y-direction. This force is $F = (3/2)(4/3)\rho_o \pi a_d^3 . dU/dt$, where the extra $(3/2)$ accounts for the additional "virtual" mass of the sphere, due to the inertia of the surrounding fluid set into motion. The dipole pressure field can then be written as

$$p_D(t;\mathbf{x}) = \frac{1}{4\pi x}\frac{1}{c}\frac{dF^*_x}{dt} \tag{4.4}$$

where F_x is the component of force in the x-direction, $F_x = F\cos\theta$.

It is in this form that the dipole can be seen to represent the generation of sound by aerodynamic forces. Again a propeller is a good example, the aerodynamic thrust generated by the blades generates dipole sound.

While the disturbance caused by motion of the sphere of the monopole was constrained to move radially, the greater degree of freedom for the dipole results in most of the disturbance oscillating directly between areas of the spherical surface moving in opposite directions, in circular paths. Thus the

dipole is not as efficient at driving the far field as the monopole. These circular paths are the same as would be induced by a small vortex ring, and form the basis of the theory of aerodynamic sound generation by vorticity.

4.1.3 The quadrupole

The third and final fundamental aeroacoustic source is known as the *quadrupole* and can be constructed by combining two point dipoles of opposite sign, a very small distance z apart, shown in figure 4.3.

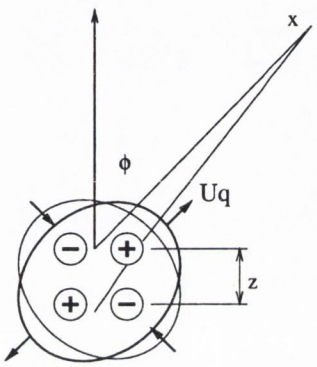

Figure 4.3: The quadrupole

The pressure field of a quadrupole is given by

$$p_Q(t;\mathbf{x}) = \frac{x\cos\theta}{c}\frac{dp_D}{dt} = \frac{\rho_o a_m^2}{x}\left(\frac{z\cos\phi}{c}\frac{y\cos\theta}{c}\right)\frac{d^3U_m^*}{dt^3} \tag{4.5}$$

In terms of the velocity $U_{q,x}$ in the direction of x of a point on the sphere of radius a_q, the pressure can be written as

$$p_Q(t;\mathbf{x}) = \frac{\rho_o a_q^2}{x}\left(\frac{a_q}{3c}\right)^2\frac{d^3U_{q,x}}{dt^3} \tag{4.6}$$

with $U_{q,x} = U_q\cos\phi\cos\theta$. The fluid near the sphere has a greater degree of freedom, and so is even less efficient at driving the far field than the dipole. It can be seen that with the quadrupole source there is no fluctuation of volume of the sphere, as for the monopole, nor is there any resultant force, as for the dipole. For the quadrupole an elliptical distortion of the sphere is the

cause of radiation and this motion is associated with aerodynamic turbulence. One variation of the quadrupole is where the four poles are colinear, in this configuration the source is known as a line quadrupole and it exhibits the same basic characteristics as the lateral quadrupole.

4.1.4 Summary of source characteristics

This analysis illustrates clearly the relationship between the fundamental components of an aeroacoustic system and the associated aerodynamic phenomena. These relationships can be summarised as follows.

- The volumetric fluctuation of the monopole is associated with the volumetric displacement of a fluid by a solid body, such as the periodic displacement of air by a rotating propeller blade.
- The fluctuating force of a dipole is related to unsteady aerodynamic loading, such as the blade loading associated with propellers.
- The elliptical distortion of a quadrupole is related to the fluid dynamics of turbulence.

Each of these sources has its own distinctive radiation characteristics. The most efficient radiator is the monopole, due to the radial motion of the imaginary sphere of fluid. This is followed by the dipole, the efficiency of which is decreased due to the extra degree of freedom evident on the surface of the sphere. The quadrupole's efficiency is decreased once again, as a result of yet another degree of freedom. These extra degrees of freedom cause more energy to be expended in the aerodynamic near field, leaving less energy for driving the acoustic far-field.

Another important property of these sources is the relationship between their sound intensity and the local fluid velocity.

- Monopole intensity varies with the fourth power of velocity.

- Dipole intensity varies with the sixth power of velocity.
- Quadrupole intensity varies with the eight power of velocity.

Depending then on the aerodynamic system under consideration, the dominance of each of the sources will vary. With relatively low speed systems, such as propeller driven aircraft, the dominant sources are monopole and dipole, where, as well as low fluid velocity, there are very obvious periodic volumetric and force fluctuations. In jet or rocket propelled aircraft however, due to the higher velocities involved and the absence of periodic solid body interaction in the free field, the dominant source is quadrupole.

4.2 Source identification in aeroacoustics

The complexity of an aeroacoustic system is due to the fact that often the basic sources all combine to generate the resultant acoustic field, and so a single sound measurement taken from such a system usually consists of a superposition of these three source types. In order to develop a more comprehensive understanding of the fundamental aeroacoustic phenomena, a more detailed analysis is necessary, in which the system can be broken down into a collection of simpler component models which can then be examined in isolation. In this way source estimates can be made which lead to the development of better global source-models. The distinctive characteristics of the individual source components provide a basis for the development of these component models, and, combined with spectral analysis, a framework for more sophisticated analysis methodologies. Whereas spectral analysis separates sources according to frequency, beamforming separates acoustic energy based on spatial location and so a combination of the two constitutes a more powerful experimental tool. However, the standard beamformer is fully efficient only when the source region is constituted of monopole sources. When the source region begins to exhibit non-monopole type propagation, the beamformer is liable to generate

data which may be easily misinterpreted. In order to illustrate this, the effect of both monopole and dipole sources on a standard beamformer are now examined using numerical models, which are later validated and further assessed in an experimental environment.

4.2.1 The monopole source

The monopole mechanism described earlier (see figure 4.1) causes omnidirectional radiation of *spherical* waves into the local sonic medium. Thus, all acoustic energy generated at the source at a given time propagates equally in all directions. When this energy reaches a microphone array the sound pressure distribution shown in figure 4.4 results (this is for a single monopole source located c). The sound

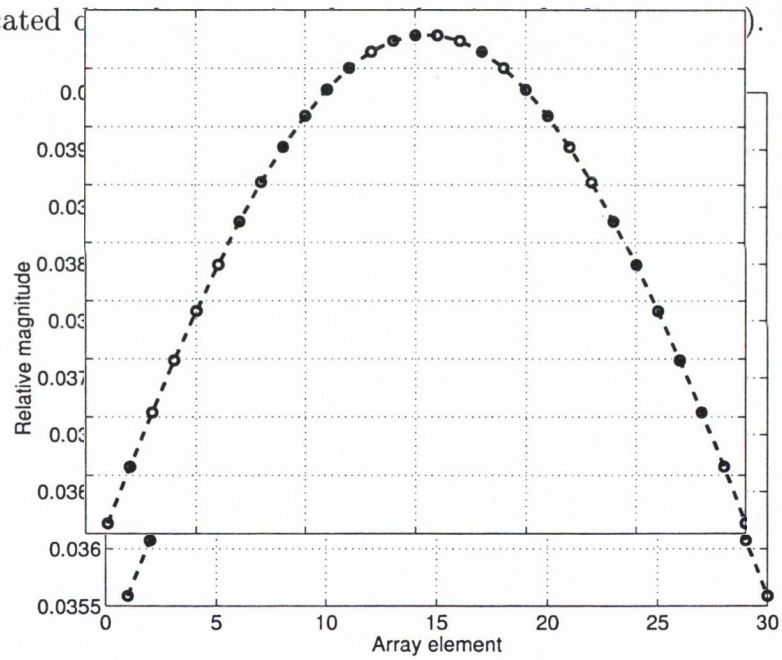

Figure 4.4: Sound pressure magnitudes on array for a monopole source

pressure is a maximum at the centre of the array because the microphones here are closer to the source, and a minimum at the array extremities where the microphones are furthest from the source. This is due to the inverse relationship between sound pressure magnitude and distance from the source.

The phase distributions across the array before and after weighting are shown in figure 4.5. It can be seen here that prior to phase-weighting the phases

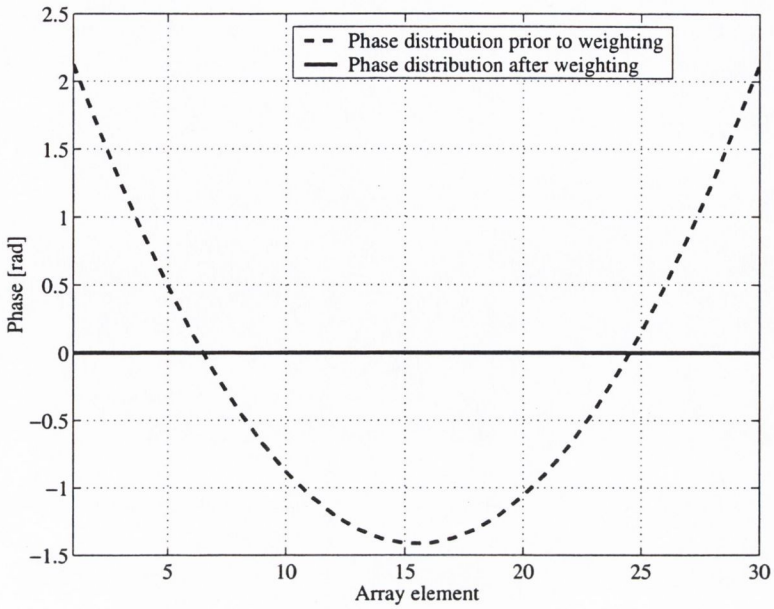

Figure 4.5: Monopole phase distributions before and after weighting

of the individual signals are misaligned, due to the different distances from the source to each of the microphones. After weighting however, due to the omnidirectional nature of the monopole, the phases are all aligned, so that summation will yield a maximum of constructive interference. It can be seen from this that the beamformer is best equipped for measurement of sources which exhibit omnidirectionality. For directional sources, where waves propagate in different directions with different phase, it is clear that the phase weighting used in standard beamforming will not be effective in aligning, and so any measure of the source strength is likely to be in error. The directivity corresponding to a monopole source is shown in figure 4.6. Due to the constructive interference which occurs when the beamformer is focused on the source, a maximum is measured. For all other positions in the source region the measurement is attenuated, due to varying degress of destructive interference when the signals are summed.

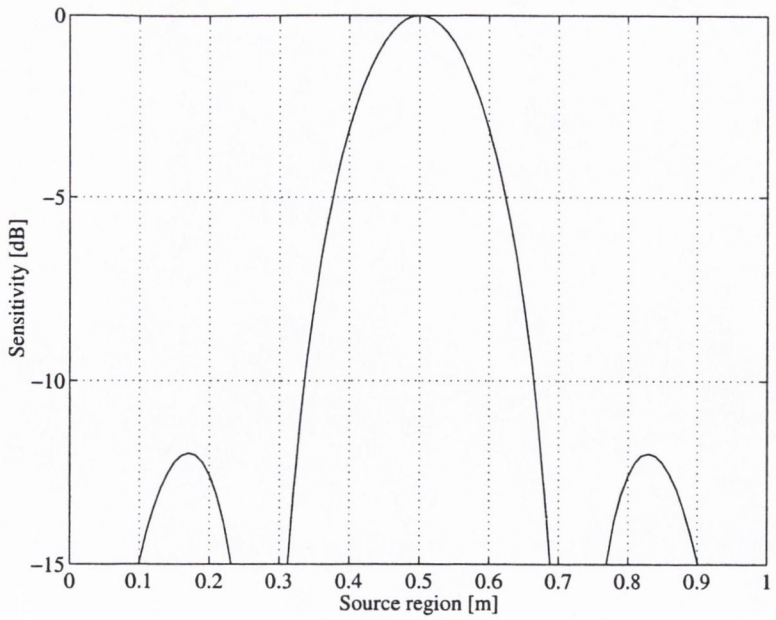

Figure 4.6: Monopole directivity

4.2.2 The dipole source

Considering the physical significance of the mathematical expression for a dipole as given by equation 4.2 (shown below as equation 4.7),

$$p_D(t;x) = \frac{y\cos\theta}{c}\frac{dp_M}{dt} = \frac{\rho_o a_m^2}{x}\left(\frac{y\cos\theta}{c}\right)\frac{d^2U_m^*}{dt^2} \tag{4.7}$$

the acoustic field of a point dipole can be thought of as follows. A dipole can be considered as a system where two adjacent volumes of fluid (modelled as points) fluctuate alternately, and so are 180° out of phase with one another, as illustrated in figure 4.7. Each consecutive pulse generates a pressure disturbance (a sound wave) which propagates spherically into space. Because the sound waves are being generated perfectly out of phase, there exists a planar region between the two poles and perpendicular to the dipole axis (shown in two dimensions in figure 4.7 as the axis of total cancellation), where sound waves from the two poles combine to achieve complete destructive interference. This is the same as saying that the null is due to the difference in propagation delay from each of the poles. An observer in the plane of total

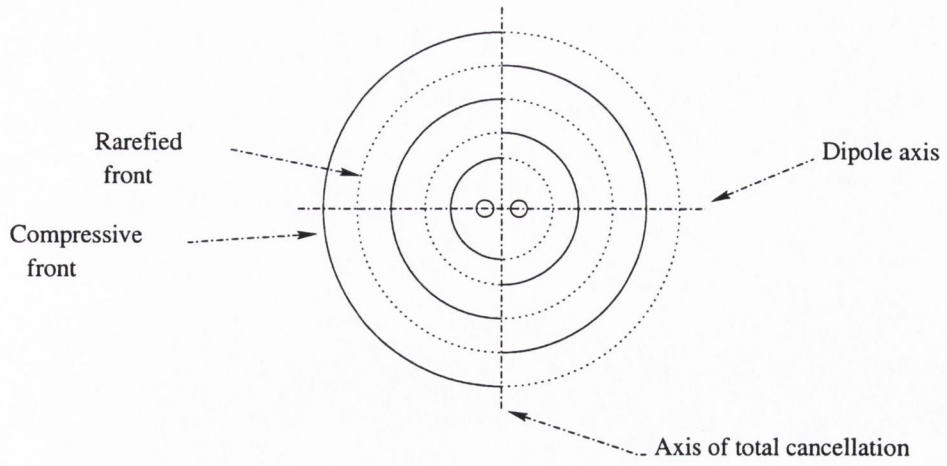

Figure 4.7: Sound pressure field of a dipole

cancellation will hear no sound. As the observer moves around the dipole this cancellation becomes less efficient, until a point is reached on the dipole axis where there is no cancellation and the sound pressure observed is a maximum. In this region the sound pressure is the same as would be found if the second pole did not exist (a monopole). As an observer moves around the dipole, at a constant radius, the change in cancellation efficiency gives rise to a gradual increase in sound pressure as the dipole axis is approached. This is illustrated in figure 4.8. It is assumed that the distance between the poles of a dipole is small compared with a wavelength so that the net result of this gradual cancellation is a single spherically propagating sound wave with the unusual characteristic of two hemispheres which are 180° out of phase. In addition to this, the sound pressure amplitude around the sphere varies with $\cos\theta$ (due to cancellation), according to equation 4.7. Figure 4.8 shows a two dimensional polar plot of absolute sound pressure. The far-field acoustic properities of the dipole are dependent on $\cos\theta$, and so the expression for the acoustic field of a monochromatic dipole can be simplified and written as

$$P(x,\theta,k) = \frac{-B}{x}\cos\theta e^{jkr} \tag{4.8}$$

where $k = \omega/c$ is the wavenumber, B the sound pressure magnitude and ω the sound frequency in radians. Using this expression a far field radiation pattern

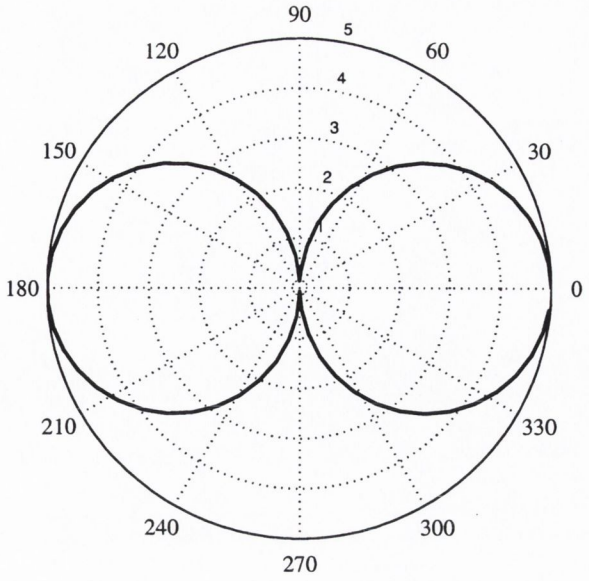

Figure 4.8: Polar Pressure Distribution of a Dipole

for a dipole was generated using Matlab code. A polar plot of absolute pressure generated by this simulation is shown in figure 4.8. Using this acoustic field, signals corresponding to a linear array of thirty microphones arranged parallel to the dipole axis and at a distance D were generated, these are shown in figures 4.9 and 4.10.

Figure 4.9 shows the magnitude of sound pressure measured by each of the microphones for the dipole. It can be seen that the pressure is a maximum towards the outer edge of the array where the microphones are closer (in terms of angle) to the dipole axis. Comparison with figure 4.4, which shows a similar sound pressure distribution for a monopole, illustrates very different signatures for the two kinds of source. In the presence of a dipole, the microphones towards the centre are closer to the region of complete cancellation and so measure much lower sound pressure. Figure 4.10 shows 10 fully reconstructed signals. Here it can be seen that there is variation in both pressure amplitude and phase across the array.

If the orientation of the dipole is changed the microphone signals will

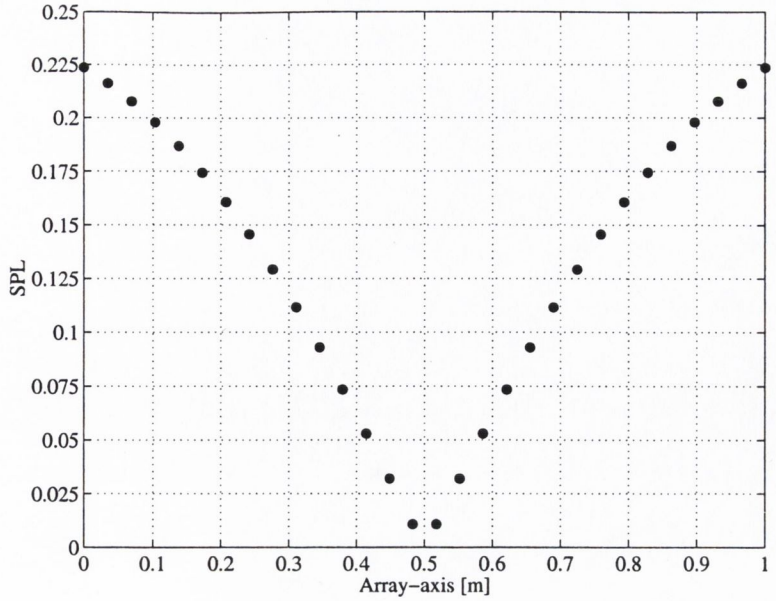

Figure 4.9: Sound pressure magnitude distribution on array for dipole source

change accordingly, as seen in figures 4.11 and 4.12. It can be seen that as the dipole is rotated, the far-field radiation pattern changes significantly. It is necessary to examine how this information can be best utilised in order to identify the location, orientation and strength of a dipole source.

4.3 Beamforming for a dipole source

Ordinarily, when source localisation is necessary, a beamformer can be used to perform a sweep of the region of interest in order to identify the source. On the application of an ordinary beamformer to a point dipole source however it was found that the source is not identified. In fact the beamformer measures zero sound pressure at the source location. Figures 4.6 and 4.13 show directivity patterns for monopole and dipole sources respectively.

It is clear from this that ordinary beamforming is insufficient for the measurement of dipole sources. The dipole directivity pattern does however give an indication as to how one might proceed in the development of a dipole location technique, that indicator is the null seen at the source origin (fig-

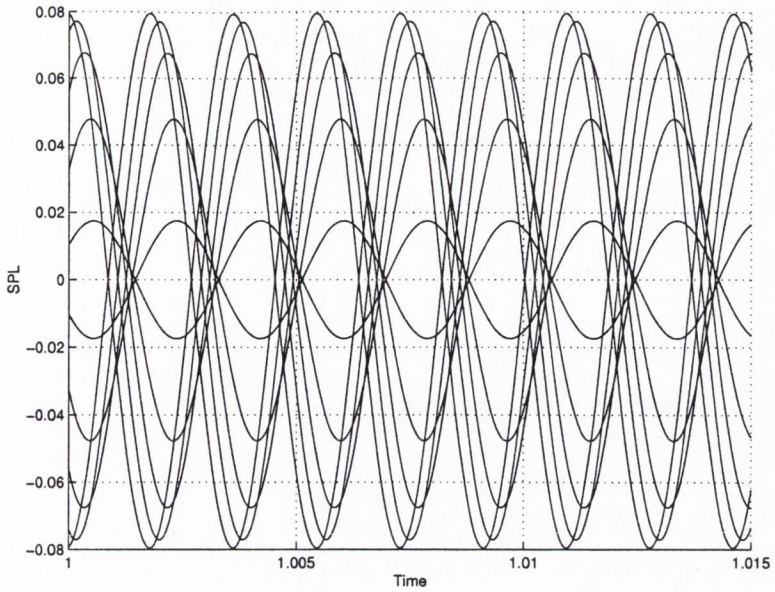

Figure 4.10: Fully reconstructed microphone signals for linear array

ure 4.13). In order to identify the mechanism which generates the null, the phase weighted microphone signals for that location were reconstructed. The result is shown in figure 4.14.

From figure 4.14 it can be seen that the signals prior to summation are such that complete destructive interference will occur, this explains the null seen at the source location. Figure 4.15, shows the first 15 microphone signals (those on the left of the dipole zero-plane), all perfectly in phase. Signals from right of the dipole zero-plane exhibit the same similarity of phase. There is however, a difference in phase between the two sides of the dipole zero-plane of 180°. The result of this is that when the entire array of signals is combined (illustrated in figure 4.14), half of the signals are out of phase with the other half, leading to perfect destructive interference, and hence the null seen when the beamformer tries to focus on the dipole origin. This of course is due to the two hemispheres of each spherical wave being 180° out of phase.

Complete cancellation will only occur when the dipole axis is parallel with that of the array, and the dipole is located at the array mid-point. It is only in this set-up that the two sides of the array are identical, but for being perfectly

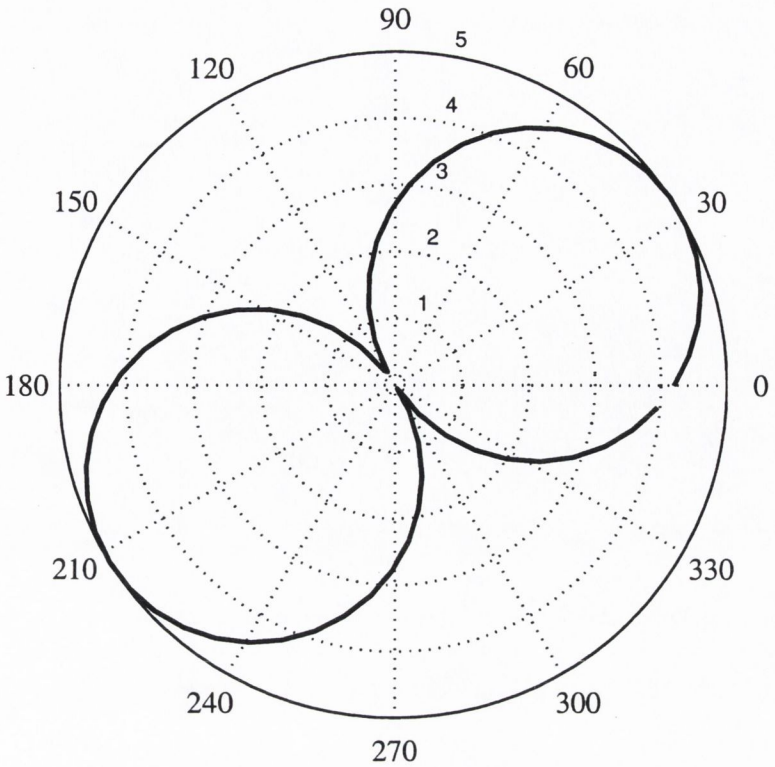

Figure 4.11: Dipole rotated through 30°

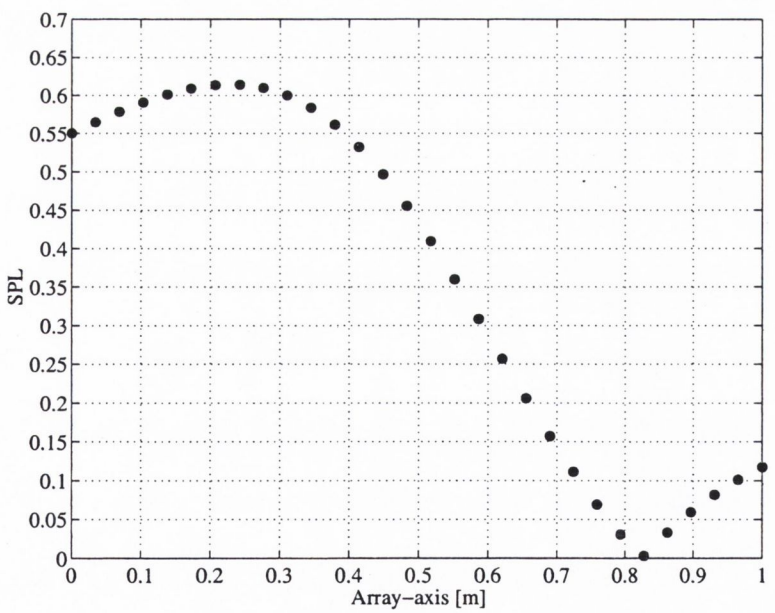

Figure 4.12: Array sound pressures for rotated dipole

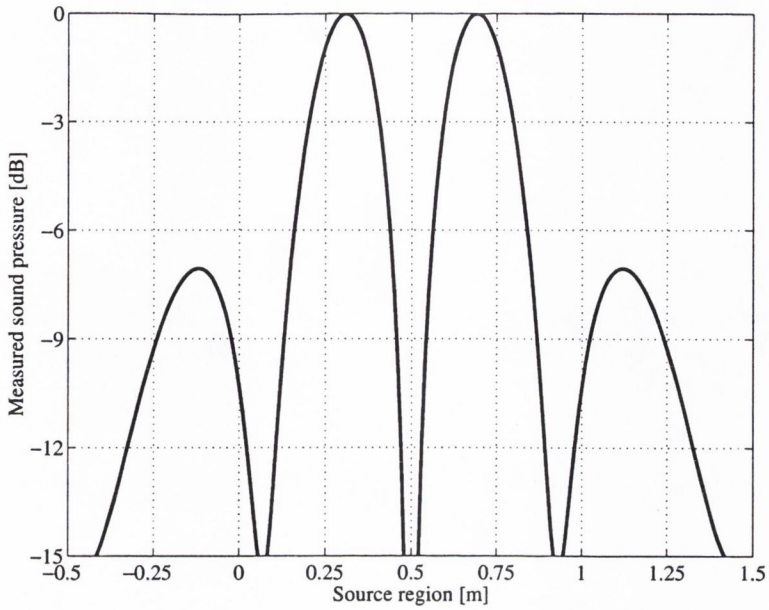

Figure 4.13: Beamforming with dipole source

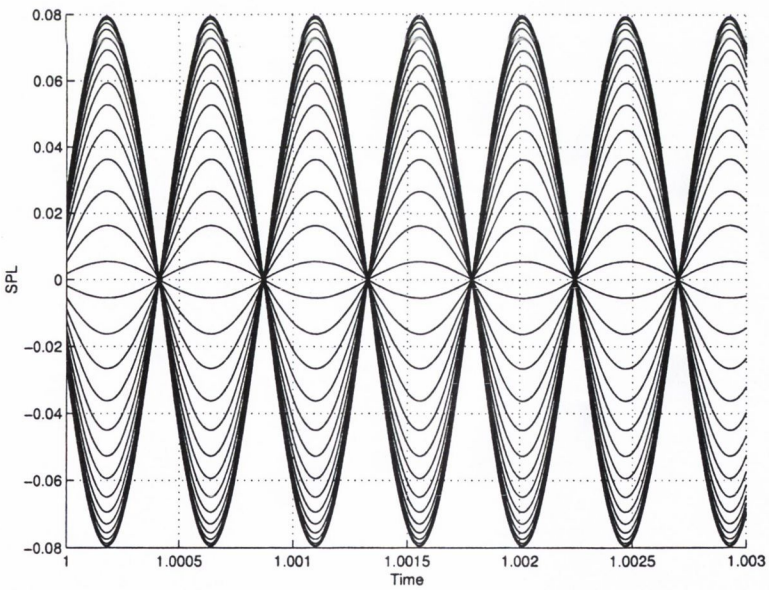

Figure 4.14: Microphone signals phase weighted for focus on dipole origin

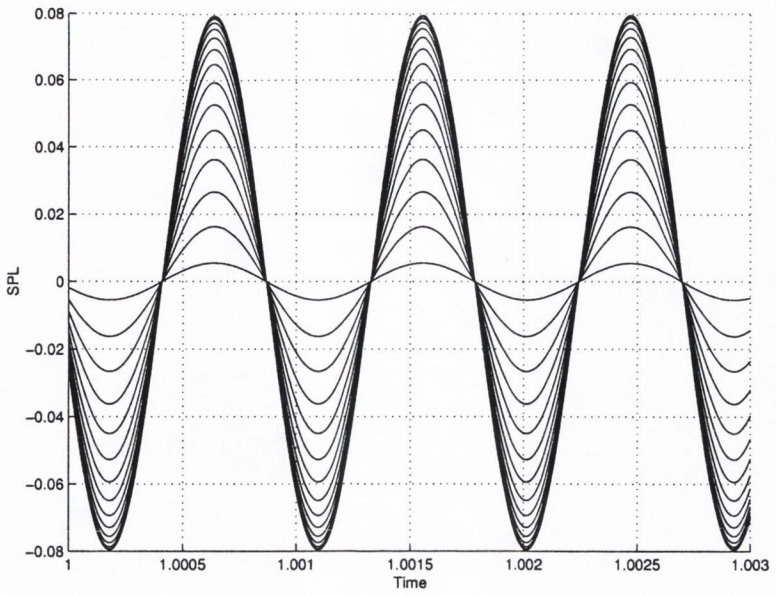

Figure 4.15: Microphone signals from one side of cancellation axis

out of phase. If the dipole axis is rotated relative to the array axis, or if the dipole is not exactly positioned over the array mid point, instead of a null being generated at the source origin, there will be a lesser attenuation. An attenuation of this kind is equally misleading, as it looks like a sidelobe, and may easily be identified as such.

4.4 Source location

The distinctive characteristics of the dipole, and the problems that these pose for an ordinary beamformer have been illustrated. The beamforming principle is based on an assumption of propagation from a monopole source, and so, when a source exhibits a more complicated propagation pattern, the beamformer will generate unreliable data. A source can only be successfully identified and measured by an array if some model is initially assumed, and then, based on this model, a correction is introduced to the array processing which accounts for any deviation from monopole propagation. The following development is based on an ideal point dipole, whose acoustic field propagates

through a homogeneous medium. Although a significant simplification of an aeroacoustic system, this model provides an illustration of how a beamformer can be adapted to the characteristics of a given system.

Consider once again a 30 element microphone array arranged parallel to a point dipole, which is again positioned opposite the mid-point of the array at some distance, D. The beamforming process consists in choosing a point in space and weighting the individual microphone signals such that waves emanating from that point come into phase. The focus of the beamformer can be made to perform a sweep of a region simply by choosing weights corresponding to a set of points within that region. The microphone signals corresponding to each focus position can then be analysed as follows.

Let

$$\phi_i = [\phi_1, \phi_2, \ldots, \phi_N] \tag{4.9}$$

be the set of microphone phase angles for a given focus position. If that focus position contains a dipole source, the phase angle of any signal will be either 0 or π (for an ideal, point dipole). If the focus position does not contain a source the phase angles will differ (displaying some pattern which is a function of the microphone weighting and the phase characteristics of the appropriate spectral component). A dipole source can then be identified by performing the following operation on the set of signals.

$$b = \frac{1}{\pi} \sum_{i=1}^{N} \phi_i$$
$$b_\phi = [b - round(b)]$$

This division by π and subsequent subtraction of the result from the nearest integer to that result gives a measure of the nearness in phase of the microphone signals. This value will be a minimum when the focus lies on a point in space which contains a source, be it monopole, dipole or otherwise, and so the source location is given by

$$\text{Source location} = \min |[b_{\phi i}]| \tag{4.10}$$

In order to decide the type of source, the phase distribution for that focus position must be examined and compared with any knowlege of what is located at that point in space. The search algorithm will not differentiate between individual sources, but it will identify the presence of a source. In order to identify the specific type of source, the phase signature for that focus point must be examined.

4.4.1 Source orientation

If the source is a dipole then calculation of its orientation is straightforward by considering the phase angles of the microphone signals when the beamformer is focused on the source, (equation 4.9). All signals corresponding to microphones lying to the left of the dipole zero-axis will have phase angle equal to π, whereas those lying to the right will have phase angle equal to zero. The

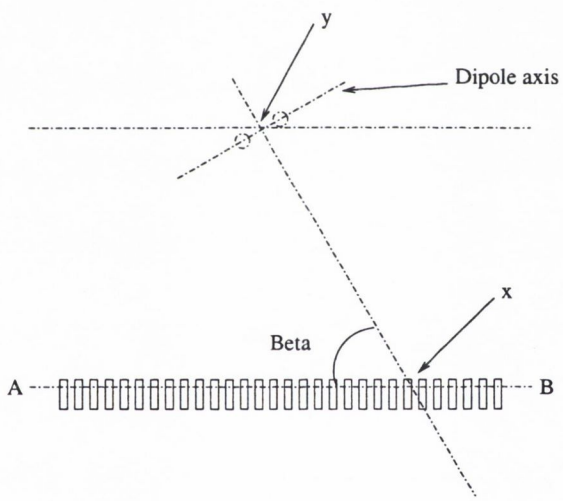

Figure 4.16: Dipole orientation

intersection between the dipole zero-axis and the array is that point where the transition from $\phi = \pi$ to $\phi = 0$ occurs. This is shown as point x in figure 4.16. This is enough information to calculate the dipole orientation (which will lie at 90° to the vector joining the dipole location and the zero-axis/array

intersection). Thus, from figure 4.16

$$\beta = \cos^{-1}\left[\frac{(\mathbf{x}-\mathbf{y})\cdot\mathbf{AB}}{|(\mathbf{x}-\mathbf{y})|}\right] \tag{4.11}$$

which gives the angle between the array axis and the vector $(\mathbf{x}-\mathbf{y})$, where $\mathbf{x}$ is the intersection between the array axis and the dipole zero-plane, $\mathbf{y}$ is the source position and $\mathbf{AB}$ the array axis. The dipole orientation is at 90° to the vector $(\mathbf{x}-\mathbf{y})$. The orientation of a dipole source is of interest for two reasons. First, the dipole axis and zero-axis correspond to directions of maximum and minimum acoustic radiation respectively. Secondly, the dipole axis gives the direction of the corresponding aerodynamic force. Identification of source orientation gives valuable information concerning both the acoustic directivity of the source and the associated aerodynamic force map.

4.4.2 Source measurement

Thus it is clear why ordinary beamforming fails to measure correctly a dipole source. Correct measurement of the dipole's acoustic energy, in the direction of the array, requires that the microphone signals be in phase before the summation process is employed, and so, the signals must be appropriately weighted prior to summation. This involves augmenting the signals from one side of the dipole zero-axis with a correction of π radians. Figures 4.17 and 4.18 show directivity patterns for beamformers measuring dipoles with and without modification. The dipole was located at 20cm from the left hand side of the array and at 30° (distance of source region from array is assumed known). The ordinary beamformer shows an attenuation at this point (figure 4.17), whereas the modified beamformer shows a maximum (figure 4.18), and the algorithm successfully calculates the dipole orientation.

4.4.3 Conclusion

The technique developed here provides a means for detecting the presence of a dipole source, calculating its orientation in space (which corresponds to

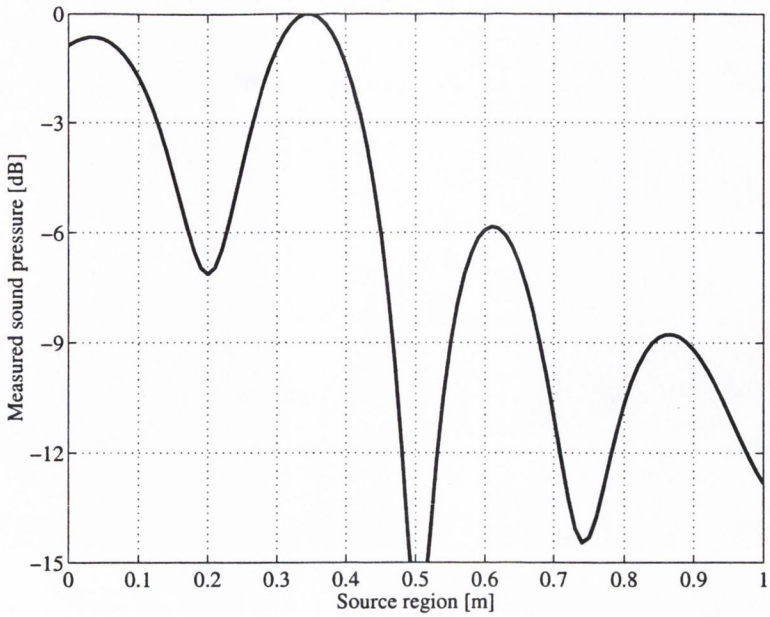

Figure 4.17: Beamformer response before dipole modification - for a dipole at 0.2m, orientation=30°

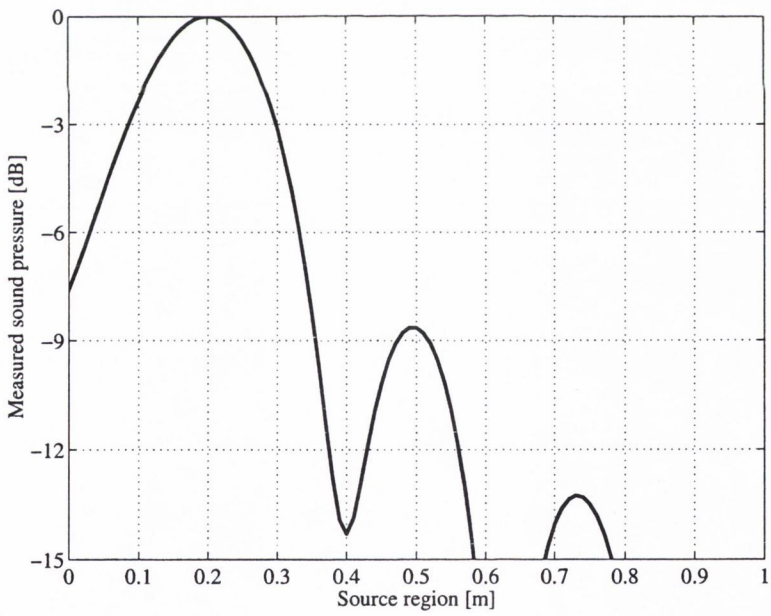

Figure 4.18: Beamformer response after dipole modification for a dipole at 0.2, orientation=30°

the direction of the corresponding aerodynamic force) and then modifying a beamformer in order to focus on the source so that its strength can be measured. The strength which this beamformer measures is not the maximum strength (which is seen on the dipole axis), but an average of the strength in the direction of the array. The individual microphones do however contain a record of the pressure distribution and so once the source location and orientation have been established, and a good source model is available the actual source strength can be calculated. This can be shown as follows. Each of the microphone signals can be written as

$$M_i = \frac{S \cos\theta e^{jkr_i}}{4\pi r_i} \tag{4.12}$$

where S is the true source strength, r_i are the distances from each of the microphones to the source, θ is the source orientation and k is the wavenumber. Once the source location and orientation have been determined the source strength can be found. In fact, if a number of sources have been identified, and good models are available for all of them, then 30 source strengths can be calculated before the equation system becomes undetermined. This will be discussed in the next chapter.

This technique was developed for an ideal point dipole. In dealing with real data a more robust method will be necessary. This is developed in the next section.

4.5 Experimental validation

4.5.1 Introduction

In using a microphone array to perform measurements on a system containing a real aeroacoustic dipole, allowances must be made for the fact that the real source will adhere only approximately to characteristics defined by a numerical model. The following development outlines a series of tests which serve both

to ascertain the validity of the numerical model used in the last section, and also to examine how, using real data, the distinctive nature of an actual dipole source can be used in order to identify its location.

4.5.2 Experimental set-up

A linear array of thirty microphones of length $1.015m$ was designed with an element spacing of $35mm$, so that the upper limit of the array's operating range is $4.9kHz$. This is shown in figure 4.19. The experimental facility, shown in figure 4.24 was designed to minimise acoustic reflection from the wall, floor and ceiling. The rest of the laboratory was treated as a half-space.

Two sources were used, the first was an acoustic source, consisting of a louspeaker rotated with its principle radiation axis parallel to the array axis. The second source was a cylinder in cross-flow, a typical example of an aeroacoustic dipole. Each microphone was calibrated in an impedance tube, and the processing algorithms automatically corrected for magnitude and phase discrepancies over a frequency range of $3.2kHz$.

4.5.3 An acoustic source

The set-up for the acoustic source is illustrated schematically in figure 4.20 The speaker in this orientation approximates a dipole due to its sound generating mechanism. An acoustic source was used in order to guarantee a clean signal, with a high SNR. The frequency of the source was $800Hz$. The test procedure was similar to the procedure followed for the numerical model. Choosing a linear source region, parallel to the array axis and including the source (shown as AB in figure 4.20), the focus of the array was swept incrementally over this region and the beamformed signal recorded at each point. Plotting this measurement as a function of the focus position generates the directivity pattern shown in figure 4.21. There are two different ways in which this result can be used. If the source position is unknown, then the directivity is a means for es-

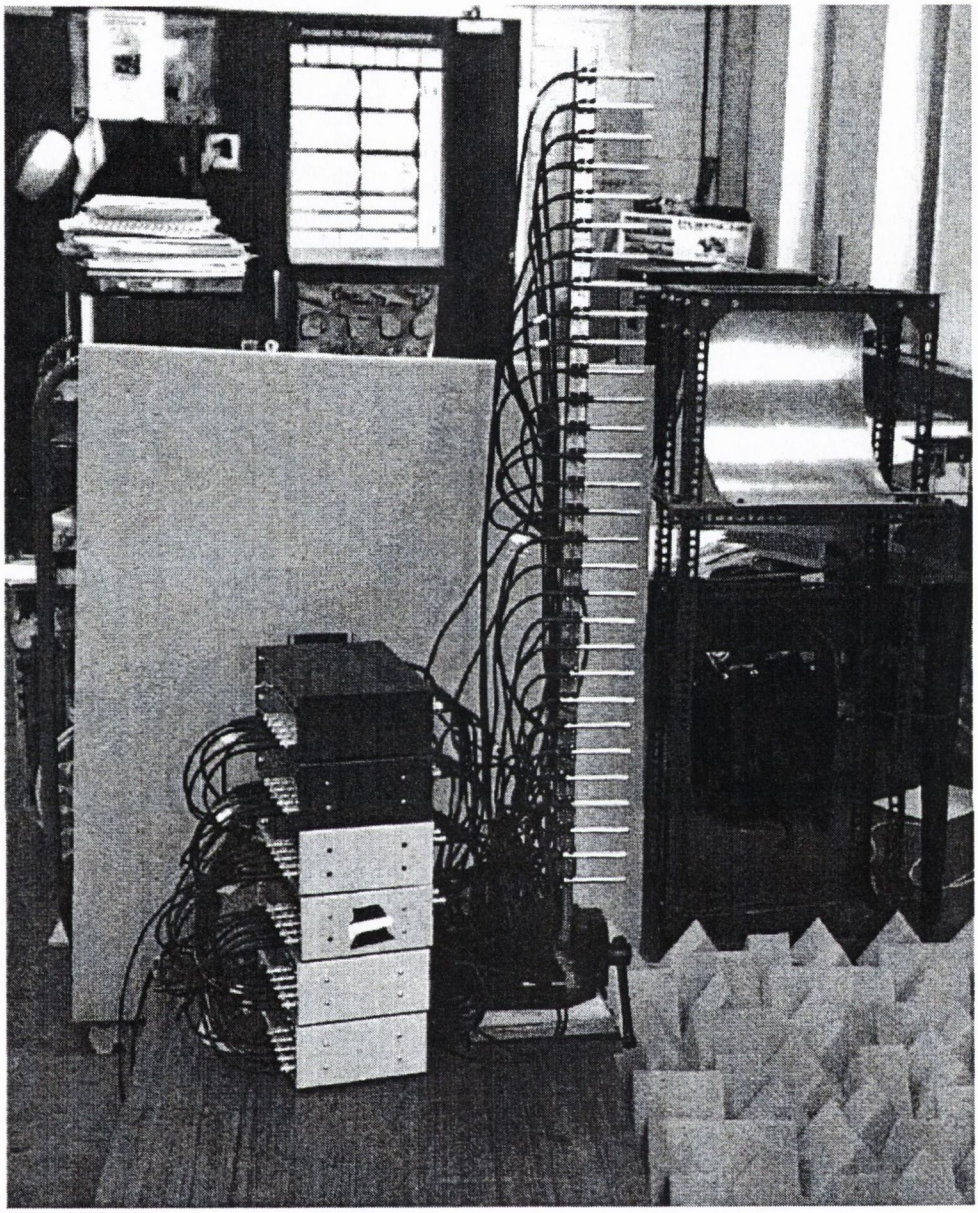

Figure 4.19: Microphone array

timating its location. If the source position is known then by focussing on that location the beamformer can be used to estimate the strength of the source, while filtering out noise coming from other regions of space. It is clear from figure 4.21 that the beamformer has failed in both these modes of application. The source position is not identified, nor is a measure of the source's strength obtained, when focused on the source position it measures -23dB relative to the maximum strength measured. This is the pattern predicted by the numerical model. Extracting the phase and magnitude values from the appropriate

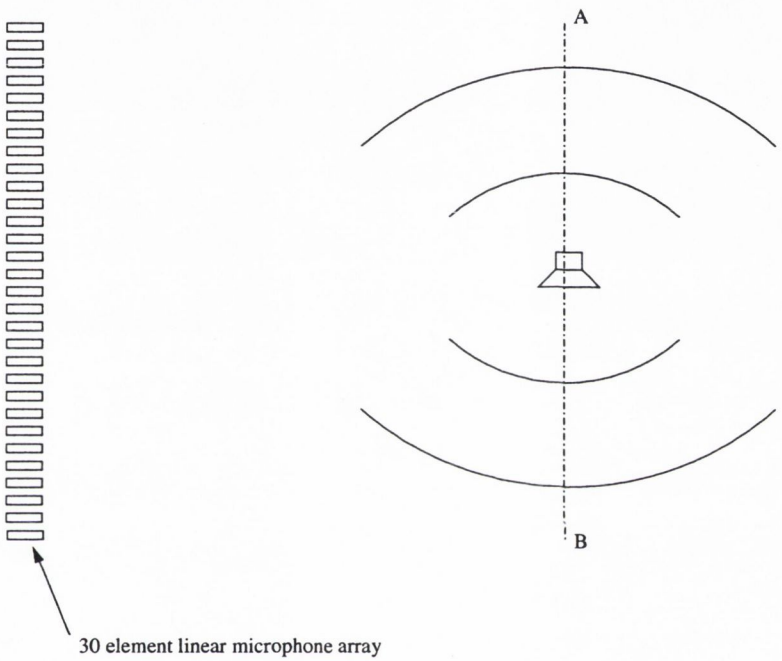

Figure 4.20: Test setup

spectral component of the Fourier transforms of the microphone signals, after they have been phase weighted so as to focus on the source position, and plotting them as a function of array element gives the distributions shown in figures 4.22 and 4.23. Both distributions show characteristics indicative of the dipole mechanism. The magnitude distribution shows maximum values towards the extremities of the array, where the microphones are closer (in terms of angle) to the dipole axis along which the sound pressure radiated is

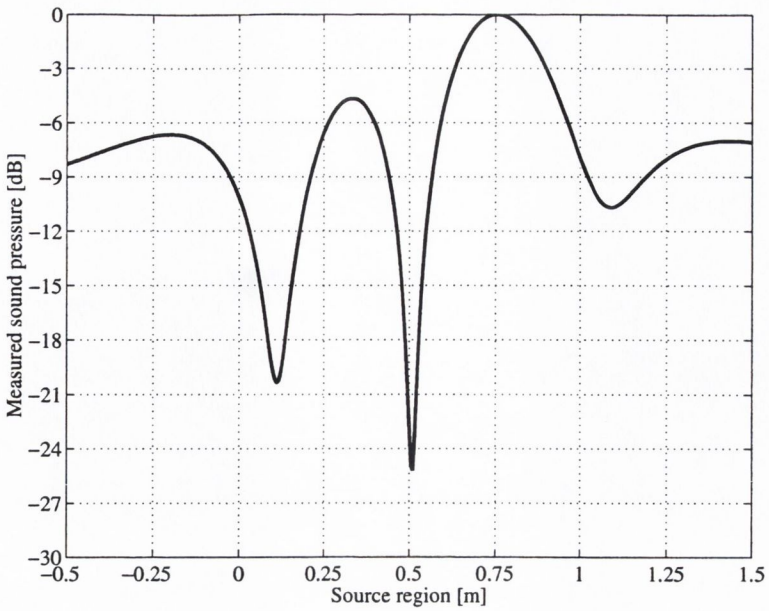

Figure 4.21: Acoustic dipole directivity pattern

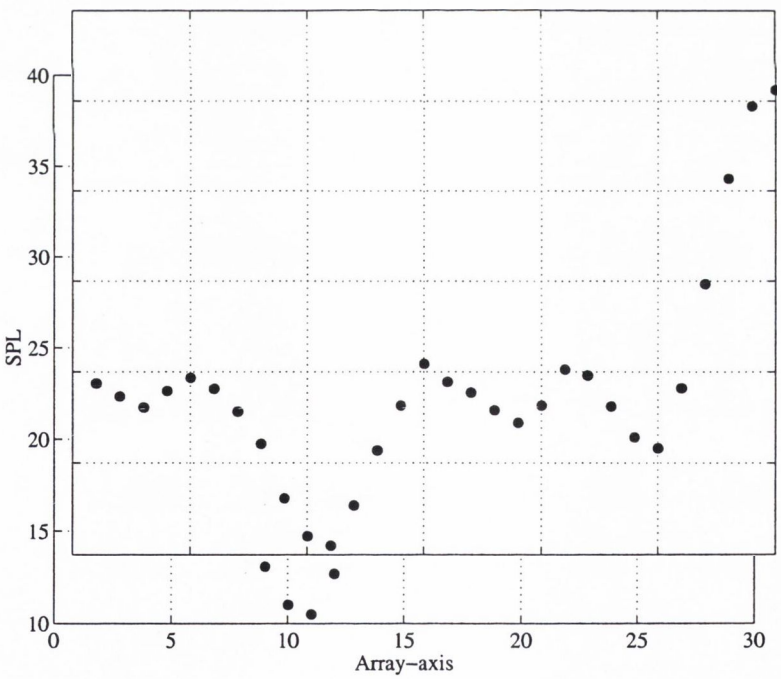

Figure 4.22: Magnitude distribution for focus on source

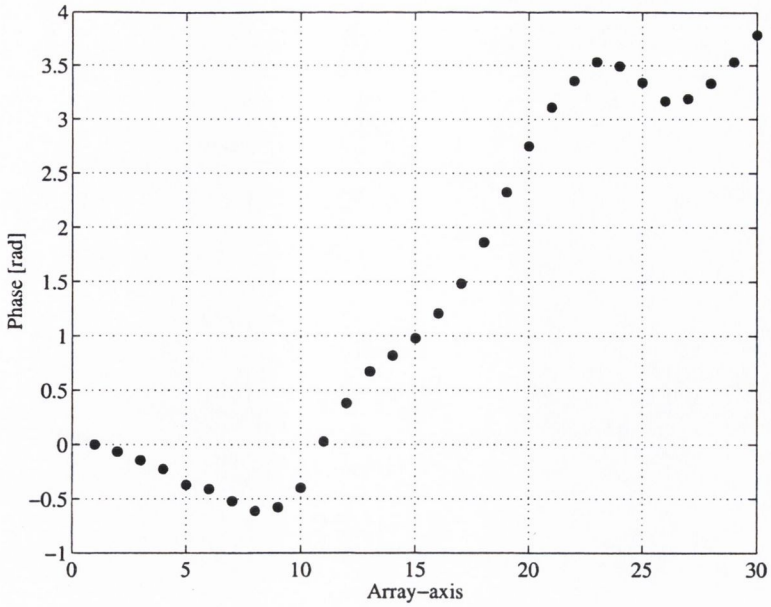

Figure 4.23: Phase distribution for focus on source

a maximum. The minimum values are towards the centre of the array, where the dipole's cancellation axis intersects the array axis. The asymmetry of the sound pressure distribution is due to the shape of the loudspeaker, which is designed to radiate efficiently in one direction only. The back side of the loudspeaker consists of a large magnet which interfere's with the sound waves which try to propagate in this direction. The phase distribution clearly shows a difference of π radians on either side of the array mid-point.

4.5.4 An aeroacoustic source

The experimental facility for aeroacoustic testing (shown in figure 4.24) consists of a fan and nozzle arrangement, capable of generating a jet of up to 50m/s through the semi-anechoic chamber. This chamber was designed to minimise acoustic reflection for frequencies down to 500Hz. The fan and nozzle setup, shown in figure 4.25, has a steel support structure attached to the end of the nozzle to hold the aeroacoustic test specimen. The aeroacoustic specimen consisted of a 6mm diameter solid cylinder in a cross flow of $50m/s$,

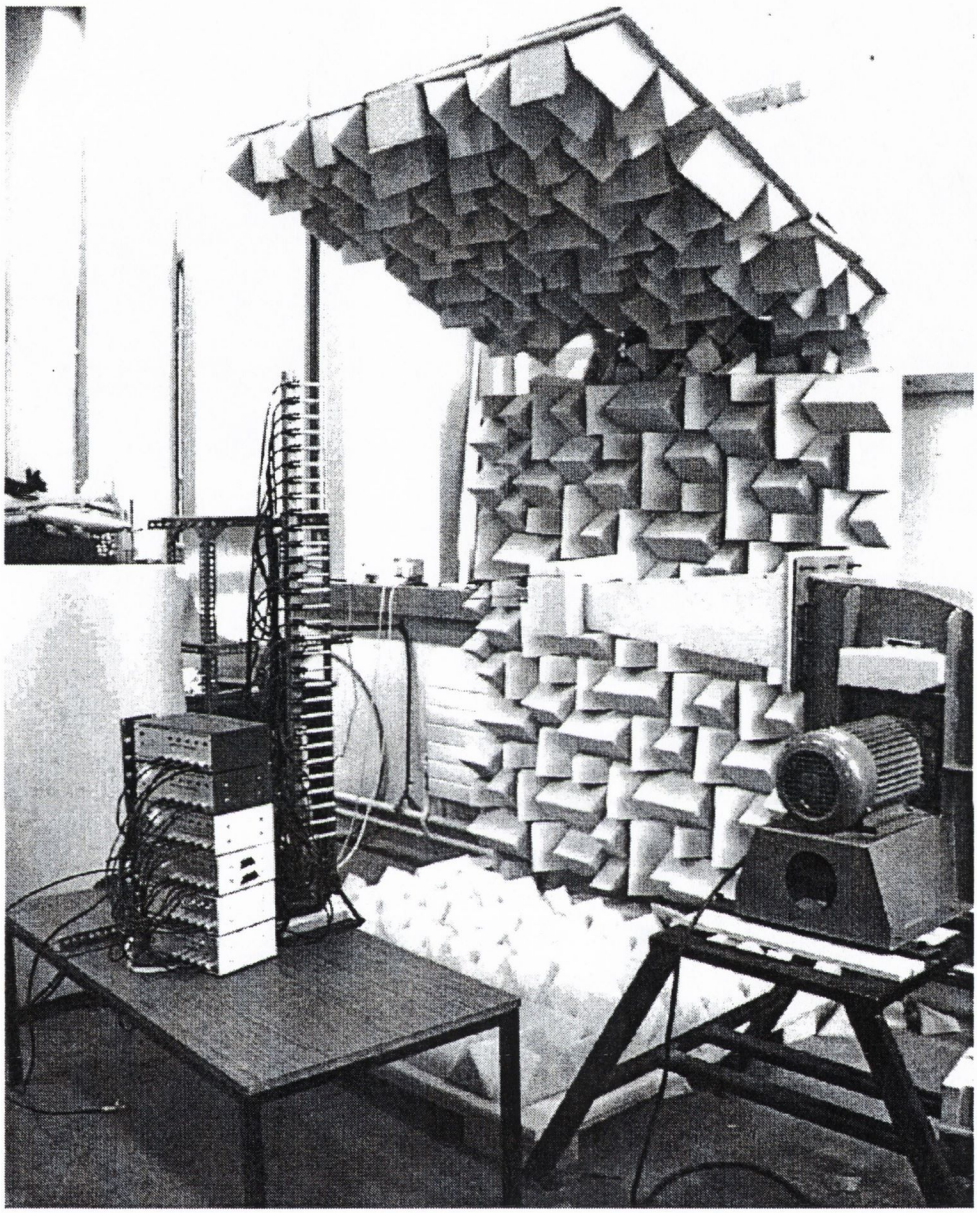

Figure 4.24: Experimental setup

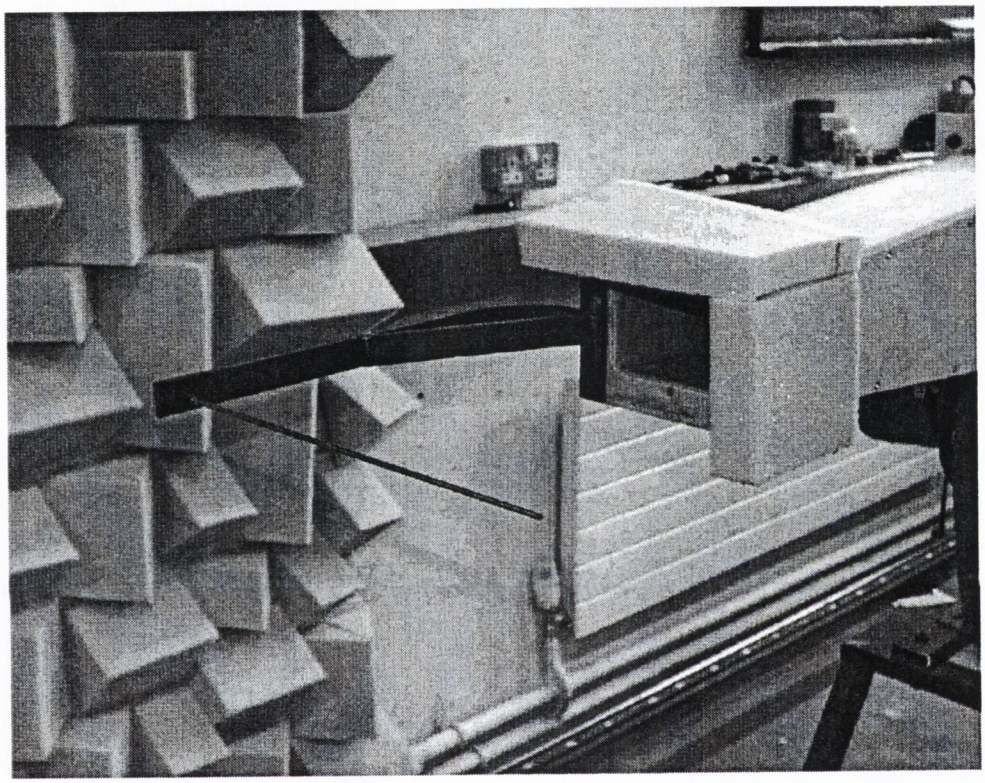

Figure 4.25:

and generated sound at $1650Hz$. This is a typical example of an aeroacoustic dipole. The sound which it generates is often referred to as Aeolian tones, named by the Greeks after the sound the wind used to make blowing through the trees on an Island called Aeolus.

4.5.5 Aeroacoustic testing

Aeroacoustic testing was performed in the same manner as the acoustic tests. Once again the focus of the array was swept over a linear region (shown as AB in figure 4.26(a) containing the source, and the sound pressure measured by the array at each focus position. The resulting directivity pattern is shown in figure 4.26(b). As with the acoustic source, it is clear that the beamformer has again failed to identify the source. It does not give a measure of the source strength, nor does it represent the source distribution over the region AB. It could be argued that the double peak shown in figure 4.26(b) identifies the presence of a dipole, however the position and width of these peaks are a function of the array geometry, its position and the source frequency. The phase and magnitude distributions (generated in the same way as for the acoustic test) shown in figures 4.27 and 4.28, again show dipole characteristics. In this case the patterns agree more closely with an ideal point dipole. The magnitude distribution is more symmetrical than for the acoustic source, and the phase distribution is more like that of an ideal dipole. This is a reflection of the fact that the aeroacoustic source is a better approximation of a point dipole.

These magnitude and phase distributions are the distinctive dipole characteristics, and so, it is by searching for these trends that the source can be identified. The location technique proposed for a numerical dipole will not be applicable to a real dipole as the phase of the microphones will be subject to experimental uncertainty. An alternative method must be developed which will allow for this variation.

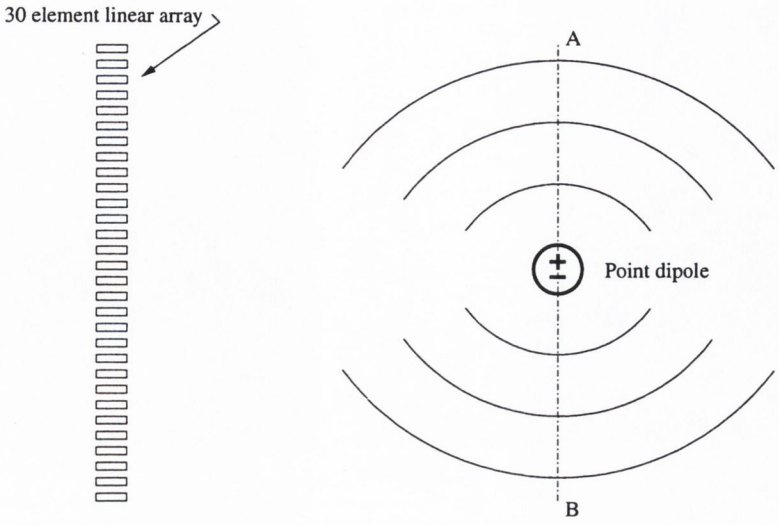

(a)

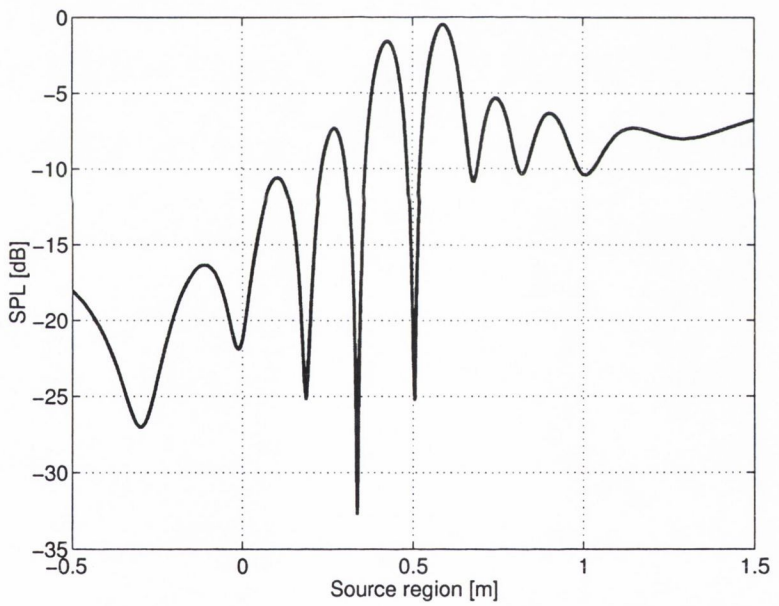

(b)

Figure 4.26: Test setup and resulting directivity pattern

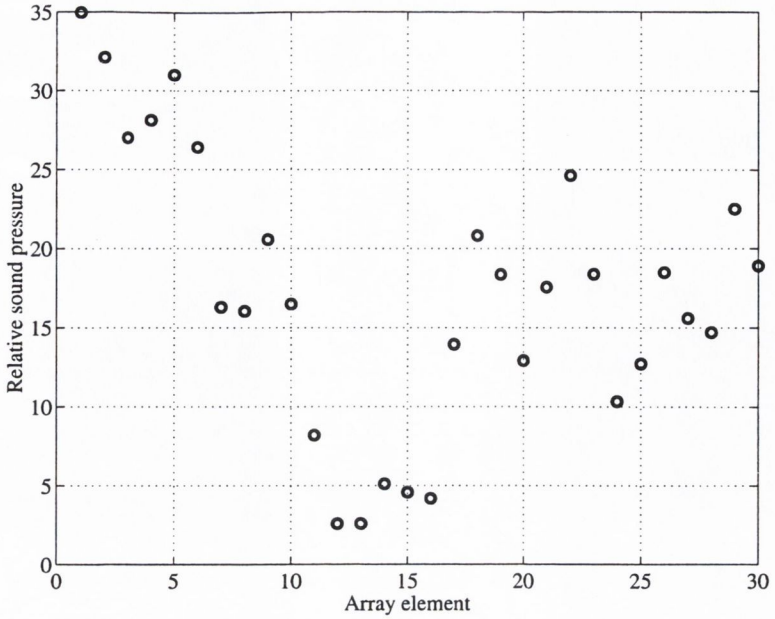

Figure 4.27: Magnitude distribution for aeroacoustic source

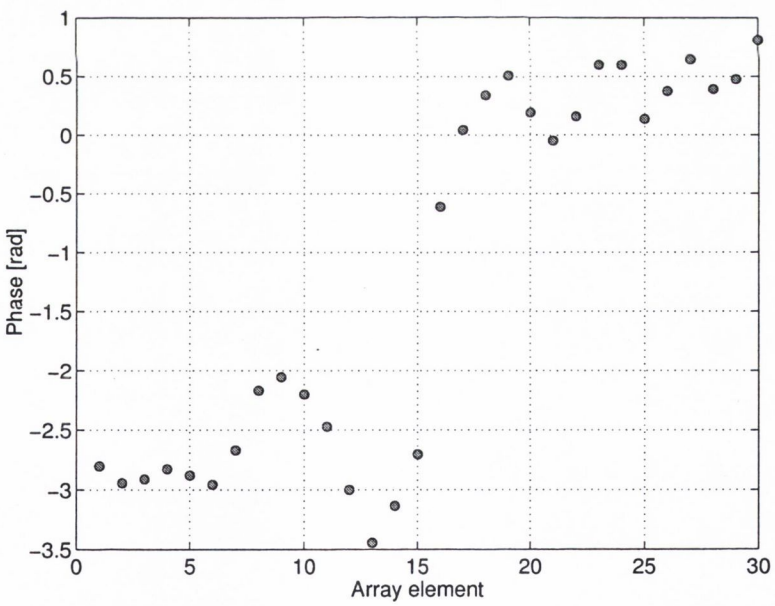

Figure 4.28: Phase distribution for aeroacoustic source

4.5.6 The search algorithm

As the phase of the weighted array-signals represent the phase of a source at the focus position corresponding to that set of weights, any technique for source location must be designed to use this data. In order to search for the phase signature of a dipole for real data, where noise will contaminate the phase data, an algorithm must be capable of identifying a trend in the data which corresponds to the source characteristics. For a dipole these trends are

- A difference of π radians along the array.
- A large number of the signals' phase lie in one of the two regions.
  - $\phi = +/-\pi$
  - $\phi = 0$
- At some point along the array there is a sudden phase shift of π radians.

Using these criteria an algorithm was designed to search a given region for the presence of a dipole. For each focus position in the linear region AB (see

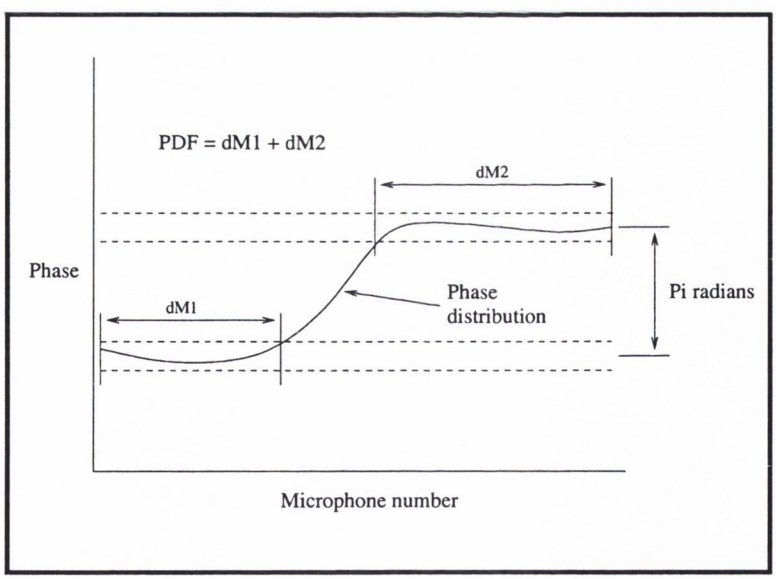

Figure 4.29: The dipole signature

figure 4.26(a)), the relative phase of each signal is calculated by means of a Fourier transform. Thus, the distribution of phase over the array for each focus position is obtained. Each distribution is tested for dipole characteristics by examining the degree of concentration of phase values within the phase bands indicated in figure 4.29. Shown in this figure is a sample phase distribution, and a pair of 'phase bands', indicated by the dashed lines. These phase bands are separated by a distance of π radians. If the array is focused on a dipole source, the phase distribution will show a high concentration of points in these phase bands. If not focused on a dipole, the distribution will show a phase characteristic whose points are scattered outside these phase bands. For each focus position the algorithm counts the number of signals whose phase falls within these bands. The focus position with the highest concentration of phase in these regions is the most likely location for finding a dipole. Shown in figure 4.30 is phase distribution as a function of focus position for the aeroacoustic source. Each line in this graph represents the phase distribution for a single focus position, from A to B. Application ot the search routine to this data results in successful identification of the dipole location. The distribution indicated by the circles in figure 4.30 is the dipole signature, and the focus position corresponding to this distribution is the dipole location. This technique is also successful in locating the acoustic source, whose phase signature is less like that of a point dipole, as shown in figure 4.31. These dipole distributions can be compared with the monopole distribution shown in figure 4.32, which was generated when the loudspeaker was oriented with its radiation axis perpendicular to the array axis. Here the phase distribution is approximately linear, corresponding to the propagation characteristics typical of monopole sources. In figures representing dipole distributions it can be seen that there are three phase bands instead of two. This is because the phase is calculated relative to the phase of the first microphone, and it is unsure whether the phase on the other side of the cancellation axis will lead or lag.

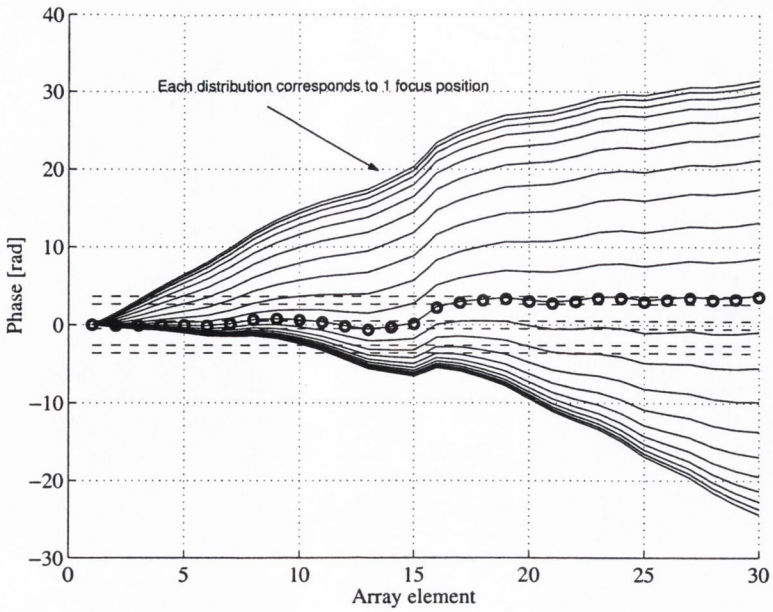

Figure 4.30: Phase distribution as a function of focus position - aeroacoustic dipole

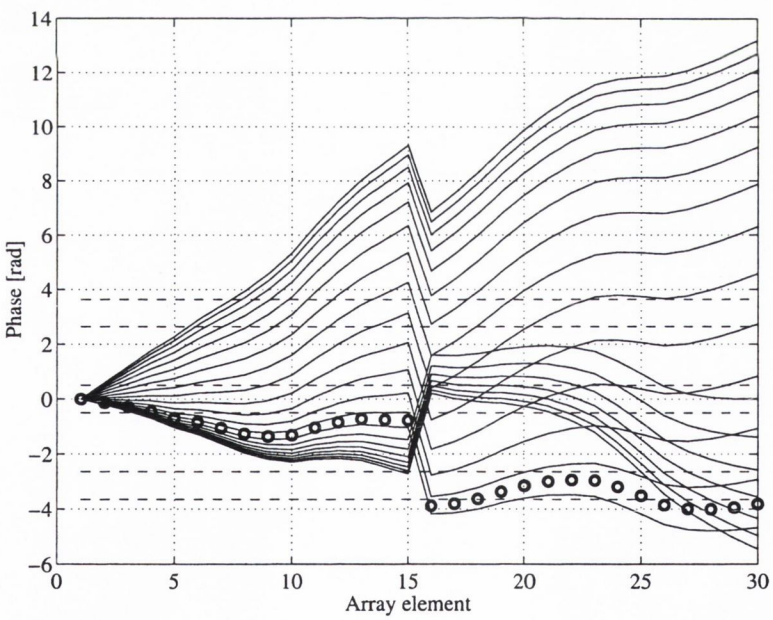

Figure 4.31: Phase distribution as a function of focus position - acoustic dipole

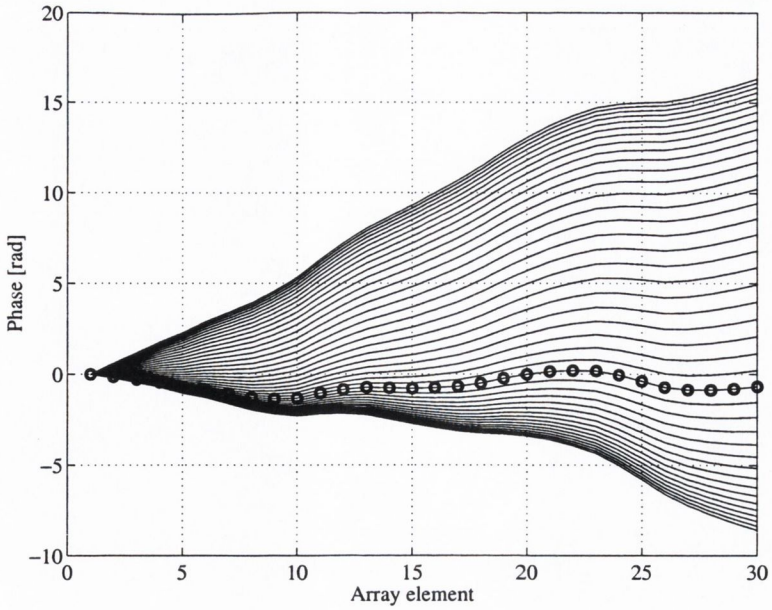

Figure 4.32: Phase distribution as a function of focus position - acoustic monopole

After the dipole location has been determined, calculation of the source orientation is straightforward, as the intersection between the cancellation axis and the array axis is given by that point at which the phase moves from one phase band to another.

4.5.7 Source measurement

Having located the dipole and calculated its orientation, the beamformer can now be modified in order to obtain a measure of the source strength. As shown in figure 4.21, when the beamformer is focused on a dipole source, it fails to give an indication of the source strength. In order then to measure the strength of the source, the phase must be aligned, in order to remove this difference. This is achieved by subtracting from the dipole phase signature the theoretical dipole signature (shown in figure 4.33). The phase distribution prior to correction is shown by the dashed line. The solid line is the theoretical dipole phase distribution and by subtracting this from the actual distribution the series of

circles results. After this operation has been performed, the phase across the

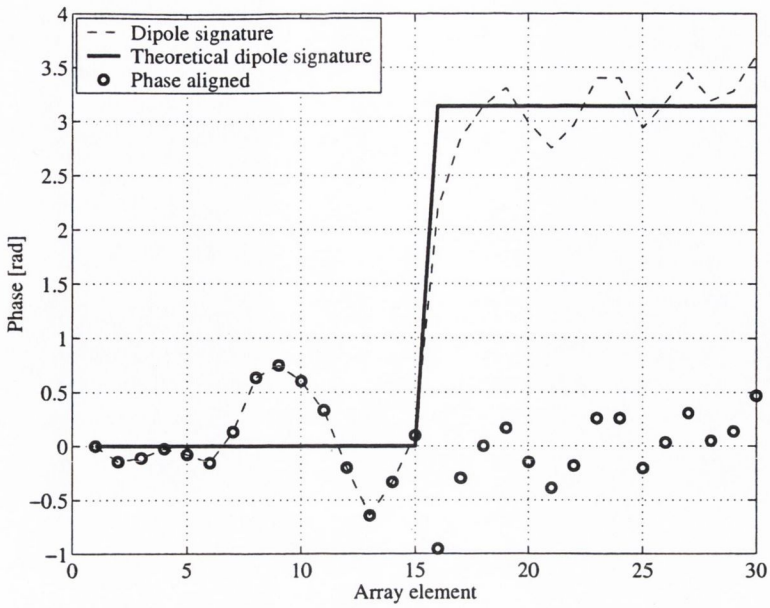

Figure 4.33: Beamformer modification

array is now aligned according to a theoretical model. When summation is performed, the signals interfere constructively, and so give a measure of the sound power radiated by the source in the direction of the array. The result of this modification is shown in figure 4.34, for the aeroacoustic source. Whereas the standard beamformer measured a minimum when focused on the source location, the modified beamformer correctly measures a maximum. Figures 4.35 through 4.37 demonstrate the full effect of this technique. Figure 4.35 shows the Fourier transform of a single microphone signal. It can be seen here that the dipole source is evident (approx. $1650Hz$), but the spectrum is dominated by lower frequency fan and nozzle noise. The effect of an ordinary beamformer on the system is shown in figure 4.36, where no real improvement is evident. Once the beamformer modification has been applied however, it can be seen from figure 4.37 that the dipole power has been reinforced and the unwanted noise attenuated. The peak at $1650Hz$ represents an average of the dipole sound radiated in the direction of the array. These Fourier transforms

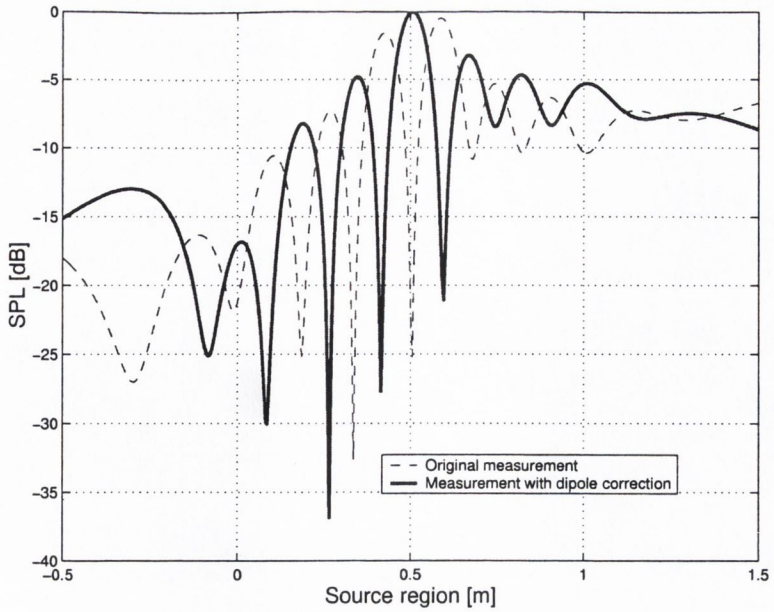

Figure 4.34: Modified directivity

were calculated using a single stream of data with no averaging, hence the noise. Averaging would produce a smoother spectral distribution, and a more pronounced spike at the dipole frequency. This development does not consider any quantitaive measure of the dipole's strength, the emphasis is on a qualitative illustration of the difficulties involved with ordinary beamforming when sources exhibit propagation characteristics which do not conform to the monopole model.

4.6 Discussion

The technique described has been shown to work well, provided a number of criteria are met, Firstly, the frequency of interest must be known, as the search is implemented only at one frequency. Secondly, it must be possible to inspect each potential source location, visually or otherwise, in order to determine if the location identified does indeed contain a source. Even if there are no dipoles present, the algorithm will identify the focus position with the

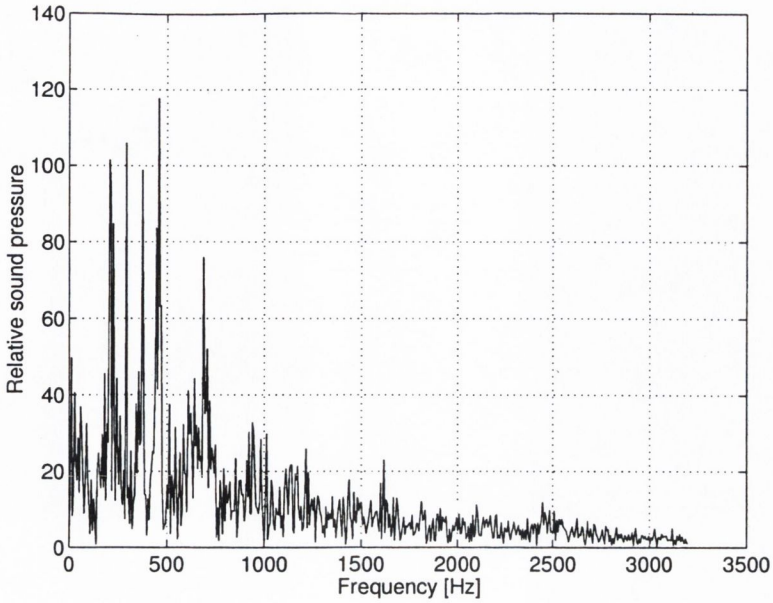

Figure 4.35: Fourier transform from a single microphone

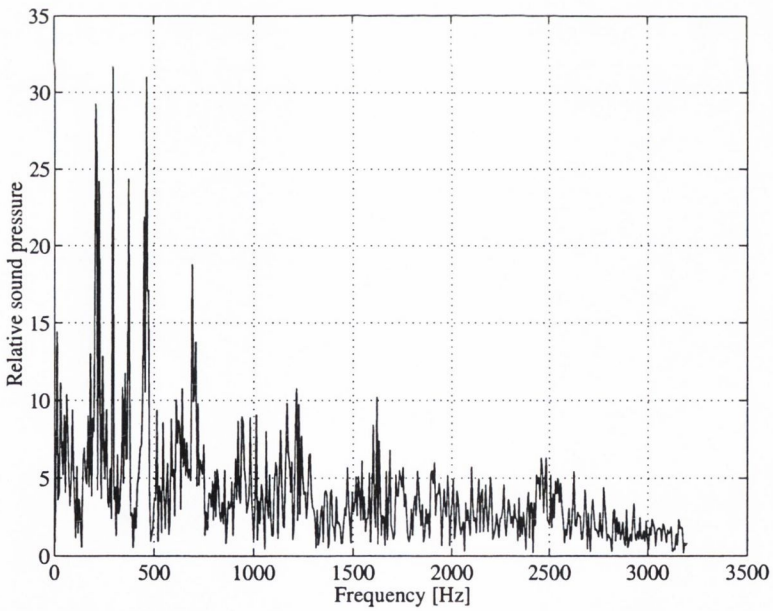

Figure 4.36: Fourier transform after ordinary beamforming

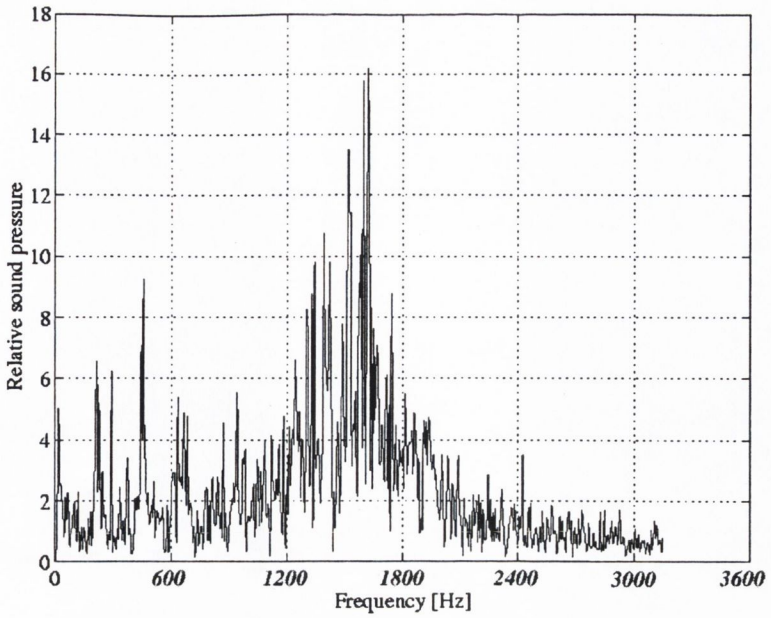

Figure 4.37: Fourier transform after modified beamforming

highest concentration of phase in the specified bands. It is important that the method be used only as an aid in the location of potential sources. Another difficulty which will be addressed in the following chapter is the problem of contamination from other sources of the same frequency.

The technique has potential for use in the determination of the physical nature of known sources if it is combined with local measurement techniques such as LDA or hot wire anemometry. If, for example, LDA is being used to analyse an aeroacoustic source at a given location, it can give information about the spectral content of that source. It cannot however determine any propagation characteristics, which are important in determining the far-field contribution of the source. Using LDA in conjunction with the proposed technique, the focus of the array can be held on the source location and the phase signature analysed as discussed. This information can then be correlated with data generated by the LDA system, giving a more complete picture of the source.

4.7 Summary

It has been shown that delay-and-sum beamforming is limited in its capacity as an analysis tool when source propagation ceases to be omnidirectional. A point dipole source was used as a test specimen in order to illustrate the nature of this problem. The results demonstrate clearly the mechanism whereby a beamformer fails, and through an identification of this mechanism an adaptive technique was developed which shows how the problem can be overcome. In using a very simple set-up, the problem of multiple source interaction has been neglected. This will be dealt with in the next chapter.

Chapter 5

Multiple sources

5.1 Introduction

A technique has been developed for the identification of an aeroacoustic dipole based on its distinctive farfield phase characteristics. The technique was developed for a system consisting of a single point dipole, free from sources of contamination at the same frequency. Aeroacoustic systems are often more complex than this, with a number of sources contributing to the resultant sound field. In light of this, the effect of other sources on the phase signature of a single dipole must be examined, in order to evaluate the usefulness of the technique for analysis of more complex systems.

5.2 Twin sources

To investigate these effects, a system was simulated (again using Matlab), which consisted of a point dipole, as before, and a point monopole, whose position and strength could be varied. This system is shown in figure 5.1. The thirty element array was $1m$ in length, and the source region parallel to the array axis at a distance of $0.8m$. The dipole source position was directly opposite the array mid-point, while the position of the monopole was varied over a $1m$ region in increments of $0.1m$ (shown in figure 5.1 as XY, from

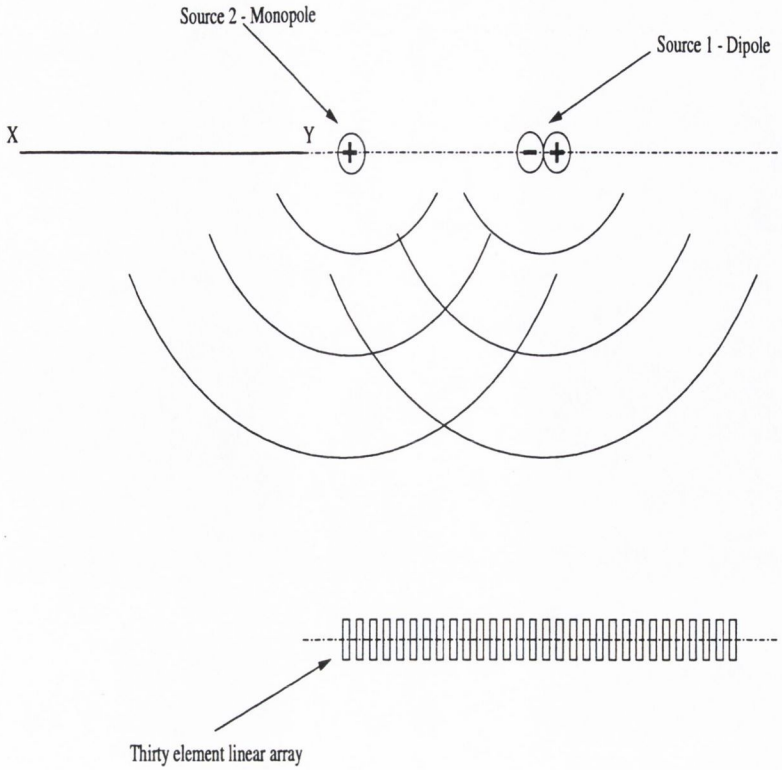

Figure 5.1: Twin source system

$1m$ at Y to $2m$ at X). The monopole was restricted to this region so as to keep the separation between the sources greater than one acoustic wavelength. For each position of the monopole, its strength was varied from one tenth dipole strength to full dipole strength. With the focus of the array maintained on the dipole, phase distributions were calculated for each case, in order to give an indication of the degree of contamination caused by the monopole for different strengths and positions. These are shown in figures 5.2 through 5.6.

Each individual figure shows phase distributions along the array for one monopole position but different monopole strengths. The phase distribution for a single point dipole is shown by a series of circles (i.e. no contamination) while distributions including the said monopole contributions are shown by the dashed lines. In each figure, i.e. for each monopole position, there are a number of phase distributions which retain the basic dipole pattern. These

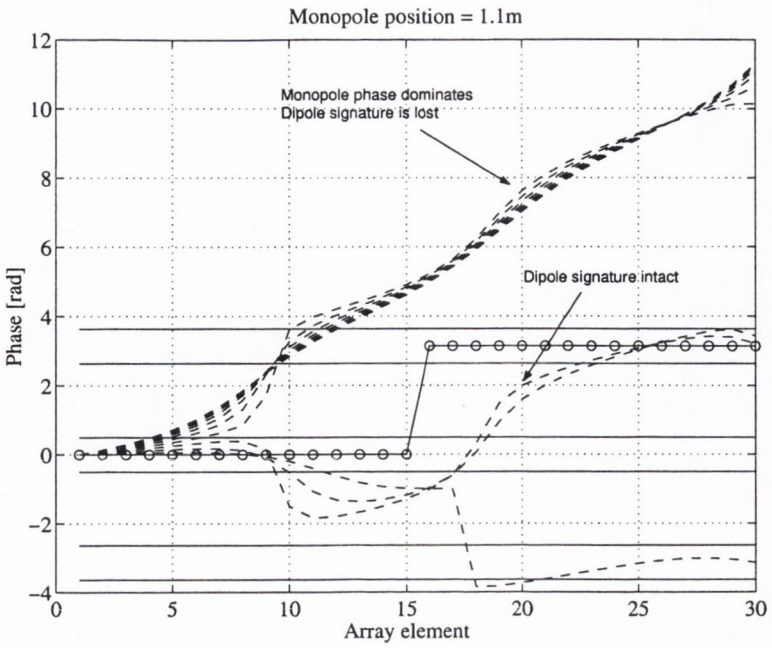

(*a*)

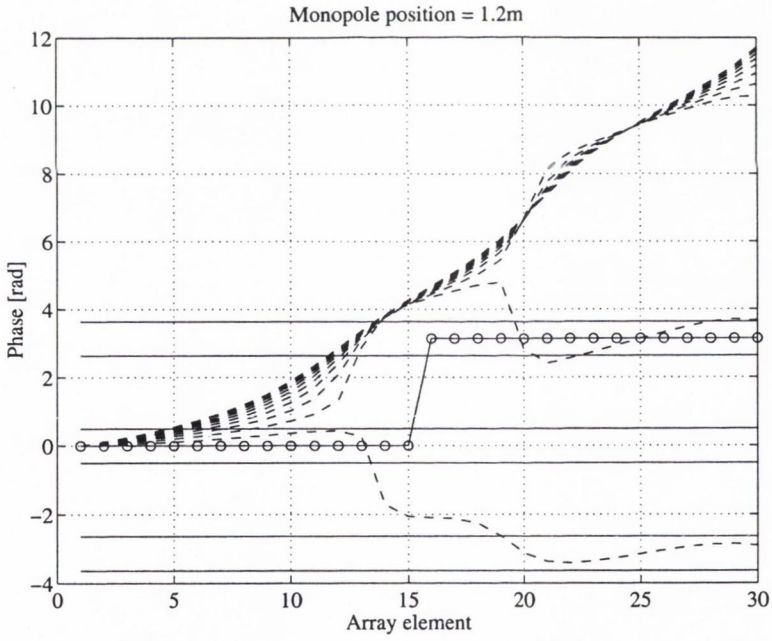

(*b*)

Figure 5.2: (*a*) 1.1m, (*b*) 1.2m

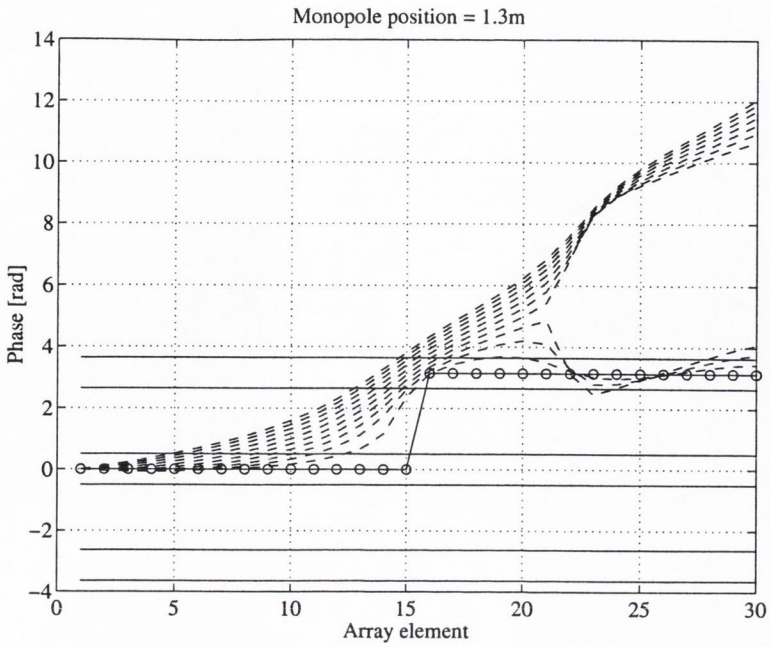

(a)

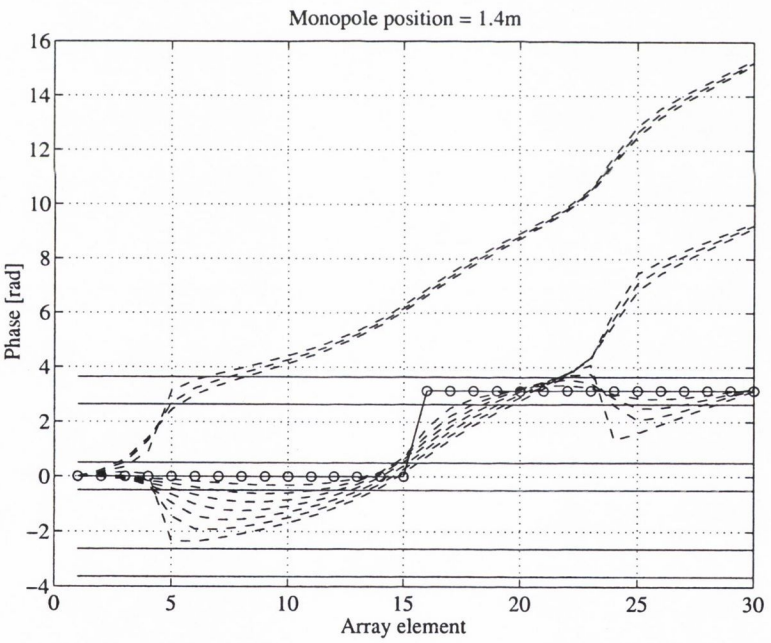

(b)

Figure 5.3: (a) 1.3m, (b) 1.4m

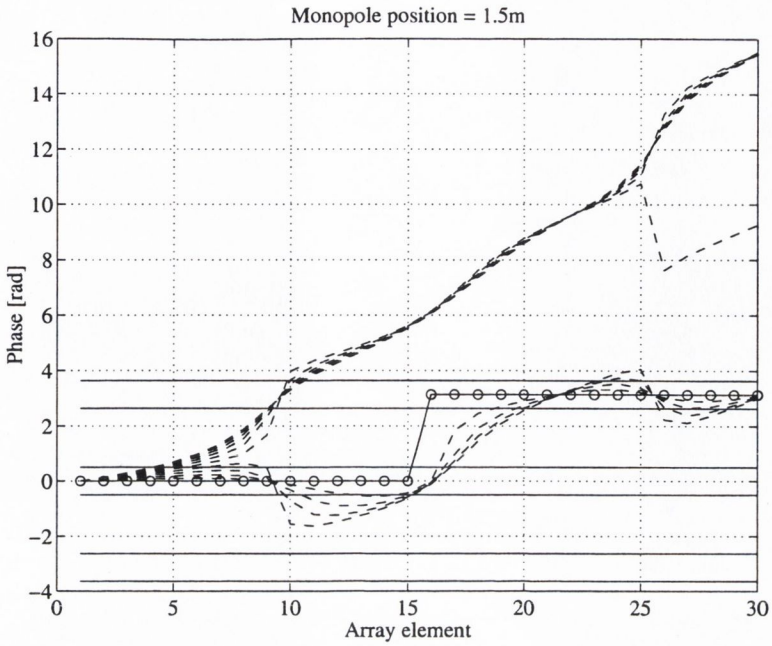

(a)

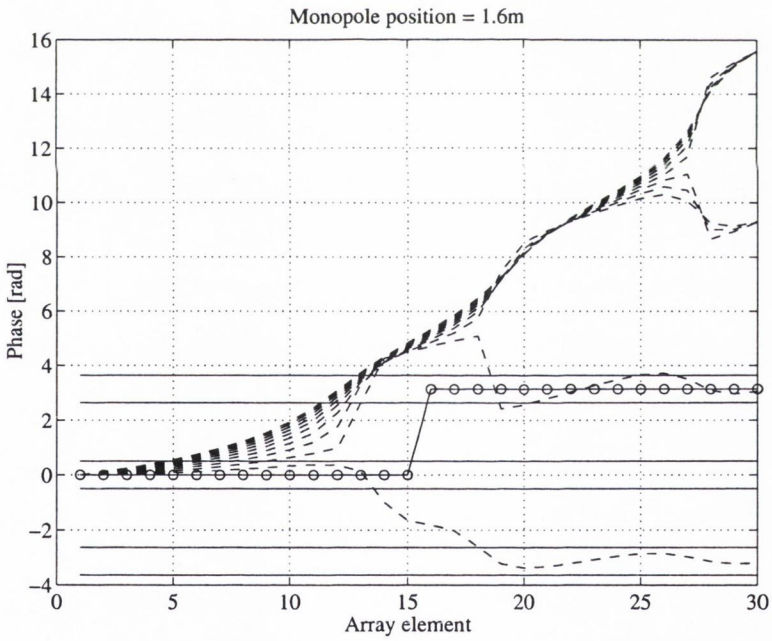

(b)

Figure 5.4: (a) 1.5m, (b) 1.6m

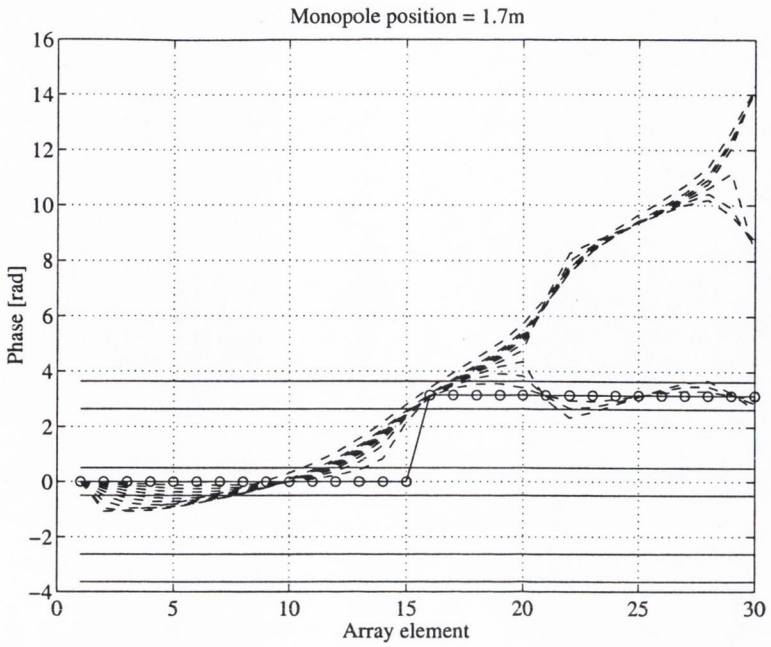

(a)

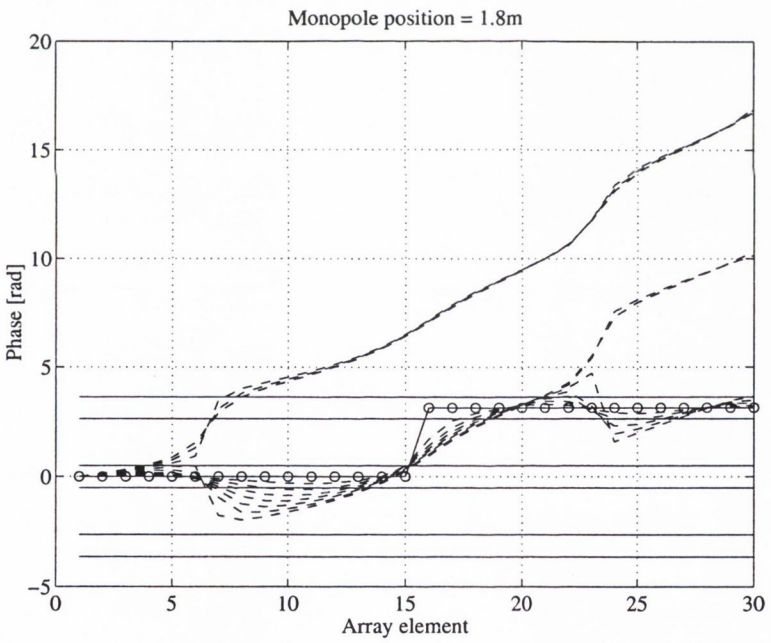

(b)

Figure 5.5: (a) 1.7m, (b) 1.8m

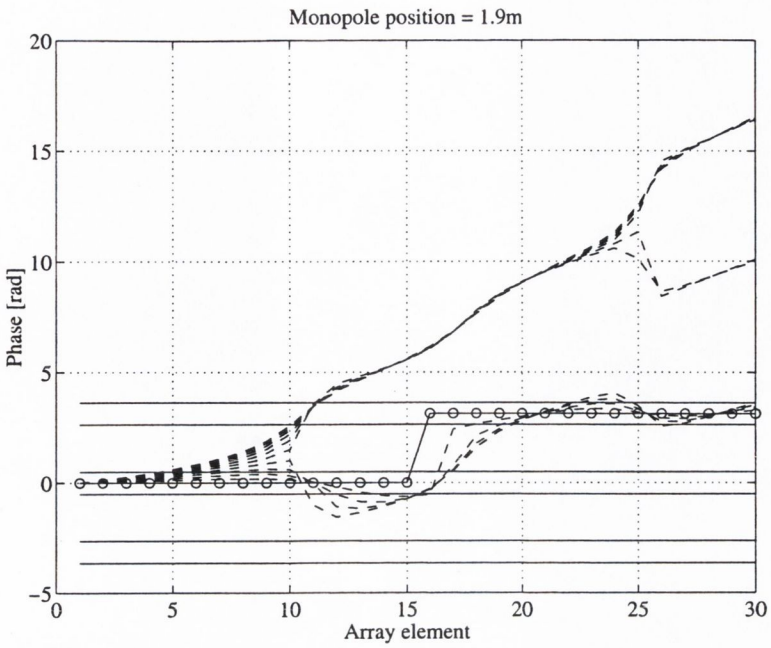

(*a*)

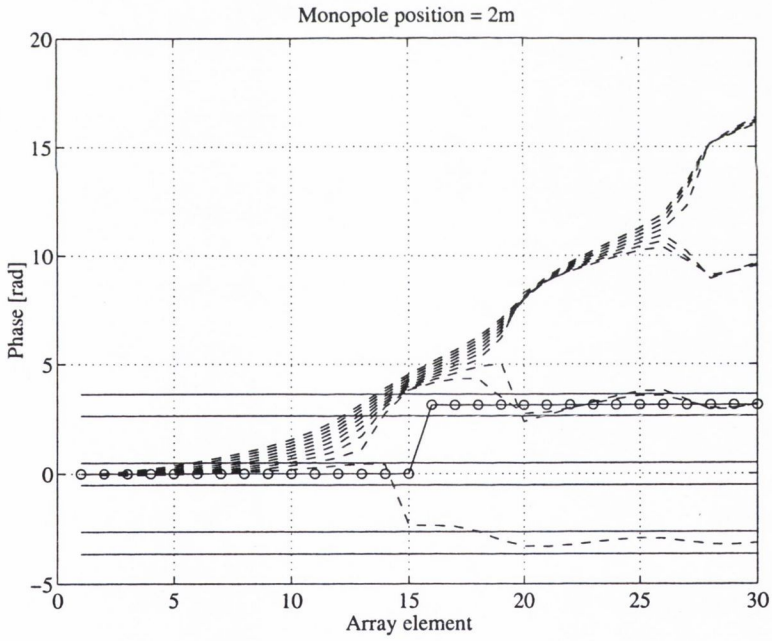

(*b*)

Figure 5.6: (*a*) 1.7m, (*b*) 1.8m

are the distributions whose values remain roughly within the bounds of the phase bands (shown as solid horizontal lines). When this basic pattern is evident, the identification technique will be able to identify the presence of the dipole. As the strength of the contaminating source increases however, the monopole phase characteristics begin to dominate and the dipole signature is lost. This can be seen in each figure as that set of phase distributions which have entirely lost the characteristic dipole pattern and have moved away from the dipole phase bands. From this data it is difficult to characterise the effect of a second source on the identification technique. Figures 5.2 through 5.6 do not show any obvious pattern as the monopole strength and position is varied. In each figure there are a number of distributions which retain the dipole characteristics and others where the monopole dominates, however it is difficult to see any relationship between the monopole strength and position and the degree of dipole phase distortion. This is a consequence of using only the signals' phases as search criteria.

5.2.1 Dealing with magnitude and phase

The technique proposed for dipole identification in the last chapter uses the physical characteristics of dipole sources, and the signature these leave in the far field, as a means for identifying their location and orientation. These characteristics are features of its distinctive propagation pattern, and are represented by the phase distribution across a focused beamformer. Using the phase alone in this way has certain drawbacks. The first of these is that the magnitude characteristics are neglected, even though these are an equally important property of any source. The reason for neglecting the magnitude distribution is because it is independent of the beamformer focus - the essence of the technique consists in searching for characteristics which are a function of the focus position. The second problem in dealing with phase is that the phase of a microphone signal which results from two separate sources at different spatial locations, can not be simply broken down into two additive components, one

for each source. It is this difficulty which makes the contamination effect of a monopole so difficult to characterise. It appears from figures 5.2 through 5.6 that the contamination is not simply dependent on the monopole position (which amounts to a change in phase), but also its strength. The magnitude and phase components of a signal are convenient parameters because of their obvious physical significance, but they are difficult quantities to deal with in this kind of study.

5.2.2 Real and imaginary components

In order to investigate the effect of a second source on the absolute contamination of a dipole signature, that is, to identify at what point the dipole characteristics are lost to the monopole, it is useful, instead of looking at the phase characteristics of a dipole, to examine its real and imaginary components. This is a different abstraction of the physical properties of the source, which, while less intuitive, is equally representative of the dipole nature. The

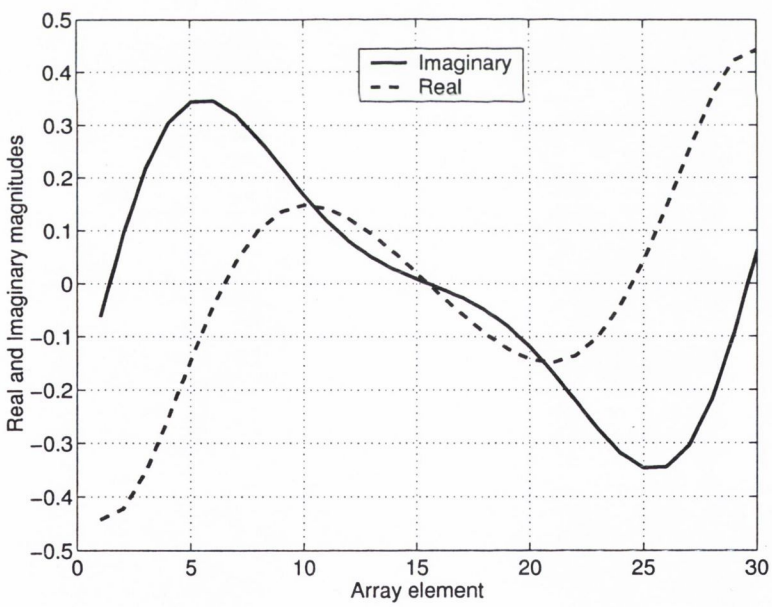

Figure 5.7: Real and imaginary distributions prior to focussing

real and imaginary distributions for a setup which consists again of a thirty

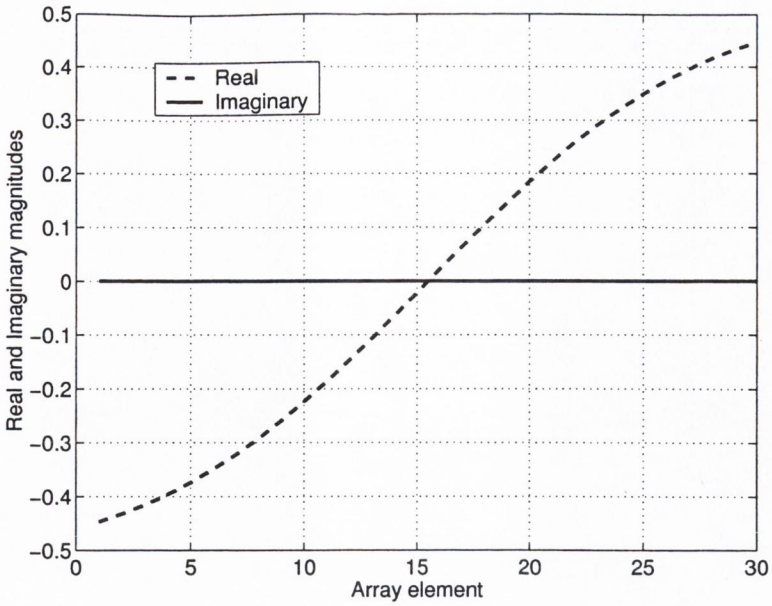

Figure 5.8: Real and imaginary distributions for focus on point dipole

element microphone array opposite a single point dipole with no contamination are shown in figure 5.7. Although these distributions represent the farfield signature of a point dipole and include both magnitude and phase effects, they do not lend themselves to the same physical interpretation as do the phase and magnitude representations. It is for this reason that they are less attractive as a means for identifying the source.

The dipole identification technique relies on changes in the dipole signature brought about by the focus of a beamformer. This change is shown in figure 5.8 which shows the real and imaginary distributions which result when the microphone signals are phase weighted to focus on the source. It can be seen here that the imaginary distribution is zero, corresponding to the alignment in phase brought about by focusing, whereas the real distribution retains its assymetry, corresponding to the fact that when the pressure is positive on one side of the cancellation axis it is negative on the other (a further demonstration of the mechanism which generates the null when an ordinary beamformer tries to measure a point dipole). In this representation of the dipole field

characteristics, the distinctive nature of the dipole is still evident. Thus, abstractions using the real and imaginary components of a source field retain the distinctive characteristics of the source, and, as they have the additive properties lacking in phase and magnitude representations, their use in the characterisation of monopole contamination is more straightforward. The real and imaginary distributions equivalent to figures 5.2 through 5.6 are shown in figures 5.9 through 5.13.

The effect of monopole strength and position on the dipole signature is much easier to see when the data is presented in this form. As the monopole strength is increased, the deviation of the real and imaginary distributions about their mean values becomes larger, this is evident in the larger oscillations of the dashed and solid lines about their mean. The same effect is evident as the monopole position is changed. Compare the maximum amplitude of the real distributions in figure 5.9(a) (corresponding to the closest monopole position) with those in figure 5.13(b) (corresponding to the most distant monopole position). Also note that depending on the position of the monopole, the frequency of undulation of the real and imaginary distributions varies. This is caused by variation, with monopole position, of the angle between the propagation direction and the array axis. For larger angles, as the sound field passes the array, more microphones are contained within a single wavelength. Conversely, when the angle is smaller fewer microphones are contained within a single wavelength.

Despite the contamination caused by the monopole, the presence of the dipole can still be recognised from the asymmetry of the real distribution, and this is an indication that a search technique based on the real and imaginary distributions might be a better approach to dipole identification. One further abstraction of this kind is to base a search algorithm on the full complex signal.

Figure 5.14 shows the complex distribution for a dipole source before and after focusing. In this form the data is again further removed from an intuitive grasp, but mathematically it remains a valid representation of the dipole

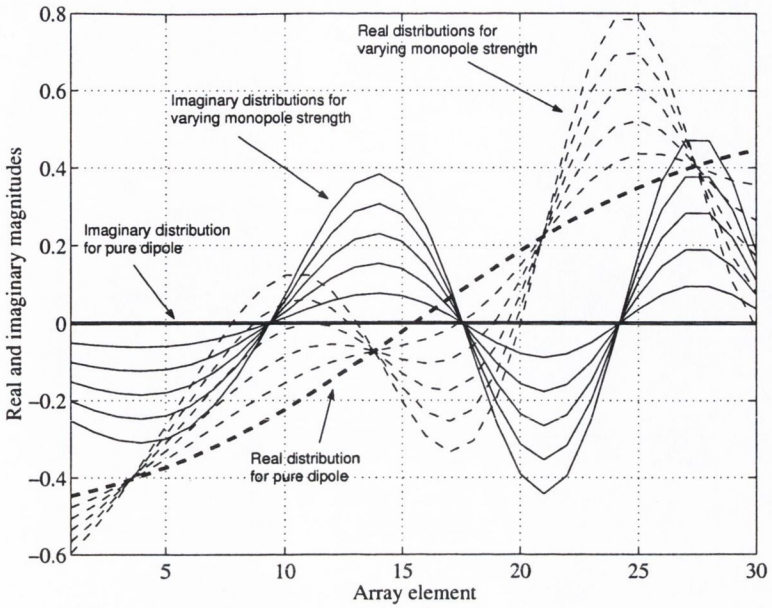

(a)

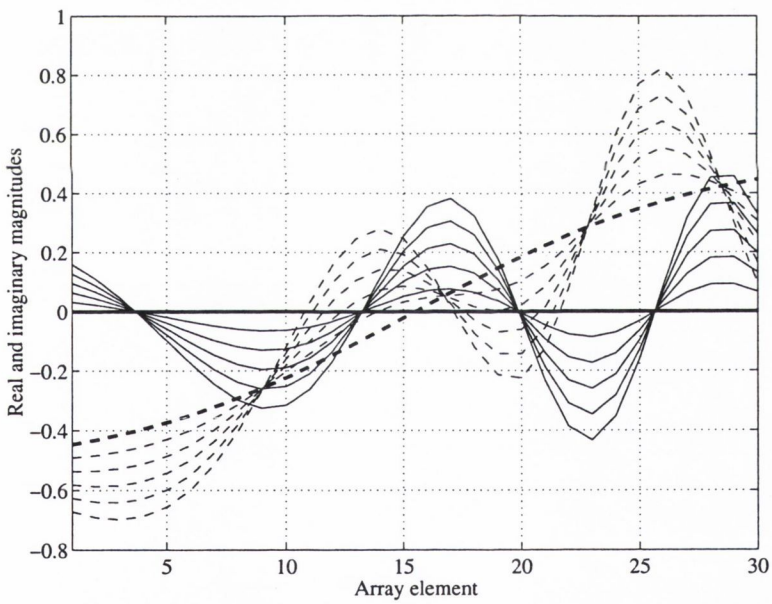

(b)

Figure 5.9: (a) 1.1m, (b) 1.2m

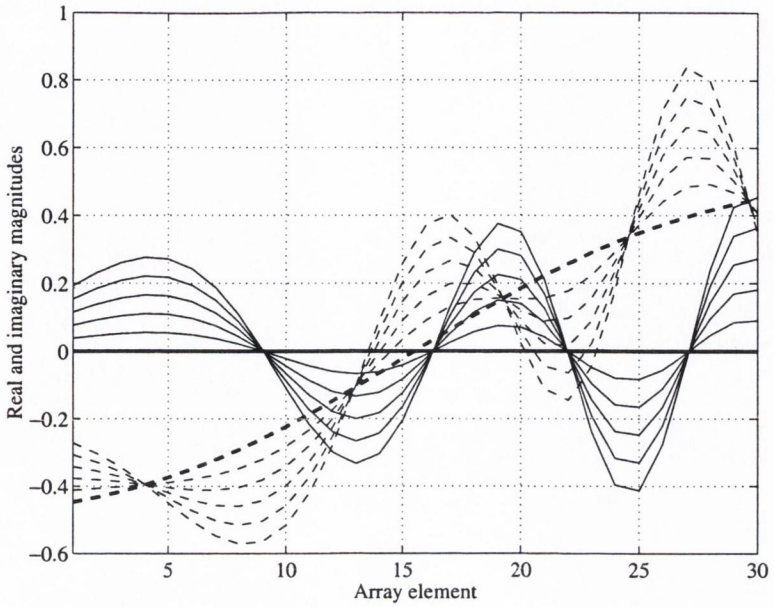

(a)

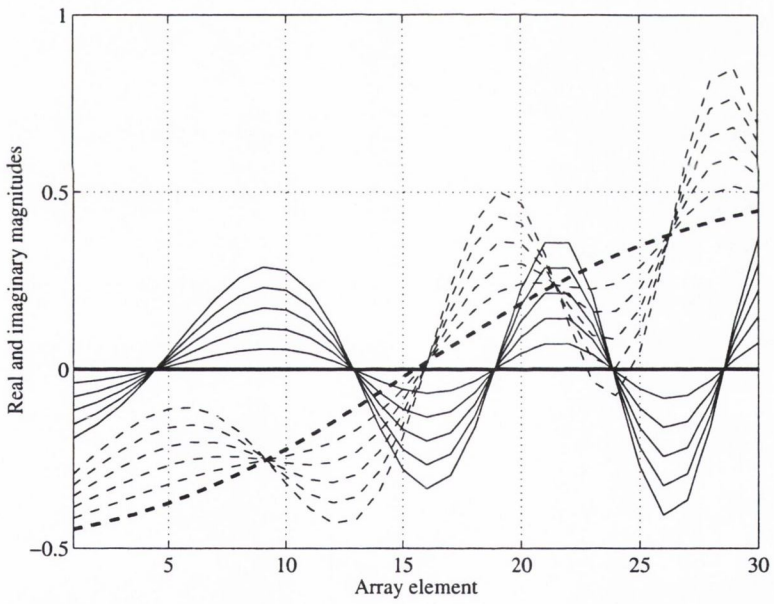

(b)

Figure 5.10: (a) 1.3m, (b) 1.4m

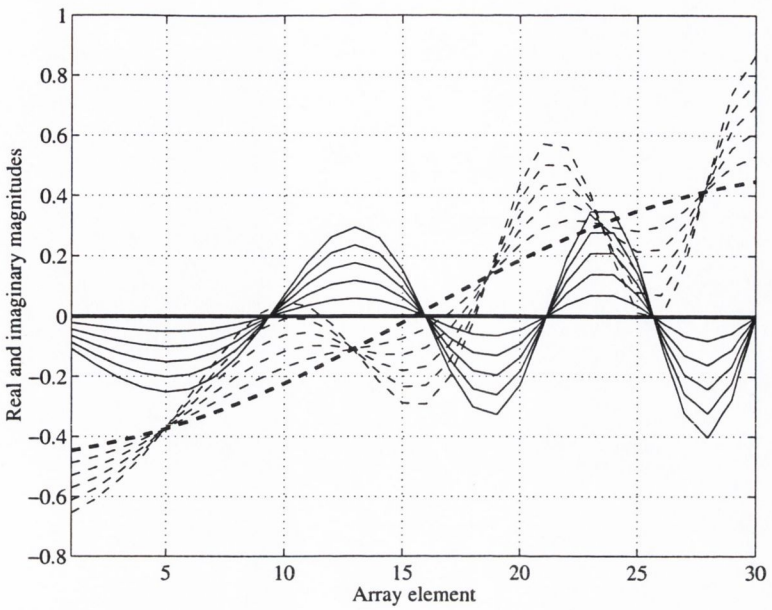

(a)

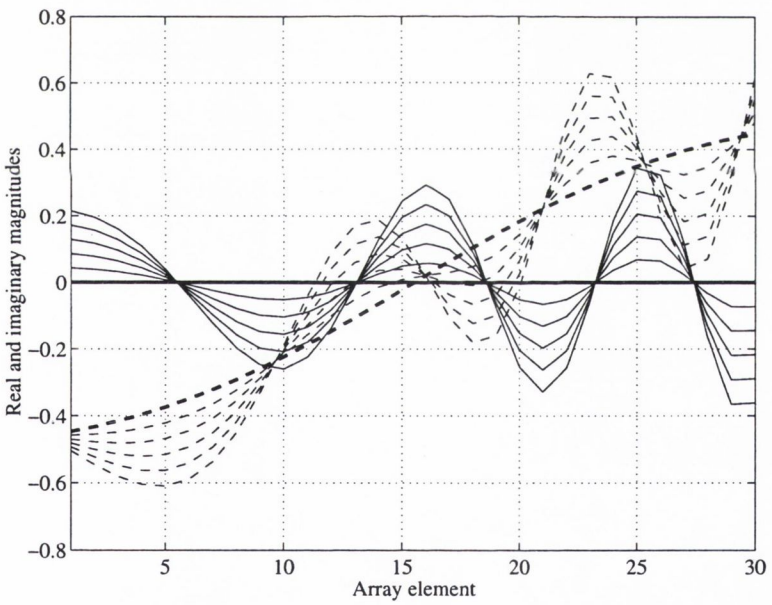

(b)

Figure 5.11: (a) 1.5m, (b) 1.6m

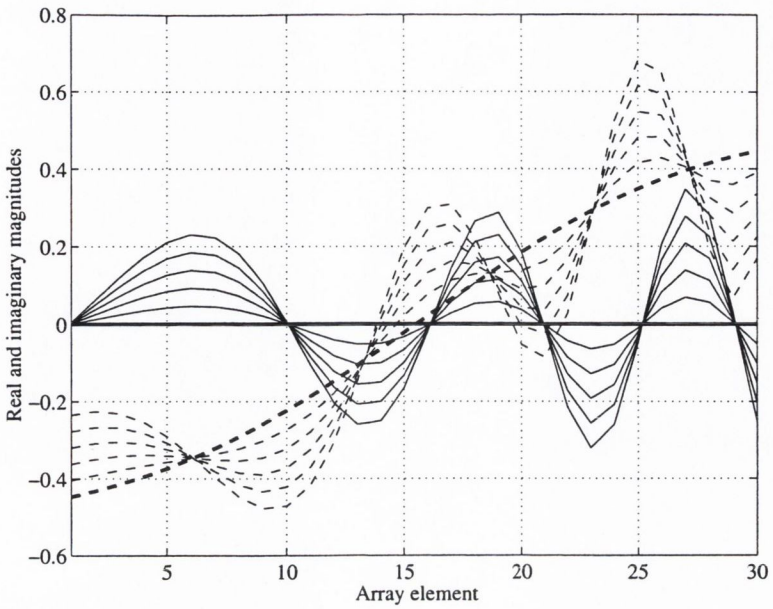

(a)

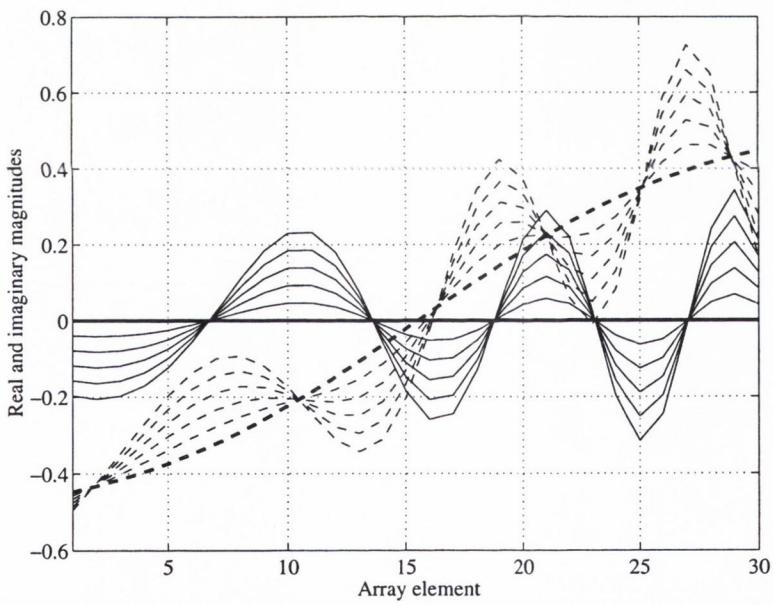

(b)

Figure 5.12: (a) 1.7m, (b) 1.8m

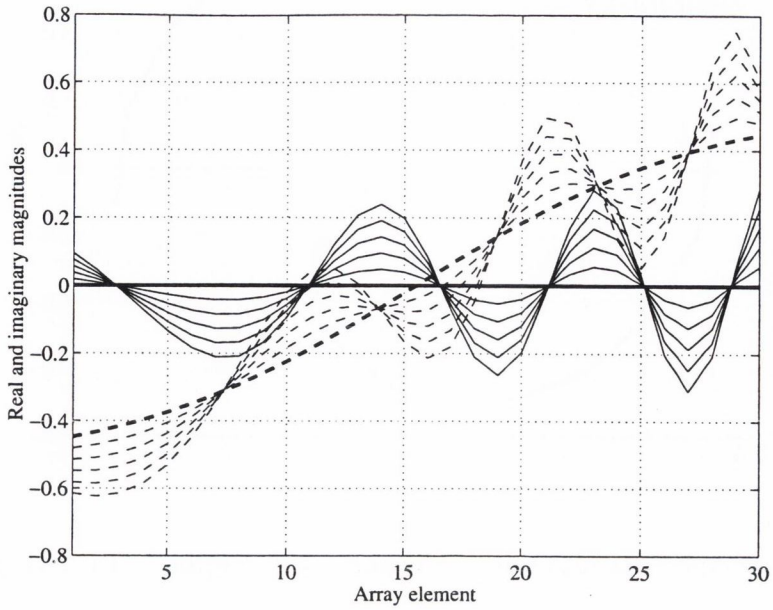

(a)

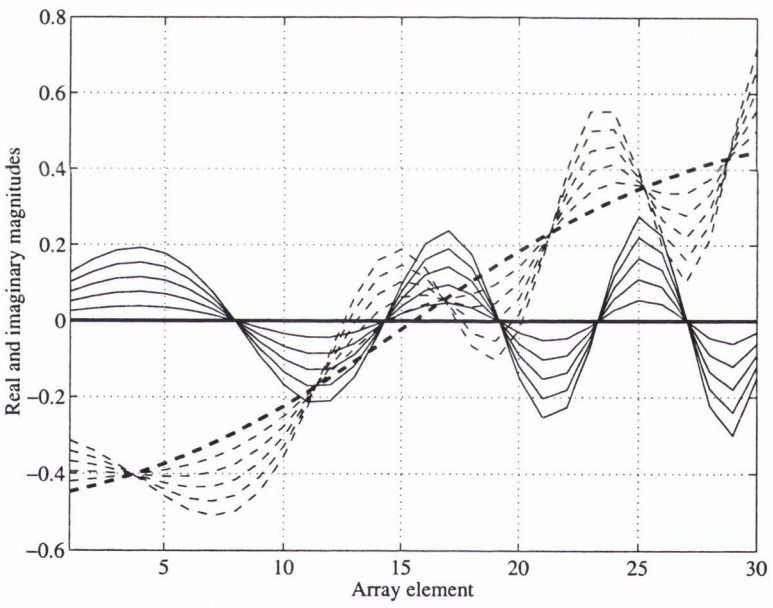

(b)

Figure 5.13: (a) 1.9m, (b) 2m

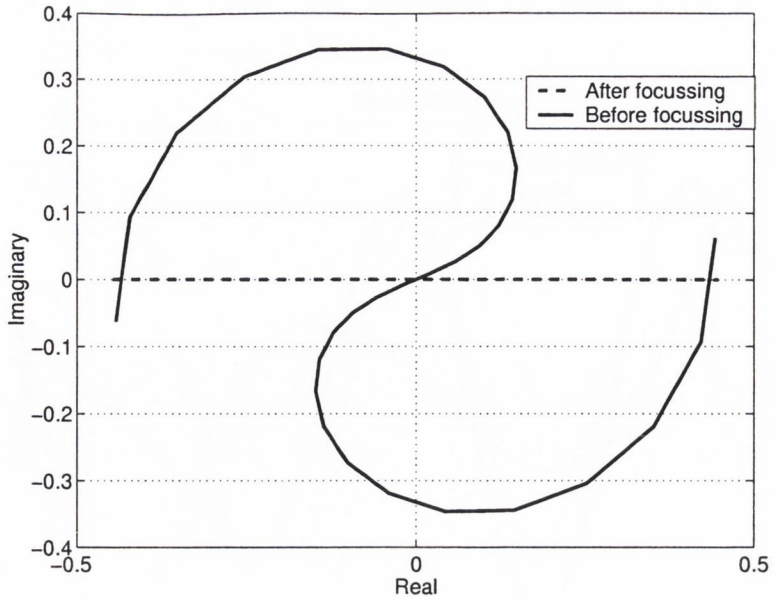

Figure 5.14: Complex distributions before and after focussing

nature and so, as the basis of a search technique, is perfectly acceptable. This analysis gives an indication of the potential for improvement in the dipole identification technique, by the application of search criteria which include both magnitude and phase characteristics.

5.3 Calculating source strength

Using a microphone array simply as a collection of microphones, it is possible, through knowledge of source position and type, to determine the strengths of the individual sources.

For an array of N microphones, the strength of N sources can be determined, provided a good propagation model is available. Consider the twin source system shown in figure 5.1. This consists of a point monopole and a point dipole, the propagation characteristics of which are well known. The real and imaginary distributions corresponding to these sources, for given locations, are shown in figures 5.15(a) and (b). Due to the additive nature of real and imaginary signal components the total distribution over the array in

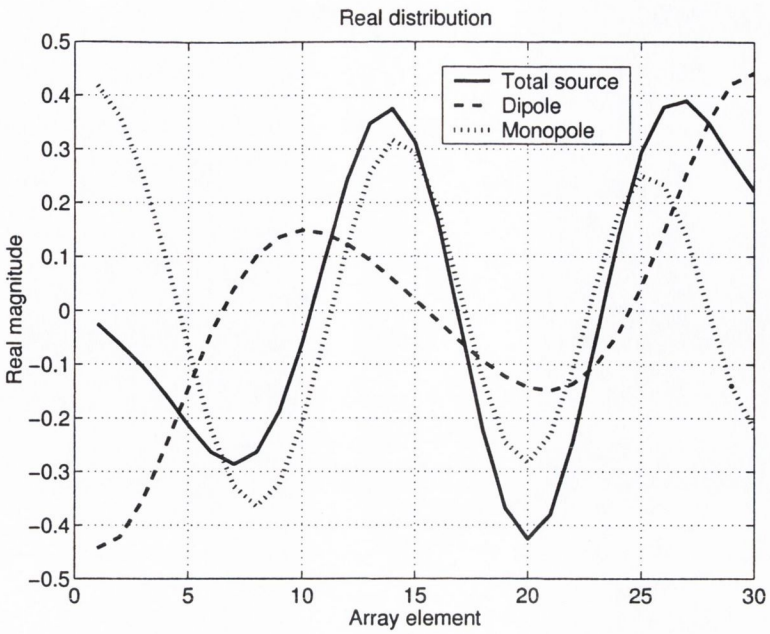

(a)

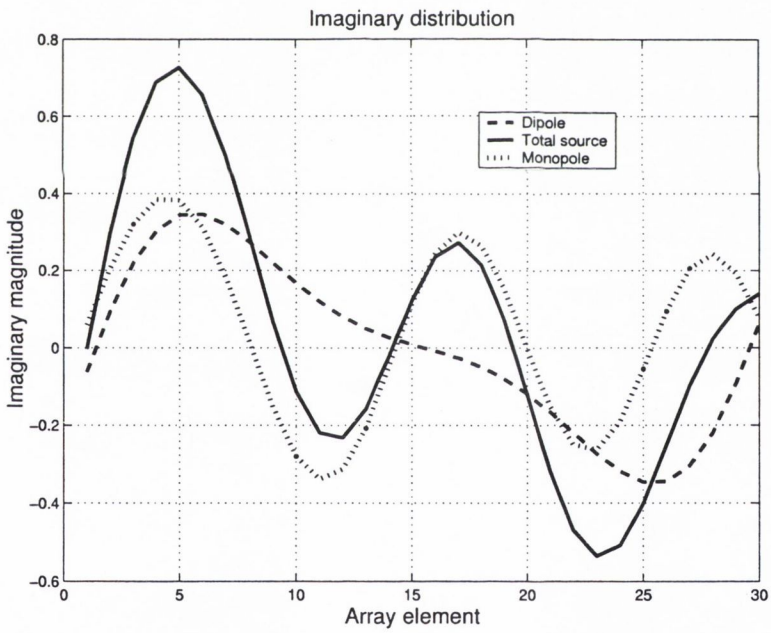

(b)

Figure 5.15: Real and imaginary distributions

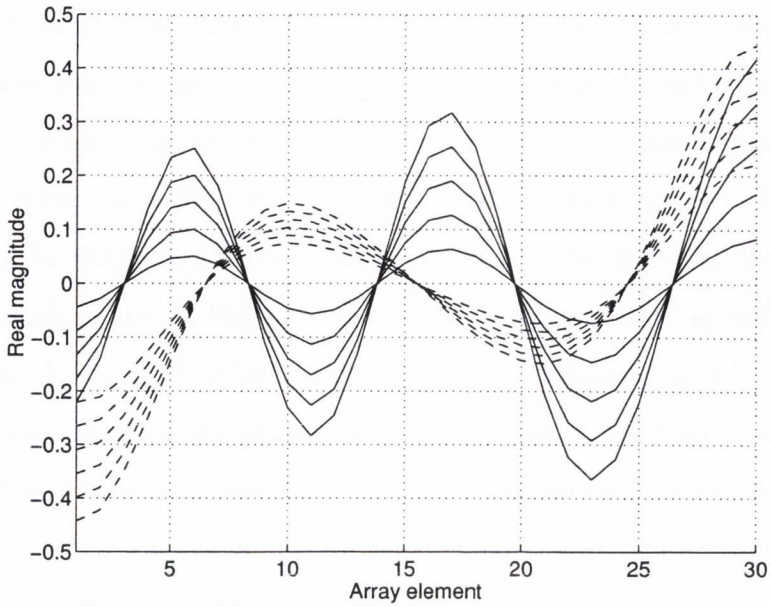

(*a*)

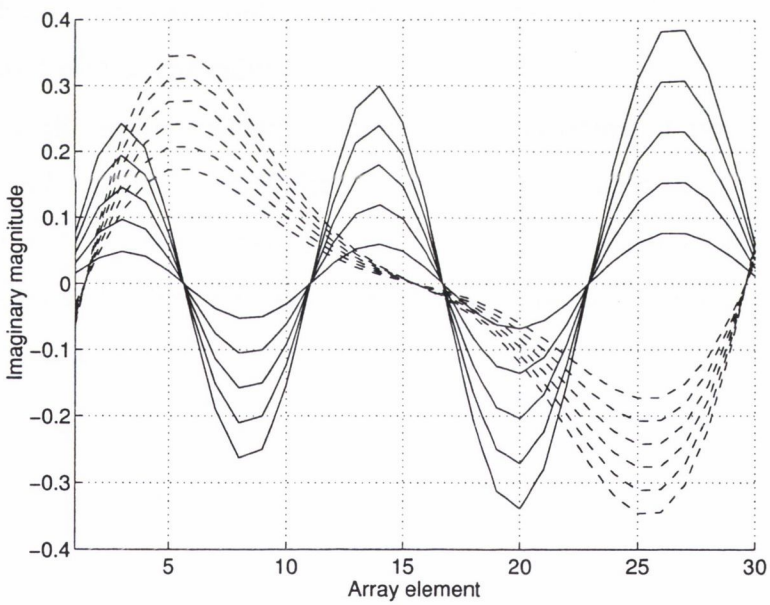

(*b*)

Figure 5.16: Real and imaginary distributions for varying source strengths

both cases is simply the sum of the individual distributions. Figures 5.16(a) and (b) show real and imaginary distributions for monopole (solid line) and dipole (dashed line) sources of varying strength. From these figures it can be seen that the basic shape of the distributions remains the same for all source strengths, it is only the size of the deviation about their means which varies. As mentioned previously, the actual distribution over the array (which is known) will simply be the sum of these distributions. So, for given source positions and types, the shape of the associated real and imaginary distributions are known, and the total distribution over the array is known in full. This leaves two unknowns, namely, the extent of the deviations of the distributions, which are related to the source strengths by the propagation model. As there are thirty microphones, a system of thirty equations and two unknowns can be set up and the sources strengths thus determined. It is clear from this that there is room for another 28 unknowns in this equation system, and so, with 30 microphones a system containing 30 sources can be evaluated. This can be demonstrated mathematically as follows.

Consider the system shown in figure 5.1, consisting of two sources, one monopole and one dipole. Let the sound pressure distribution over the array resulting from this source system be denoted by the 30 element vector S. Each microphone signal will consist of contributions from each of the sources, which can be written as

$$P_M = A_M \frac{e^{-jkR_M}}{4\pi R_M}$$

$$P_D = A_D \frac{\cos(\theta - \phi) e^{-jkR_D}}{4\pi R_D}$$

where P_M is a 30 element vector containing contributions from the monopole, P_D is a vector of the same length containing the dipole contributions (in this case the real and imaginary components are not separated, the signals are maintained in complex form). A_M and A_D are the actual source strengths

while R_M and R_D are vectors containing the distances from the array elements to the monopole and dipole sources respectively. The remaining terms in each expression contain details of the source propagation characteristics. In matrix form the equation system can be represented as

$$[Prop][A] = [S] \tag{5.1}$$

where $[A]$ is a two element column vector containing the source strengths, $[Prop]$ is a $[30 \times 2]$ element matrix containing the propagation models, and $[S]$ is a thirty element column vector containing the actual sound pressure distribution across the array. The source strengths can thus be solved for through the following operation.

$$[A] = [Prop]^{-1}[S] \tag{5.2}$$

The matrix $[A]$ can contain up to thirty source strengths before the equation system becomes underdetermined. Thus with an N element array N individual source strengths can be determined.

5.3.1 Limitations

This technique requires a substantial quantity of information concerning the source region, and in systems where the source mechanisms are uncertain, the technique will be weak. It is clear that any of these techniques used alone will be limited to a certain extent, and for this reason it is important that aeroacoustic analysis be approached with a variety of tools, both experimental and theoretical. By combining the strengths of the various methods, information regarding the source region can be gradually gathered and distributed to the appropriate tools for analysis. It is only in this way that an aeroacoustic system will ever be fully understood.

Chapter 6

General discussion

6.1 Beamforming for specific applications

In many array applications, emphasis is on the maximisation of measurement gain, (gain is defined as the difference in levels between the main-lobe and the highest side-lobe). This is because of the way in which a beamformer is most often applied - to perform a sweep of a region where both the spatial and spectral source distributions are unknown. Applications of this kind are susceptible to varying degrees of error, depending on the characteristics of the system. One source of error is the change in beampattern which occurs with varying frequency. This difficulty is addressed by Marcolini and Brooks [8], where they demonstrate how an array can be weighted in order to maintain constant beamwidth independent of frequency and look-angle. Meadows et al. [9] combine this technique, applying it to their small aperture directional array (SADA), with a spiral array configuration known as LADA (large aperture directional array), which minimises sidelobe levels for broadband applications. By this combination the arrays have been further improved, to give constant mainlobe beamwidth in the case of the SADA, and maximum gain in the case of the LADA. The arrays have thus been designed to best suit the particular characteristics of the system they are being used to analyse.

For the APIAN application, described in chapter 3, the source region con-

sists of two major narrowband sources of similar strength and an array is to be used to perform quantitative measurement of one of the sources. The requirements of the array are thus quite different from the application of Meadows et al.. Even if the techniques applied in their case were applied to the APIAN array, the measurement capacity would still vary as a function of frequency. This is because of the comparable strengths of the sources. Despite maximised gain and constant mainlobe beamwidth, measurement at frequencies where the sidelobes fall on the second propeller will be subject to more contamination than frequencies where this is not the case. For this application the array must again be designed to suit the characteristics of the system being investigated. It was demonstrated in chapter 3 how a linear array can be controlled so as to keep the major source of contamination - the second propeller - in a region where attenuation is a maximum, and this independent of frequency. This technique allows a good degree of accurate directivity control which is useful in systems where quantitaive measurements are required, and the positions of the major sources of contamination are known.

This comparison demonstrates the importance of designing an array to suit the specific characteristics of a given system. Each of the arrays, while suited to their own specific application, would be considerably weakened if they were applied to the opposite system. The setup of Meadows et al., because it consisted of broadband sources up to very high frequencies, is an example of a case where the most important array characteristic, for source localisation, is its gain. The APIAN application, consisting of low-frequency narrowband sources, is a system where the more important array characteristic is the particular shape of its sensitivity pattern and the positions of the sidelobes. Rather than simply using a configuration which gives the best gain, by looking a little closer at the system under analysis an array can be customised to suit that application and so provide better performance characteristics.

6.2 Aeroacoustic sources

In most aeroacoustic systems there exist fluid-structure interactions which result in unsteady aerodynamic loading. This is one of the major sources of dipole sound and such systems will exhibit a degree of source directionality which is not allowed for in standard beamformer algorithms. It was demonstrated in chapter 4 how failure to account for source-directivity can lead to erroneous interpretation of array data. Using a simple system consisting of a single aeroacoustic dipole, it was demonstrated how, once a source model is available, sources can be identified through a search for the appropriate characteristics, and the beamforming analysis procedures subsequently modified so as to perform a true measurement of that source.

This investigation illustrates how, in order to perform effective measurements using a microphone array, some attention must be given to the possibility erroneous interpretation due to source-directivity. If directional sources can be identified and modelled, then beamformer algorithms can be adapted in order to perform effective quantitative source measurement.

6.3 Analysis techniques

Each of the techniques discussed in the foregoing chapters have had their associated weaknesses and limitations. It is clear, that due to the impossibility of specifying a unique source distribution for a given set of field measurements, no method which is restricted to this kind of data can ascertain the actual source responsible. A general methodology is now proposed which combines these techniques in order to perform a more effective analysis of aeroacoustic systems.

6.4 Summary of analysis tools

- **Basic array optimisation :** The relationship between the response characteristic of an array and any combination of array/source parameters is well known and can be modelled. Using models such as these, the measurement capacity of an array for a given system can be readily determined. With a basic knowledge of the system to be analysed, array geometry can be optimised for that application.

- **Further optimisation - Directivity control :** By weighting the individual signals of an array, the response characteristic can be manipulated to suit a given system. For nonlinear array configurations the control parameters (weights) can be chosen based on results from numerical simulation of the array's response. However, there is no way of calculating a set of weights for a desired response characteristic. For a linear array, using the technique described in chapter 3, a set of microphone weights can be calculated which will effect an accurate repositioning of the directivity's sidelobes. Thus, a certain degree of directivity control can be achieved.

- **Dipole identification :** The technique developed in chapter 4 is capable, under certain conditions, of determining the location and orientation of an aeroacoustic dipole. The limiting factors for this method are known, and so again, with a basic knowledge of the aeroacoustic system under investigation, the applicability of the technique can be assessed.

- **Source strength calculation :** If the location of the dominant sources of a system are well known, and good propagation models are available, then using the technique discussed in chapter five, with an array of N microphones, N source strengths can be evaluated.

For thorough investigation of a given system, these tools must be used so as to compliment one another and thus improve their overall analysis capability.

6.5 General methodology

The flowchart shown in figure 6.1 proposes a general procedure for the analysis of an aeroacoustic system. The first step involves assumptions concerning the source region, which are made using a priori knowledge combined with a basic visual inspection. From these assumptions an initial estimate is made regarding the source distribution, which includes a rough estimate of both the spatial extent of the source region and its spectral content. Based on these assumptions an initial array is designed and optimised through consideration of the expected source distribution. This design will most likely be planar. Using this array design, initial measurements are made, giving an indication of the spatial distribution of dominant sound sources. By comparing the results of this measurement with the initial source estimate, the array configuration is reassessed in order to determine if further optimisation is necessary. Once the array has been well optimised, the next stage involves the design of a linear array for more localised analysis. This array should be mobile, so as to allow the determination of source directionality (by moving the array around a source, changes in the signature left on the array can be used to infer source propagation patterns) and is applied in two different ways. The first is for measurement of monopole-type sources for which it can be controlled using the technique described in chapter 3. The second mode of application is for the detection of dipole sources using the technique described in chapter 4. By combining the results of these measurements, a third estimate is made of the source region which includes details of the source types and their propagation characteristics. This estimate is then used as the basis for a calculation of the individual source strengths using the technique described in chapter 5. In order for this operation to yield a good estimate of the source, the models developed in the last stage of the analysis need to be accurate. If the estimate is very different from the previous estimate, the models must be reassessed and the operation repeated. Once some degree of convergence has been achieved,

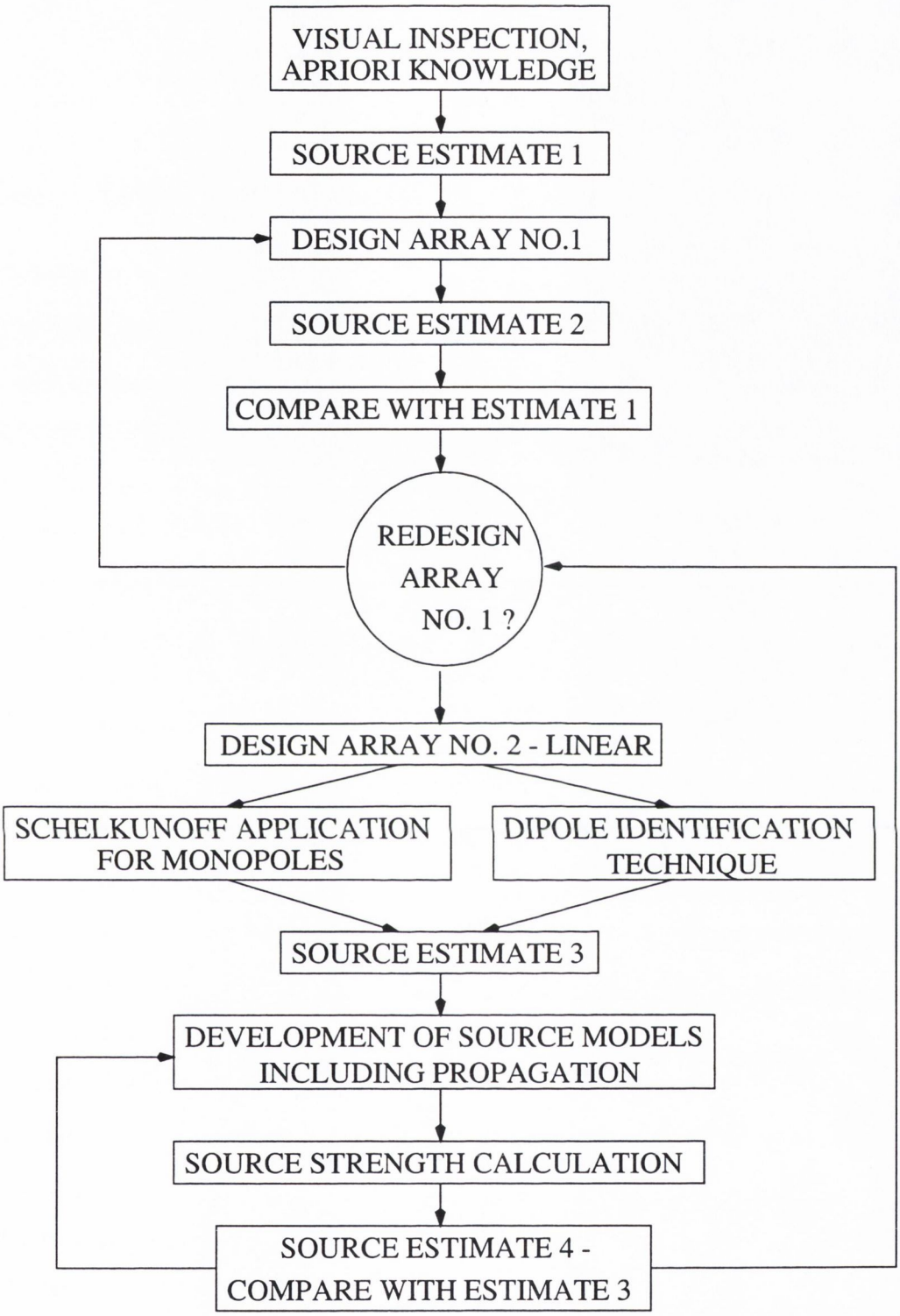

Figure 6.1: Analysis methodology

and estimates 3 and 4 are in good agreement, the design of array 1 can be reevaluated in light of the source information available from estimate 4, and the entire procedure repeated if necessary.

6.6 Discussion

Because of the impossibility of attaining a unique solution for a source region, given any amount of field data, analysis of a source region using measurements taken in the farfield will be limited in some form or another. This is evident in every technique described in this thesis. Given these limitations, the only option open to the aeroacoustic engineer is to approach the problem in a way similar to that described in the previous section. This involves making assumptions about the source region, and, by combining these with far-field measurements, arriving at an estimate of the source distribution. It is sure that this estimate will not be an exact solution, but should be used as a means for sharpening the intial assumptions, in order, through a process of iteration, to cause the subsequent series of estimates to converge. If in-flow measurements are also available, in the form of LDA or hotwire anemometry, these measurements will serve to further condition the analysis methodology, (the same goes for CFD and theoretical analysis). It is clear, that in order to fully evaluate the nature of an aeroacoustic system, the engineer must use every tool available, combining their strenghts and abating their weaknesses by mutual support, in order to arrive at a valuable set of conclusions concerning the nature of any system. With this more rounded appreciation of the workings of an aeroacoustic system, attempts to reduce, enhance, and generally manipulate those phenomena responsible for the sound will be made more effective.

Chapter 7

Conclusions

Array techniques have been developed which can be used to improve the measurement capacity of a microphone array. This was achieved by focussing on the two major weaknesses of array measurement systems, namely, the effects of source-frequency and source-directivity on the performance of an array. It has been demonstrated how, due to these difficulties, measurements may often be prone to erroneous interpretation.

- Sidelobe contamination can lead to spurious source identification when the array is used for source localisation, or incorrect source measurement when it is used to take measurements from a single source.
- The directional nature of certain aeroacoustic sources can lead to erroneous source measurement and localisation.

To address the sidelobe problem, a technique was adapted from microwave antenna theory for application to a linear microphone array. This technique gives control of the array's directivity pattern such that the sidelobe positions can be manipulated. In this way sources of contamination can be kept in regions of maximum attenuation. The implementation of this technique was demonstrated in the design and optimisation of an array for a specific aeroacoustic application.

The problem of erroneous source measurement due to the directional nature of a dipole source was demonstrated by means of a numerical model, which was then validated using a simple aeroacoustic system - a cylinder in cross flow. Based on these investigations a technique was developed which is capable of identifying the location and orientation of a point dipole, thus overcoming the problems posed by the directivity of that source.

The limitations of these techniques were assessed and shown to be due largely to the same limiting factors which arise in all analysis techniques based on farfield measurements, i.e. the impossibility of determining the actual source distribution responsible for a given sound field.

A general methodology for aeroacoustic analysis is proposed which combines the relative strengths of the different techniques.

7.1 Future work

This work has addressed a number of aspects of microphone array technology, and in each case developed techniques to improve array performance. There is scope for the further development of each of these techniques which is now briefly outlined.

- The technique for directivity control developed in chapter 3 will be extended to a two dimensional array to make it applicable to planar source regions. In the same way that sidelobe position can be controlled as a function of one spatial dimension, using a two dimensional array it should be possible to control the sensitivity as a function of two dimensions.

- The dipole identification technique will be improved by using real and imaginary array distributions as search criteria. It was shown in chapter 4 that the search technique based on a dipole's phase signature showed weaknesses which might be avoided through use of the complete microphone signal.

- Techniques which use array data in parallel with LDA measurement will also be developed. It was seen that some of the major difficulties in array applications arise from the fact that measurements are taken in the farfield. If these measurements are combined with measurements taken at the source, the limitations may be substantially reduced. With these improvements, the analysis methodology described in chapter 6 can be further refined.

Bibliography

[1] Merrill Skolnik. *Introduction to Radar Systems.* McGraw-Hill, 1980.

[2] H. O. Berktay and C. A. Al-Temimi. Virtual arrays for underwater reception. *Journal of Sound and Vibration*, 1969.

[3] A. D. Kuz'min and A. E. Salomonovich. *Radioastronomical Methods of Antenna Measurements.* Academic Press, 1966.

[4] C. L. Dolph. A current distribution for braodside arrays which optimizes the relationship between beam width and side-lobe level. *Proc. of institute of radio engineers*, 34:335–348, 1946.

[5] C. J. Bouwkamp and N. G. De Bruin. The problem of optimum antenna current distribution. *Phillips Res Rep*, 1946.

[6] H. J. Riblet. Microwave omnidirectional antennae. *Proceedings of institute of radio engineers*, 35:474–478, 1947.

[7] J. Billingsley and R. Kinns. The acoustic telescope. *Journal of sound and vibration*, 48(4):485–510, 1976.

[8] Michael A. Marcolini and Thomas F. Brooks. Rotor noise measurement using a directional microphone array. *Journal of the American helicoptor society*, pages 11–21, April 1992.

[9] William M. Humphreys William W. Hunter Kristine R. Meadows, Thomas F. Brooks and Carl H. Gerhold. Aeroacoustic measurement of a wing-flap configuration. *AIAA*, 1997.

[10] Michael Papazoglou and Jeffrey Krolik. High resolution adaptive beamforming for three-dimensional acoustic imaging of zooplankton. *Journal of the Acoustic Society of America*, 1996.

[11] S. R. Venkatesh and D. R. Polak. Phased array design, validation and application to jet noise source localization. In *6th AIAA/CEAS Aeroacoustics Conference*, number 2000-1934, Lahaina, Hawaii, June 2000.

[12] A Berman and C. S. Clay. Theroy of time-averaged-product arrays. *Journal of the acoustical society of America*, 29(7):805–812, July 1957.

[13] John L. Brown and Ricard O. Rowlands. Design of directional arrays. *Journal of the acoustical society of America*, 31(12):1638–1643, December 1959.

[14] R. Kinns. Binaural source location. *Journal of sound and Vibration*, 44(2):275–289, 1976.

[15] O. E. Flynn and R. Kinns. Multiplicative signal processing for sound source location on jet engines. *Journal of sound and vibration*, 46(1):137–150, 1976.

[16] S. A. Schelkunoff. A mathematical theory of arrays. *Bell System Technical Journal*, 22:80–107, January 1943.

[17] R. H. Duhamel. Optimum patterns for endfire arrays. *!.R.E.*, May 1953.

[18] G. Ziehm. Optimum directional pattern synthesis of circular arrays.

[19] R. S. Elliot F. Ares and E. Moreno. Design of planar arrays to obtain efficient footprint patterns with an arbitrary footprint boundary. *IEEE*, 42(11):1509–1514, November 1994.

[20] P. M. Woodward and J. D. Lawson. The theoretical precision with which an arbitrary radiation-pattern may be obtained from a source of finite size.

[21] R. L. Pritchard. Optimum directivity patterns for linear point arrays. *Journal of the acoustical soiciety of America*, 25(5), September 53.